JPRS-JST-91-016
9 MAY 1991

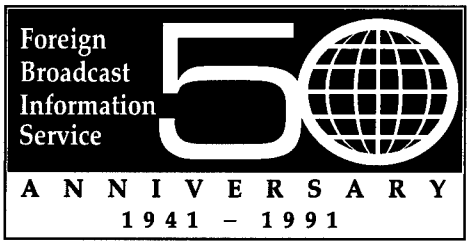

JPRS Report

Science & Technology

Japan

INTERMETALLIC COMPOUNDS SEMINAR

JPRS-JST-91-016
9 MAY 1991

SCIENCE & TECHNOLOGY
JAPAN

INTERMETALLIC COMPOUNDS SEMINAR

916C1004 Tokyo KINZOKU GAKKAI SEMINA KINZOKUKAN KAGOBUTSU in Japanese
1 Jun 90 pp 1-11

[Papers presented at The Japan Institute of Metals Seminar on Intermetallic Compounds held 21-22 June 90 in Tokyo, sponsored by The Japan Institute of Metals]

CONTENTS

Crystal Structure, Systems of Intermetallic Compounds

916C1004A Tokyo KINZOKU GAKKAI SEMINA KINZOKUKAN KAGOBUTSU in Japanese
1 Jun 90 pp 1-11

[Article by Masahiko Morinaga, School of Engineering, Toyohashi University of Technology: "Crystal Structure of Intermetallic Compounds: Theoretical Prediction of Crystal Structure of Intermetallic Compounds by Band Calculation; Crystal Structure Map"]

[Text] **1. Introduction**

Intermetallic compounds are new materials, including metallic to ceramic compounds with diverse properties. In this undeveloped field, a large number of compounds with much more excellent characteristics than conventional materials as those found in $Nd_2Fe_{14}B$ are likely to exist, raising expectations of material researchers.

It is well known that various properties and chemical characteristics of materials are closely related to their crystal structure. With intermetallic compounds, in particular, their crystal structure undergoes various changes depending upon combinations of construction elements, so predictions of these changes are very important in material design. To this end, various prediction methods have been proposed since the Hume-Rothery age. Recently, progress in band calculation is enabling predictions of crystal structure to be made in theory. This article describes the crystal structure outline of intermetallic compounds and considers the current state of predicting structure.

2. Crystal Structure of Intermetallic Compounds

Most metals form such simple crystal lattices as a face-centered cubic lattice, body-centered cubic lattice, and closest packed hexagonal lattice. About 41 percent of intermetallic compounds have a structure derived from these simple crystal types. Figure 1 shows simple examples. There are many symbols representing crystal structure and here the author uses Strukturbericht's. Division symbols (a)-(c), (d)-(g) and (h) are produced by substituting dissimilar atoms for a face-centered cubic lattice, body-centered cubic lattice, and closest packed hexagonal lattice, respectively. With AB-composition compounds, for example, TiAl has $L1_0$ type structure, FeAl B2 type structure, and LiAl B32 type structure.

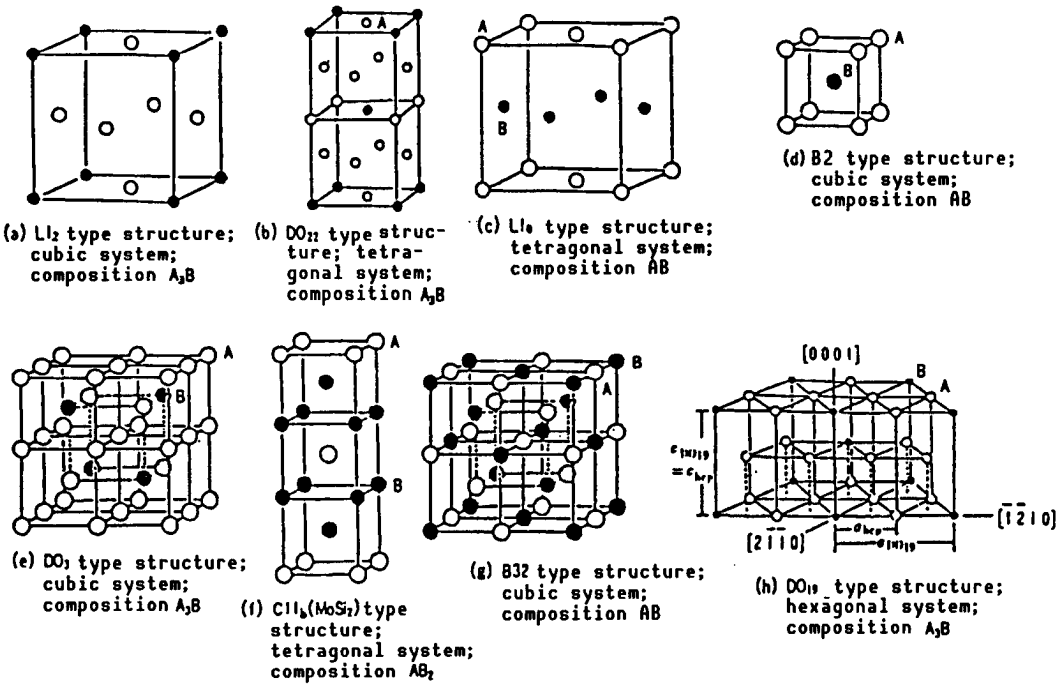

Figure 1. Structure Based on Face-Centered Cubic Lattice, Body-Centered Cubic Lattice, or Closest Packed Hexagonal Lattice

Figure 2 shows the crystal structure which appears when dissimilar atoms enter into an interstitial position of a face-centered cubic lattice (a). Enclosed in the parentheses in the drawing are names of prototype compounds. Dissimilar atoms are regularly in tetrahedral position with division symbols (b) and (c) and in octahedral position with (d). For example, those with NaCl type structure include transition metallic carbide and nitride (TiC and TiN, for example), which show interesting properties, the most important being superconductivity.

Compounds with AB_2 composition generically called Laves phase comprise 29 percent of all intermetallic compounds. Their crystal structure is represented by C15($MgCu_2$) type of cubic crystals and C14($MgZn_2$) and C36($MgNi_2$) types of hexagonal crystals. Figure 3 shows the structure of C15 and C14 types. Letting the radius of atom A and that of atom B be r_A and r_B, respectively, and when $r_A/r_B = 1.225$, Laves phase known as dimensional factor compounds has a closest packed filling structure. The radius ratio of actual compounds ranges from 1.0~1.7.

In addition to these compounds, there are compounds with various crystal structure, led by A15 type compounds (Nb_3Sn, for example) which show superconductivity and B8 type compounds (PdTe, for example). Data on the crystal structure of intermetallic compounds has recently been published.

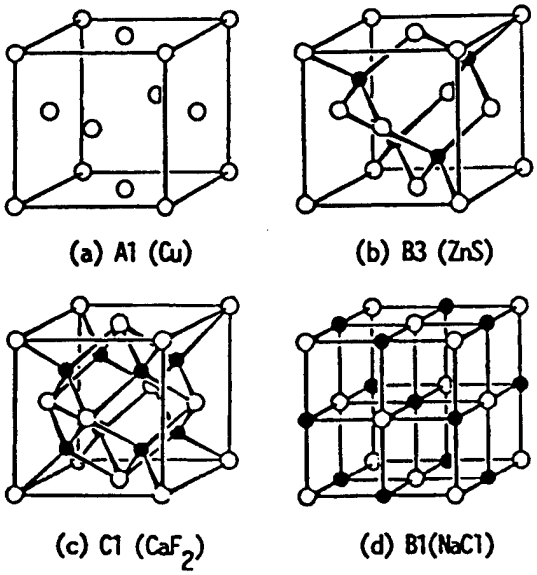

Figure 2. Face-Centered Cubic Lattice (a) and Structure (b)-(d) Generated When Dissimilar Atoms Enter Into an Interstitial Position

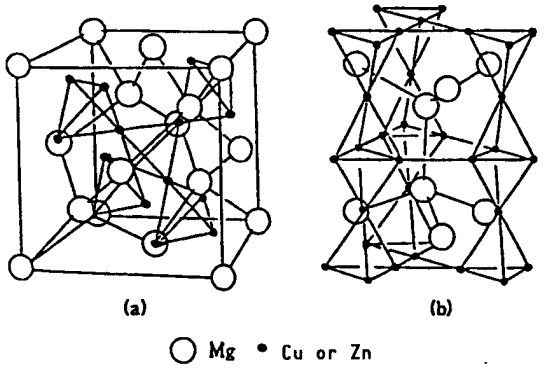

Figure 3. Crystal Structure of Laves Phase
(a) C15 cubic Laves phase ($MgCu_2$ type)
(b) C14 hexagonal Laves phase ($MgZn_2$ type)

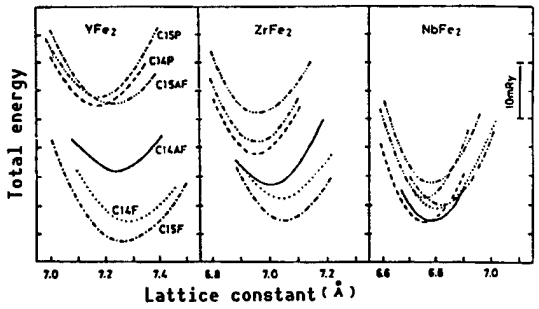

Figure 4. Calculation Results of Total Energy of Fe-System Laves Phase

3. Theoretical Predictions of Crystal Structure of Intermetallic Compounds by Band Calculation

Let us cite Laves phase which shows a variety of properties as an example. In Fe-system Laves phases, YFe_2 and $ZrFe_2$ (both are C15 type) are ferromagnetic (indicated by F) and $NbFe_2$ (C14 type) paramagnetic.

Predictions on the stability and magnetism of the crystal structure of these Laves phases have recently been made using band calculation. Figure 4 shows the total energy of the electronic system found by changing lattice constants with various crystal and magnetic structures. With YFe_2 and $ZrFe_2$, ferromagnetic C15 type shows minimum total energy, coinciding with an experimental result. With $NbFe_2$, on the other hand, the magnetic structure does not cause

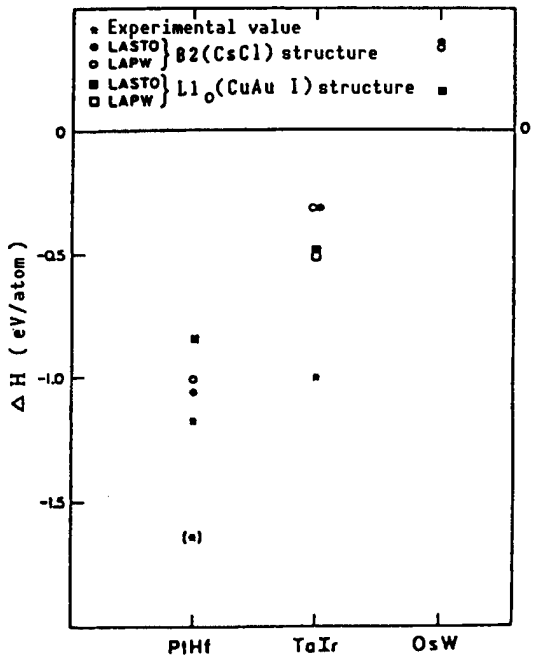

Figure 5. Comparison of Heat Generation When OsW, TaIR, and PtHf Take B2(CsCl) and $L1_0$(CuAuI) Structure Between Calculation and Experiment
Calculation results of LASTO and LAPW by band calculation are shown in the drawing.

the total energy to change much due to meager energy gain by spin polarization. The state of C14P confirmed by the experiment is barely stable, but C14AF (AF represents antiferromagnetic) is present near the C14P.

Magnetism of these Laves phases changes with lattice constants. In YFe_2 with large lattice constant, magnetic moment of Fe can exist stably as if it were in bcc pure iron with the result that it becomes ferromagnetic. In $NbFe_2$ with small lattice constant, magnetic moment of Fe is unstable, so it becomes paramagnetic.

Calculation of such total energy is tried with various compounds (hydrogen storage compound FeTi, for example). Also, based on the calculation, heat from the formation of compounds ΔH is calculated as follows:

$$\Delta H = E(AB) - E(A) - E(B)$$

where E(AB) is total energy of compound AB and E(A) and E(B) are their total energies when they exist independently. When ΔH is negative, the greater ΔH, the easier the generation of compounds. Figure 5 shows ΔH obtained with TaIr($L1_0$(CuAul)) type structure, PtHf(B2(CsCl)) type structure and a hypothetical compound OsW. Heat from the formation of TaIr is greatest with CuAuI structure and PtHf with CsCl structure. OsW, which does not develop any compounds, on the other hand, shows a positive heat of formation.

It is worth noting that compared to total energy, very little heat of formation can be predicted at present.

In addition to the above, the first theoretical calculation of alloy state diagrams based on band calculation is being made by Mori and Terakura. Also, with respect to regular and irregular transformation of alloys, such theoretical discussions are taking place.

The problem of calculating total energy lies in the assumption of some kind of crystal structure used for calculation. It can be found which crystal structure is lowest in energy and is stable, but it is difficult to define simply the crystal structure of unknown substance.

4. Crystal Structure Maps

As stated above, it has become possible to compare total energies to discuss crystal structure. However, this method does not necessarily go well. Another problem is that thorough calculation of every intermetallic compound and its crystal structure is impossible even using a supercomputer due to the amount of time required. To cope with this, adjustment of the crystal structure is currently attempted using various parameters. This attempt has been made continuously since the Hume-Rothery age, a pioneer in metallurgy.

The author has reviewed the possibility of adjusting the crystal structure of intermetallic compounds using various parameters as part of the survey by the Metallic Material Development Center. This chapter describes some of the results. The survey is targeted at Al, Si, B, and Mg intermetallic compounds recently attracting attention as lightweight heat-resistant materials. The presence of nonstoichiometric composition widths, melting points, and Young's moduli of these compounds were examined together with their crystal structure maps. Researchers from a large number of enterprises and universities participated in the survey. The names of the researchers will be identified in the figures included throughout the text.

4.1 Structure Maps and Parameters

Various so-called structure maps have so far been studied which are adjusted as two-dimensional or three-dimensional maps by selecting parameters possibly involving the structural stability of intermetallic compounds. Figure 6 shows a structure map. A structure map is aimed at predicting the crystal structure of intermetallic compounds using parameters involving interatomic chemical bonds, adjusting their properties and applying the results to material design. As parameters to be studied or adjusting methods, the following nine types were selected in view of the historical process: 1) periodic tables; 2) electronegativity and atomic radii (classical parameters); 3) group numbers of periodic tables; 4) principal quantum number and electronegativity; 5) electronegativity and electronic hole number; 6) Miedema's electronegativity and electronic density of (Wignersaissel) boundary; 7) pseudo-potential orbital radius; 8) pseudo-potential orbital radius, number of valency electrons and electronegativity (Villars' method); and 9) Mendeleev's number. The following are concrete descriptions of each result.

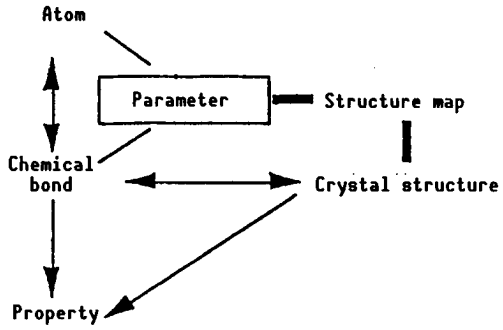

Figure 6. Concept of Structure Map

4.2 Periodic Table

In order to know the properties of elements, the periodic table is the first reference. In a periodic table, elements are arranged according to their extranuclear electron arrangement, which is naturally closely related to interatomic chemical bond format.

In Figure 7, the crystal structure of Al compounds by composition ratio is summarized in (a)–(c) and that of Si compounds in (d). To show the crystal structure, Pearson's symbols (cP2, for example) are used here in addition to Strukturbericht symbols and names of prototype compounds. These symbols comprise three kinds of letters with the English small letter representing the crystal system, the English in capital letter representing the lattice shape, and the numerical representing the number of atoms in a unit cell. As can be anticipated, it is found from these drawings that compounds taking the same crystal structure appear in the periphery of the same group.

With MAl compounds in Figure 7(a), only TiAl has $L1_0$(AuCu, tP4) type structure, while many others have B2(CsCl, cP2) type structure. Since $L1_0$ type structure does not appear in Mg, Si, and B systems, IiAl can be said to be a compound with a special structure. From Figure 7(b), it is found that Nb_3Al and Ti_3Al have A15(Cr_3Si, cP8) type structure and DO_{19}(Ni_3Sn, hP8) type structure, respectively. From Figure 7(c), Al_3Ti has DO_{22}(Al_3Ti, tI8) type structure, near which are $L1_2$($AuCu_3$, cP4) and a compound with DO_{19} type structure. It is known that the structure of $L1_2$, DO_{19}, and DO_{22} types changes according to changes in laminating fault energy and antiphase boundary energy. Also, as found in Figure 7(d), $MoSi_2$ has $C11_b$($MoSi_2$, tI6) type structure. Such an adjusting method based on the periodic table uses no quantitative parameters, which causes the problem that only qualitative discussion can be considered.

4.3 Electronegativity and Atomic Radii (Classical parameters)

Since the work of Hume–Rothery and Darken–Gurry, diagrams of alloys (solution limit, for example) have been adjusted using electronegativity and atomic radii. Figure 8 shows results of the adjustment of the crystal structure of MAl compounds using these classical parameters. Due to dispersed data, no consistency could be found.

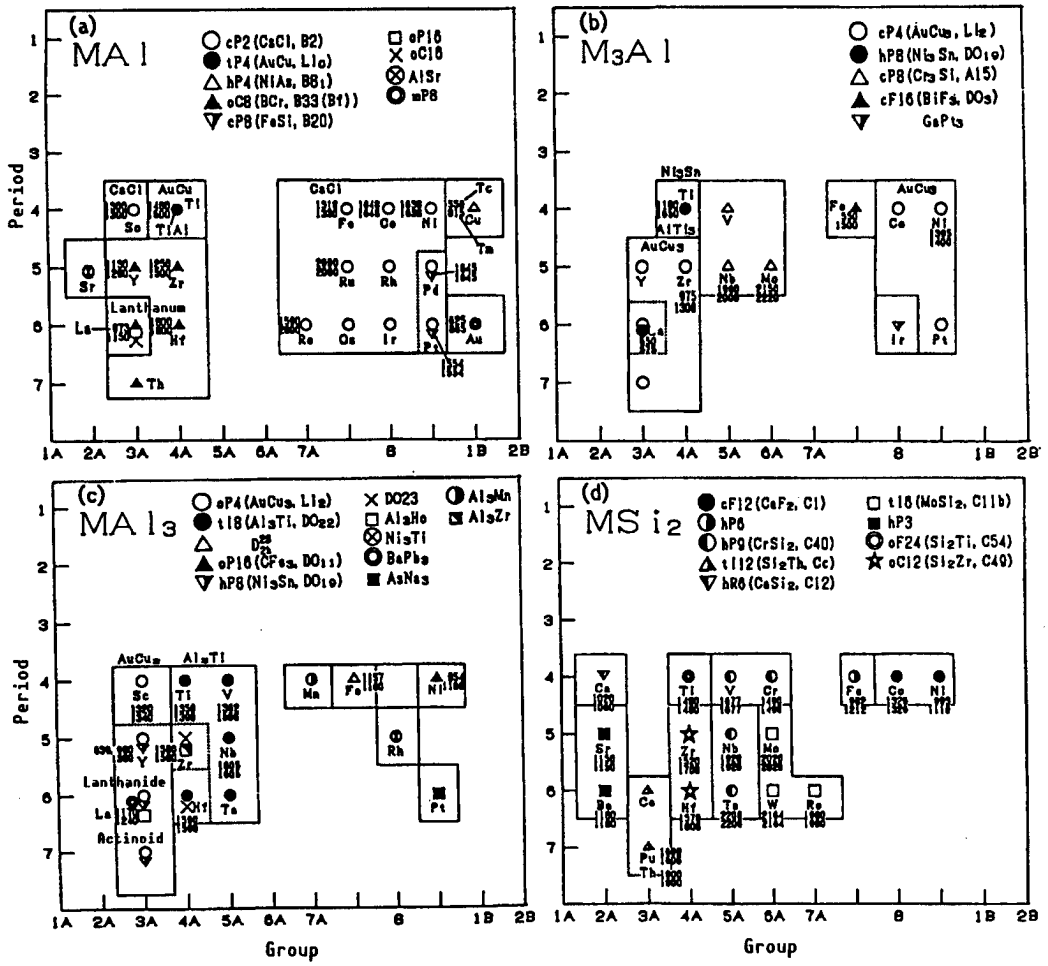

Figure 7. Adjustment of Crystal Structure With Periodic Table and Compounds of (a) MAl, (b) M_3Al, (c) MAl_3, and (d) MSi_2 Systems

With figures in two rows close to element symbols in the drawing, the upper ones represent upper limit temperature (T_c) where compounds can exist stably and the lower are melting temperature (T_m) with relevant compositions. When $T_c = T_m$, it implies that the compound exists stably until it melts.

4.4 Group Numbers in Periodic Table

These numbers are to introduce a numerical system comprising horizontal elements and their corresponding group numbers in the periodic table for the qualitative adjustment of the periodic table. However, there is no discrimination with vertical elements and their corresponding periodic numbers in the periodic table.

With this method, adjustment is made by taking the average ($\overline{N}$) and the difference (ΔN) of group number N of component elements on both axes. The use of the average and difference of parameters is a method often used for

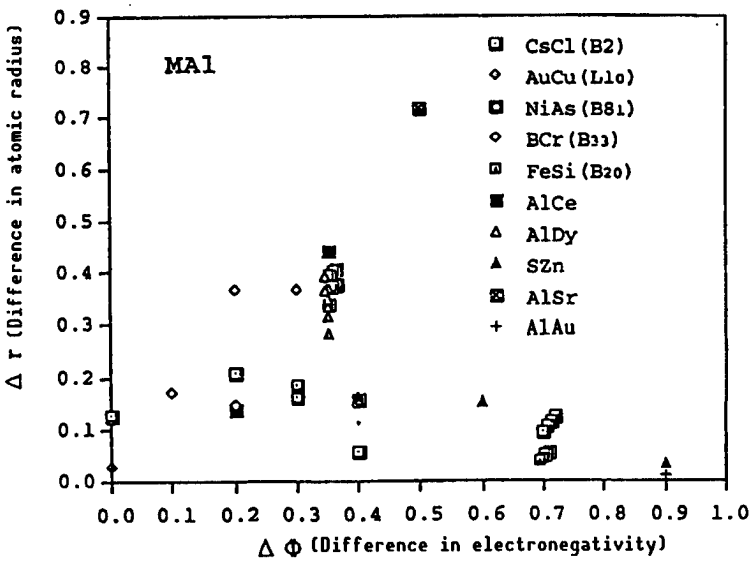

Figure 8. Adjustment of MAl Compounds With Classic Parameters

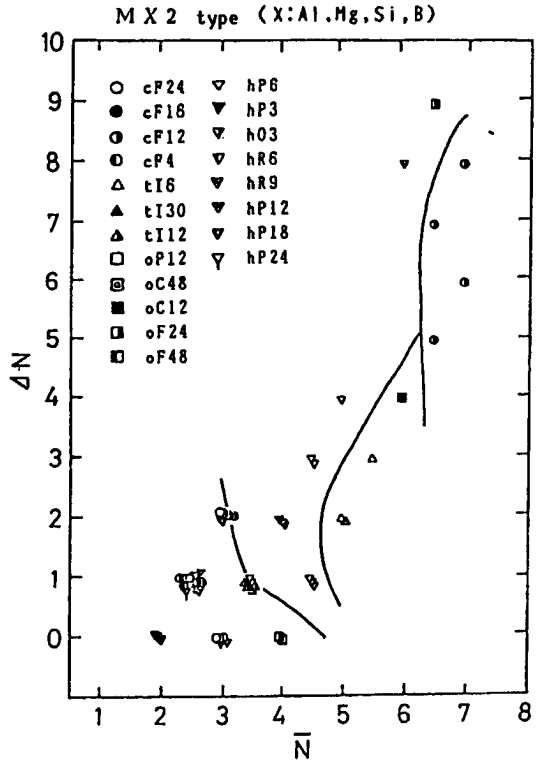

Figure 9. Adjustment of MX_2 Compounds With Group Numbers
(By Suzuki, Kawasaki Steel Corp.)

structure maps. Figure 9 shows the results of adjustment of MX_2 compounds (where X=Al, Mg, Si, B). It is difficult to adjust the crystal structure; however, crystal systems (represented by first letter of Pearson symbols) can be identified to some extent from this drawing. Similar adjustment could be made with the MX system, but not with the M_2X system.

In addition to the above, it was found that Young's moduli and melting points of compounds become highest near average group numbers ($\overline{N}$) of 4~5. Melting points of compounds are related to those of component elements, and the higher the melting point of an element contained in a compound, the higher the compound's melting point.

Group numbers correspond to the horizontal arrangement of elements in the periodic table, and can be interchangeably read with numbers of outermost electrons (numbers of valence electrons). The "valence electron" theory used for chemical substances cannot be used for metals, but this theory is the only one available to answer simple questions such as, "How many electrons are involved in bonding?"

4.5 Principal Quantum Numbers and Electronegativity

Principal quantum numbers correspond to the vertical arrangement of elements in the periodic table, which is in contrast with the above group numbers corresponding to their horizontal arrangement. Mooser and Pearson proposed the use of principal quantum numbers as a guideline to covalent bond quality. For example, they compared diamond (C, n=2) with lead (Pb, n=6) of the same MB group and found that with principal quantum numbers (n), covalent bond quality was lost as n increased. Furthermore, they used electronegativity as a guideline to show ionic bond quality. Finding many compounds having both ionic bond quality and covalent bond quality, they tried to adjust crystal structure using these two parameters.

Figure 10 shows the experiment results using Si compounds. With these compounds, areas of crystal structure can be roughly divided, but it was difficult with other compounds. Nishitani (Kyoto University) pointed out that these parameters pose a problem of not including how to arrange extranuclear electrons (i.e., an idea of valence electrons) and factors of atomic size, etc.

4.6 Electronegativity and Electron Vacancy Number

Electron vacancy number (N_v) is the number of electron vacancies for electron holes) above the Fermi level of d band of transition metals. Similarly, N_v = 10.66−(e/a) and the number of valence electrons can be used. Nontransitional metals such as Al and Si have often used 7.66 N_v and 6.66 N_v, respectively, in the past.

N_v is a parameter which has been used to predict the generation of embrittlement phases (sigma phase and mu phase, for example) in heat-resistant materials such as Ni alloys. Historically viewed, after the N_v (so-called PHACOMP) prediction method was developed, the words "alloy design" began to be used.

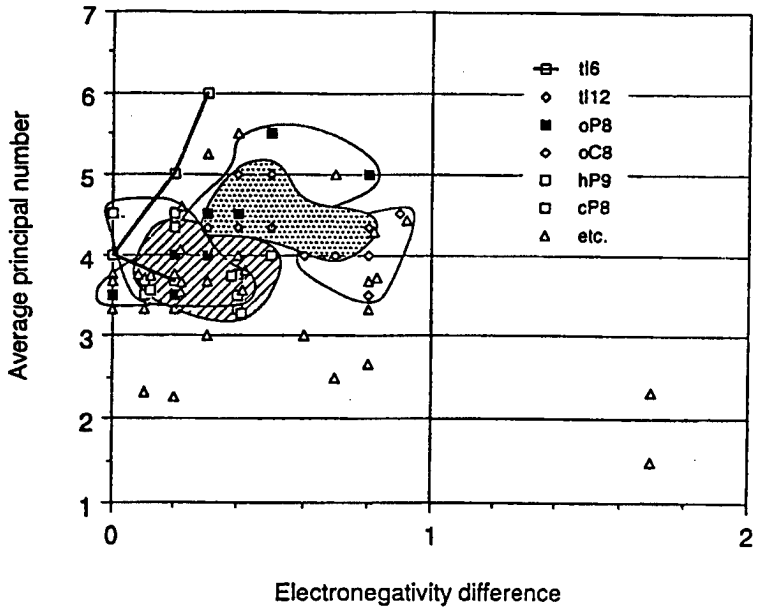

Figure 10. Adjustment of Si Compounds With Principal Quantum Numbers and Electronegativity (By Nishitani, Kyoto University)

In relation to (e/a), N_v may be read as a group number. According to Omori (Nippon Yakin Kogyo Co.), similar to adjustment results by the periodic table and group numbers, crystal structure can be divided to some extent by the number of electron cavities. However, virtually no interrelation with electronegativity can be observed.

4.7 Miedema Electronegativity and Electron Density of (Wignersaissel) Boundary

Based on his experience, Miedema presented heat of generation (ΔE) of compounds by

$$AE = -P(\Delta\phi^*)^2 + Q(\Delta n_{ws}^{1/3})^2$$

where $\Delta\phi^*$, Δn_{ws} represent the difference in electronegativity between component elements and offset of electron density in Wignersaissel boundary, respectively. P and Q constants should be determined based on experience. According to Miedema, the first term of the above expression represents energy gain of the electron system resulting from charge transition. The second term represents energy loss caused by changes in the state of electrons of component atoms from the prebond stable state to eliminate offset of electron density in the boundary between two atoms during bond. The values of ϕ^* and n_{ws} are determined experientially. Pettifor discusses the meaning of these parameters with respect to transitional metal alloys from the standpoint of the electron theory.

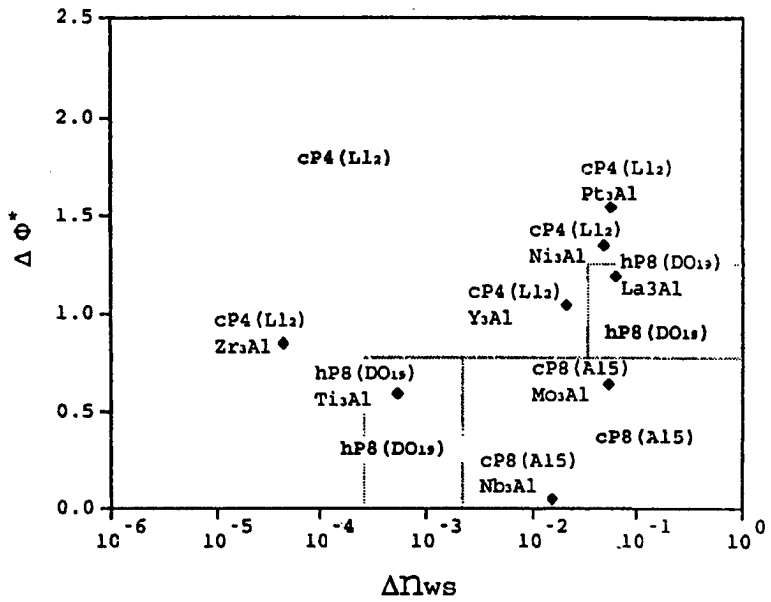

Figure 11. Adjustment of M_3Al Crystal Structure With Miedema's Parameters (By Itoh, Sumitomo Electric Industries)

The n_{ws} is interrelated with the size of the relevant atom; however, it is related not merely to the size, but to the bulk-modulus, implying the extent of the feasibility of adjusting the atomic size by alloying. In this sense, this adjustment method may be the classic correction method in section 4.3.

In fact, Chelikowsky applied these two parameters to problems of the solution limit of Mg alloys, proposing a new map called a Miedema-Chelikowsky map, indicating that the method enables better adjustment of the solution limit than the conventional classic one.

When such parameters were used for adjusting crystal structure of intermetallic compounds, its systematic adjustment was generally as difficult as it was in the past. With M_3Al compounds, however, as can be observed in Figure 11, areas can be divided relatively successfully when M is a transition metal. The similar adjustment is possible with MSi. It has also been found that, for unknown reasons, intermetallic compounds with low melting points tend to exist in groups where there are maps.

4.8 Pseudo-Potential Orbital Radius

Zunger determined a new parameter r_ι depending on angular momentum of electrons of each atom by calculating electron structure, which is an orbital radius when there is electron shielding and pseudo-potential $V_{eff}^{(\iota)}$ becomes 0.

The r_ι itself and r_ι^{-1} are interrelated with the atomic radius and electronegativity, respectively. Therefore, setting of $\{r_\iota^{-1}, r_\iota\}$ is responding to electronegativity and the classic parameter of an atomic radius. Assessing orbital radius r_s of s electron when $\iota = 0$ and orbital radius r_p of p electron when $\iota = 1$, Zunger set the following parameters for MX compounds:

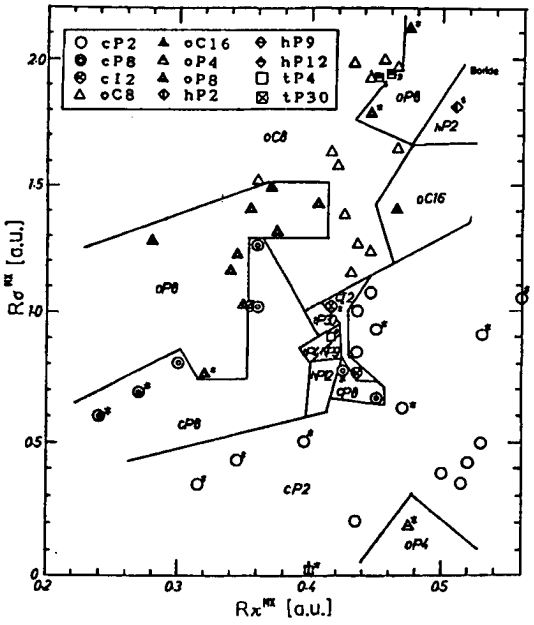

Figure 12. Adjustment of Crystal Structure of MX (X=Al, Si, Mg, B) Compounds With Pseudo-Potential Orbital Radii
* marks in the drawing represent compounds with compositional width.
(By Shimizu, Daido Steel Co.)

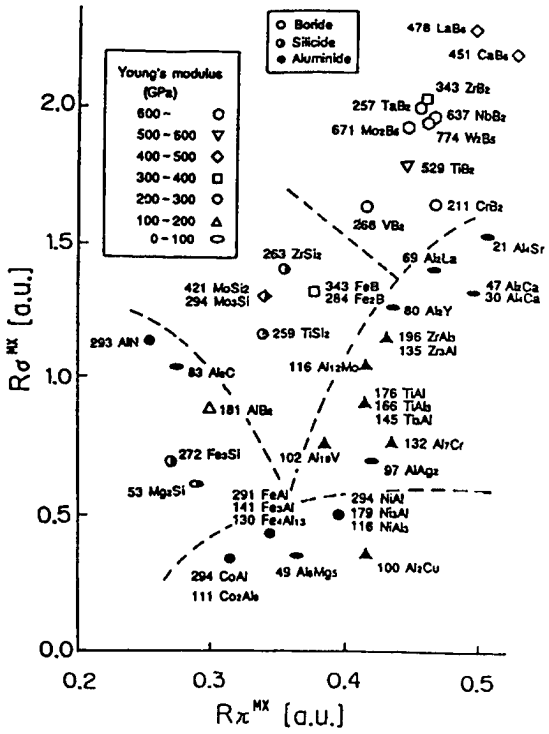

Figure 13. Results of Adjustment of Young's Moduli of Aluminide, Boride, and Siliside With Pseudo-Potential Orbital Radii
(By Tsuzuki, The Furukawa Electric Co.)

$$R\sigma^{MX} = \left| r_p^M + r_s^M \right) - \left(r_p^X + r_s^X \right) \left|$$

$$R\pi^{MX} = \left| \left(r_p^M - r_s^M \right) + \left(r_p^X - r_s^X \right) \right|$$

where $R\sigma^{MX}$ is a parameter indicating mismatching in size between M and X atoms. On the other hand, $R\pi^{MX}$ is a parameter indicating orbital delocalization of s and p electrons in their respective atomic positions.

Figure 12 presents a structure map of MX compounds (X-Al, Si, Mg, B) with $R\sigma^{MX}$ and $R\pi^{MX}$ on either axis. In the drawing, crystal structure is almost adjusted. What is interesting is that Al, Si, and Mg compounds have no compositional width when $R\sigma^{MX}$ is 1.05[a.u.] or above (where 1 a.u. = 0.053 nm). In other words, mismatching in size between M and X atoms, compositional width of compounds is lost. With the B system, however, contrary to the above, their compositional widths are lost when $R\sigma^{MX}$ exceeds 1.75[a.u.], the reason for

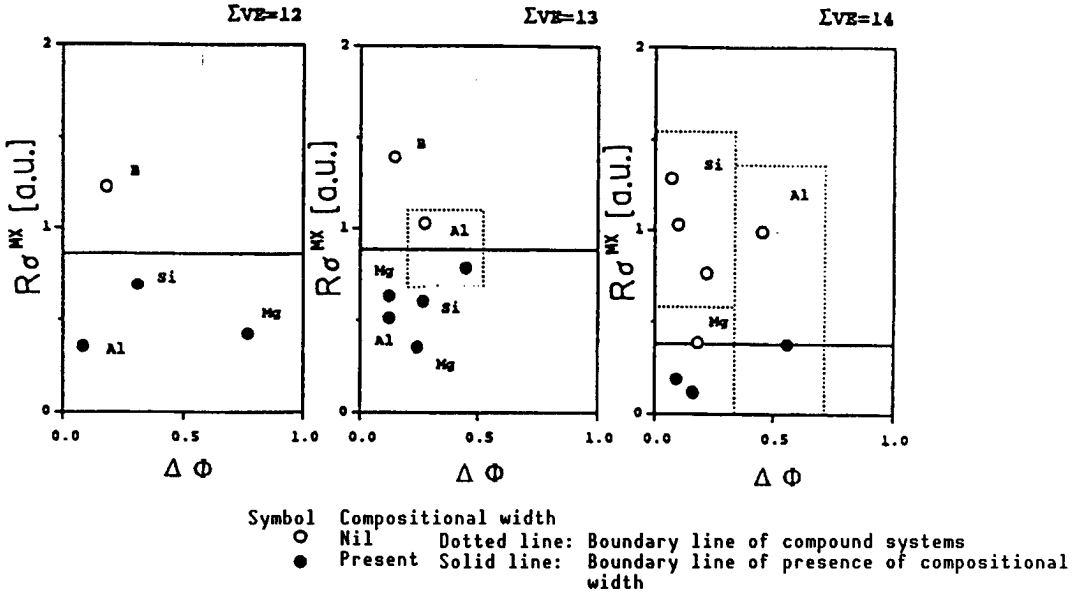

Figure 14. Adjustment Results of Presence of Compositional Width of MX System by Villars' Method (By Tetsui, Mitsubishi Heavy Industries)

which is unknown. MX_2 and MX_3 compounds were similarly handled with the result that their crystal structure could not be adjusted very successfully.

Figure 13 shows adjustment results of Young's moduli as an example of the relationship between structural maps and properties. In this drawing, compounds with different compositional ratios are also plotted. With respect to the same alloy system with several compounds, those with the greatest Young's modulus are selected to be classified according to symbols in the drawing.

With compounds comprising the same component elements, those with composition close to the isoatomic ratio show high Young's moduli. Young's modulus values are different with the Al, Si, and B systems and these three areas are roughly divided in the drawing. The Young's modulus of the B system rated highest among these compounds.

4.9 Pseudo-Potential Orbital Radius, Number of Valence Electrons, and Electronegativity (Villars' method)

Villars proposed to adjust crystal structure using three parameters of pseudo-potential orbital radius, the number of valence electrons, and electronegativity. The conventional adjustment method uses only two parameters, compared to three of this method.

With respect to crystal structure, when target compounds were limited as in this case, the number of data on each coordinate was so small that it could not be clearly evaluated whether or not this adjustment method was effective. Figure 14 shows adjustment results with respect to the presence of

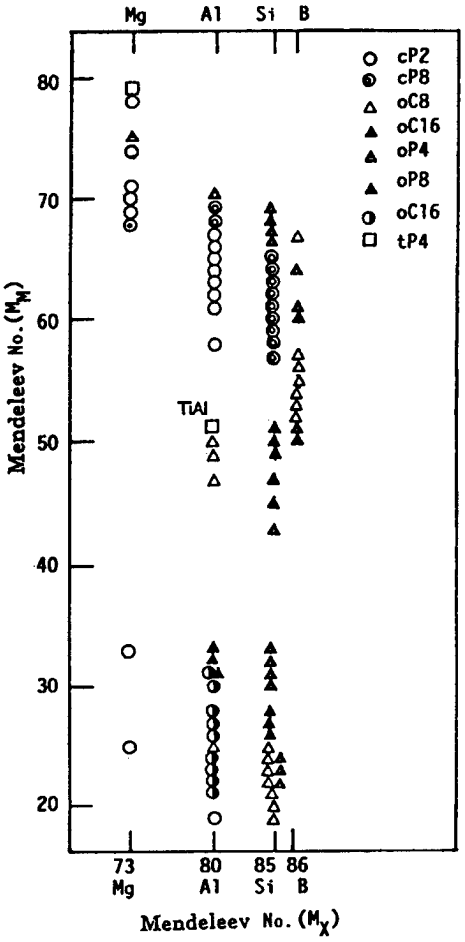

Figure 15. Adjustment With Mendeleev Numbers of Crystal Structure of MX (X = Al, Si, Mg, B) Compounds (By Matsuo, Nippon Steel Corp.)

compositional width in MX compounds (X = Al, Si, Mg, B) where $R\sigma^{MX}$ and $\Delta\phi$ represent the difference in pseudo-potential orbital radius and that of electronegativity among individual component elements, respectively. Also, ΣVE represents the sum of the numbers of valence electrons of component elements. With $\Sigma VE \geq 12$, compositional widths of compounds are lost when $R\sigma^{MX}$ exceeds a certain value, which is the same with the adjustment results of the above pseudo-potentials. With respect to the presence of compositional width, it is apparent that it does not depend entirely on the difference in electronegativity ($\Delta\phi$) taken on the horizontal axis.

4.10 Mendeleev Numbers

This is a very unique attempt to control the development of compounds and crystal structure by providing a number called Mendeleev number to elements instead of using the concept of the two-dimensional periodic table.

With MX compounds, for example, a structure map is generated with M_M and M_X, Mendeleev numbers of M and X, taken on either axis. This method proposed by Pettifor determines Mendeleev numbers on the basis of the chemical scale (X) of elements. Figure 15 shows a structure map of the MX system (X = Al, Si, Mg, B) compounds. A comparison of those with the same X finds that compounds with the same crystal structure are generally distributed in groups in this drawing. Therefore, the tendency of the generation of these compounds is likely to be decided from this map to some extent. When viewed as a whole with X changed, it is not very clear to what extent the crystal structure can be predicted from this structure map. Matsuo (Nippon Steel Corp.) pointed out based on this map that it is difficult to predict atomic substitution behavior of the third element and the way the crystal structure moves.

4.11 Evaluation of Structure Maps

Based on the results of the above investigation, Table 1 shows the evaluation of each method used for Al, Si, Mg, and B compounds.

No methods are available which enable exact predictions of crystal structure, the presence of compositional widths, melting points, and Young's moduli of intermetallic compounds, and structure maps must be used separately depending on different purposes. One of the reasons for the difficulty of this operation may be that the component elements of the majority of Al, Si, Mg, and B intermetallic compounds comprise nontransition and transition metals. With these compounds, their adjustment is rather difficult since their interatomic bond formats become complex, compared to those whose component elements comprise only nontransition or transition metals. However, the current adjustment has made clear the scope and effectiveness of the application of each structure map to these compounds.

The adjustment by the "periodic table" is effective for qualitative discussion of almost all properties, such as crystal structure, compositional width, melting point. Structure maps relatively effective in the adjustment of crystal structure and properties in addition to the periodic table were "pseudo-potential orbital radius" and "Mendeleev number." Crystal structure and the presence of compositional widths of the Al, Mg, and B systems are successfully adjusted using pseudo-potential orbital radii.

"Villars' method" involving pseudo-potential orbital radius as a parameter seems to be effective for adjusting compositional widths; however, with a small number of plots due to three-dimensional maps, it could not be decided whether they were really effective for adjusting properties. On the other hand, the adjustment by "Mendeleev number" provided maps easy to look at since atoms were adjusted in one-dimensional arrangement and was effective for adjusting crystal structure.

Also, with peaks of melting points and Young's moduli of individual systems at average group numbers of 4~5, group numbers of the periodic table may be effective for adjusting these properties. The number of valence electrons and the number of electron vacancies related to group numbers are likely to be used as parameters for these properties. However, when considered as structure

Table 1. Evaluation of Each Adjustment Method

	[1]	[2]	[3]	[4]	Remarks
Periodic table	o	Δ	Δ	—*	*Cannot be stated clearly due to data shortage; seems to be related to melting points
Classic parameter	x	—	—	—	
Group number in periodic table	o*	x	Δ	o	*Area division with M2X is difficult
Principal quantum number of electron cavities	x	x	x	x	
Electronegativity and number of electron cavities	Δ	x	Δ	—	*Regarding average number of electron cavities, both crystal structure and melting points enable area division although unclear. Regarding electronegativity, seems to be no interrelation in either case
Miedema's electronegativity, electron density (Wignersaissel) number	—	—	—	x*	*Tendency of compounds of same system gathering in group
Pseudo-potential orbital radius	Δ	Δ	—	Δ	
Villars' method	Δ*1	o*2	Δ*3	—	*1Villars' original paper claims that adjustment is possible *2Remarkable when sum numbers of valence electrons is 12 or more with 1:1 compounds *3Adjustment by separating every 500°C
Mendeleev number	o	Δ	Δ	—	

Note: Young's moduli were adjusted with aluminide, boride, siliside, and nitride.

[1] Crystal structure
[2] Compositional width
[3] Melting point
[4] Young's modulus

maps, no effectiveness of "principal quantum number and electronegativity" and "electronegativity and the number of electron cavities" can be observed.

With "Miedema electronegativity and electron density of (Wignersaissel) boundary," it is interesting to find compounds with low melting points in group in areas of certain electronegativity. With respect to the intermetallic compounds used in this experiment, it has been made clear that electronegativity has not affected their crystal structure and properties.

5. Conclusion

This is a general view of the current state of crystal structure predictions by band calculation and various structure maps by the phenomenalistic parameters with intermetallic compounds of Al, Si, Mg, and B systems. Strictly speaking, with the latter, each method is insufficient as a prediction method of crystal structure and properties, and studies on new parameters and adjusting methods are expected in the future. This paper is based on the survey report of the systematization working group, intermetallic compound session, Metallic Materials Research and Development Center.

Ni-Al Intermetallic Compounds

916C1004B Tokyo KINZOKU GAKKAI SEMINA KINZOKUKAN KAGOBUTSU in Japanese
1 Jun 90 pp 13-20

[Article by Asao Suzuki, School of Engineering, and Hideki Hosoda, Graduate School, both of Tokyo Institute of Technology: "Physical and Mechanical Properties; Grain Size Dependency of Mechanical Properties; Creep Resistance; Diffusion Speed; Oxidation Resistance; Effect of Third Element Addition; Reinforcement by Second Phase and Composition Structure and Improved Toughness"]

[Text] 1. **Introduction**

Of Ni-Al based intermetallic compounds, those likely to be used as high temperature structural materials are Ni_3Al based on fcc structure and NiAl based on bcc structure. The melting point of the former is 1,390°C and that of the latter 1,640°C. NiAl is superior in terms of heat resistance, while Ni_3Al is superior in terms of cold ductility and it also brings improved rigidity by adding a trace quantity of B. On the other hand, NiAl which contains a sufficient quantity of Al to form a continuous oxidized layer on the surface is much more advantageous than Ni_3Al in terms of oxidation resistance. While Ni_3Al is already used for a composition layer of Ni heat-resistant alloys as γ', NiAl can possibly be used as a heat-resistant structural material in the future. This article compares the two from various angles to clarify their characteristics.

2. Stable Composition Area and Physical Property

2.1 Ni-Al Binary System Structural Diagram

Figure 1 is an Ni-Al system constitutional diagram. Both β(NiAl0 and γ'(Ni_3Al) are Berthollide type intermetallic compounds with composition areas centering on stoichiometric composition. As seen from the constitutional diagram, NiAl is congruent with the highest melting point in the stoichiometric composition, while Ni_3Al is a compound generated by peritectic reactions. Binary compositional Ni_3Al single crystals can be produced only on the Ni-excess side not on the Al-excess side. For this, the peritectic reaction existing on the binary system must be shifted in a ternary constitutional diagram by adding a

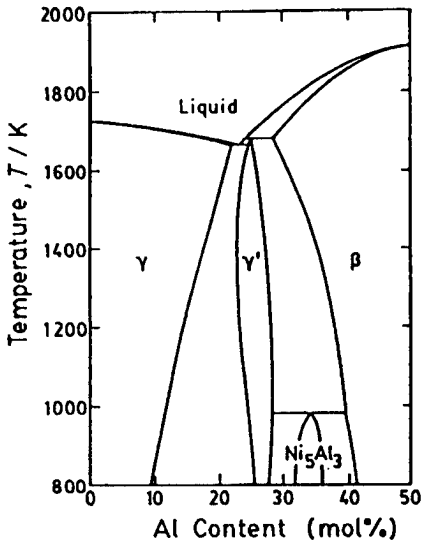

Figure 1. Binary System Structural Diagram of Ni-Excess Side
The phases existing here in addition to a liquid phase are γ(Ni), γ'(Ni_3Al), β(NiAl), and Ni_5Al_3.

third element. On the Al-excess side, a single crystal cannot be produced until a ternary composition like Ni_3(Al, X), with a third element substituted, is obtained. With NiAl, on the other hand, single crystals can be produced with relative ease. However, much more data is available on Ni_3Al than NiAl; the same applies to data on polycrystals. The difference in the number of papers on the two is tens to hundreds of times. The major reasons for this are that researchers concentrated on the particularly strong positive temperature dependency of Ni_3Al, Ni_3Al was a major structure compositional factor of Ni heat-resistant alloys, and there was the need for such data. It is expected that there will be many studies on NiAl in the future.

In the intermediate composition area between γ'(Ni_3Al) and β(NiAl), intermetallic compound Ni_5Al_3 based on fcc structure exists as a low temperature phase. Quenching from the two-phase area of γ' and β yields a metastable phase with $L1_0$ crystal structure formed by martensite transformation. Liquid ultra-quenching from the Al excess side of Ni_3Al also provides this metastable phase.

2.2 Physical Properties

With a large ratio of Al, a light element, NiAl based on bcc which does not have the closest packed structure has a specific gravity of 5.86 (g/cc). This figure is far under 3.91 of TiAl, but was smaller than expected, compared to 7.50 of Ni_3Al. This seems to be one of the reasons for the increasing interest in NiAl. Table 1 compares Young's moduli, etc., among Ni_3Al, NiAl, and TiAl.

Table 1. Crystal Constructions, Young's Moduli, Melting Points, and Densities of Ni_3Al, NiAl, and TiAl

		E (GPa)	T_m (K)	Density (g/cm^3)
TiAl	$L1_0$	25.5	1773	3.91
NiAl	B2	42.7	1913	5.86
Ni_3Al	$L1_2$	25.9	1663	7.50

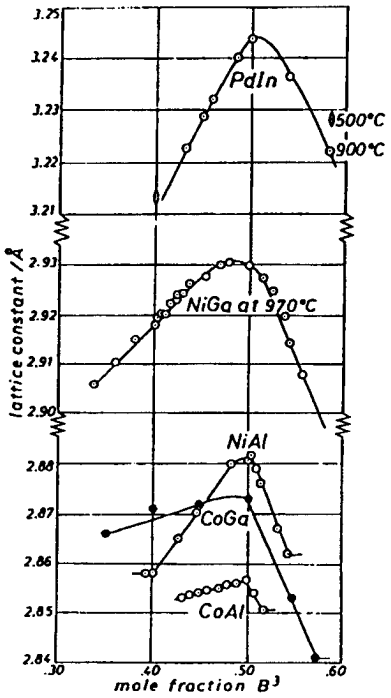

Figure 2. Changes in Lattice Constants of Various B2 Type Intermetallic Compound Phases

3. Mechanical Properties at Ordinary Temperature

3.1 Influence of Displacement From Stoichiometric Composition

From a Berthollide type intermetallic compound with compositional width to exist stably when displaced from stoichiometric composition, some structural defect must be introduced into its crystal structure. Let us consider a cavity type structural defect and a substitutional type structural defect. The former is a structural defect in which excessive atomic species persistently exist in their intrinsic lattice positions, while other species are insufficient in number to fill all the other lattice positions, so some cavities are left as they are. The latter is a structural defect in which excessive atomic species are substituted for lattice positions of short atomic species with no structural cavities existing.

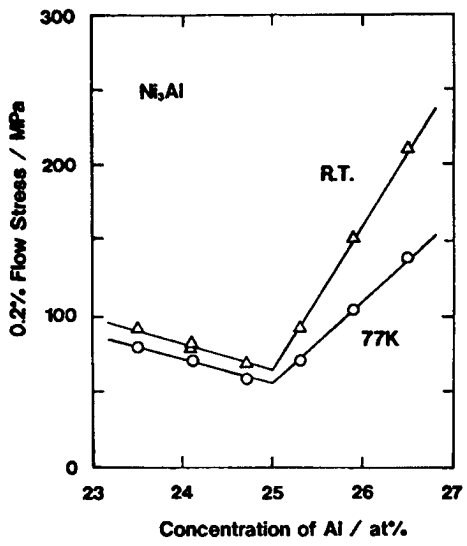

Figure 3(a). Influence of Dislocation From Stoichiometric Composition Affecting Strength of Ni_3Al at Ordinary Temperature and 77 K

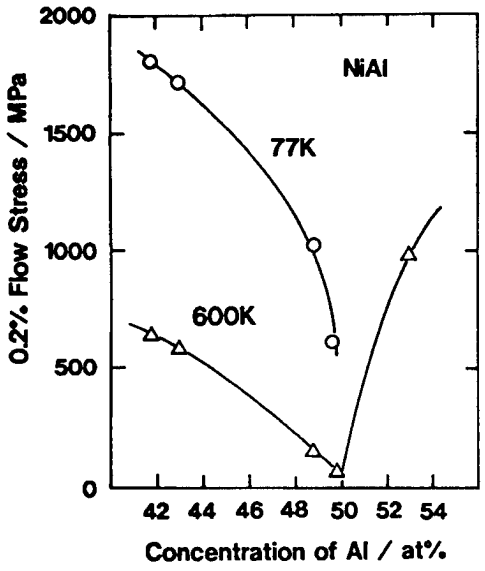

Figure 3(b). Influence of Dislocation From Stoichiometric Composition Affecting Strength of Ni_3Al at 77 K and 600 K

With Ni_3Al, substitutional type structural defects are introduced into both sides of excess Ni and excess Al, while with NiAl, they are introduced into the side of excess Ni. The cavity-type structural defects are made to occur on the side of excess Al of NiAl. NiAl is a kind of electronic compound. It is believed that structural cavities are produced in response to the need to keep constant an electron-to-atom ratio in a unit cell. Here, Al is trivalent, but the number of electrons in cavities is naturally 0 and that of Ni is also 0. Cavity type structural defects can be observed on the excess side of 3B subgroup elements of CoAl, CoGa, NiGa, and PdIn with B2 type crystal structure the same as NiAl. Here, a change in lattice constant has, as shown in Figure 2, a (chnnik) or a peak in 1:1 composition. This proves that the excess side of B subgroup elements of these compounds has cavity type structural defects.

These structural defects affect not only physical but mechanical properties. The great influence of cavity type structural defects is shown in Figure 3 which indicates the influence of strength on the dislocation of stoichiometric composition of the two compounds. In either case, reinforcement on the Al excess side is remarkable. With NiAl, the reinforcement is attributable to the introduction of cavity type structural defects. The remarkable reinforcement on the Al-excess side of Ni_3Al, compared to the Ni-excess side, seems to be related to the closest position of Al. However, there have been no theoretical studies on the reinforcement of structural defects to date. With respect to Ni_3Al, an increase in the intensity due to compositional displacement is more remarkable at room temperature on the Al excess side than an intensity of 77 K. This is because positive temperature dependency of intensity becomes remarkable as the amount of Al increases.

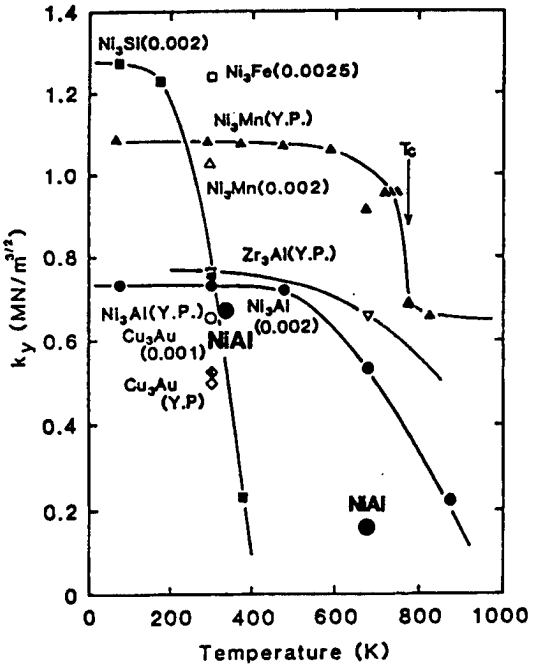

Figure 4. Comparison of Hall-Petch Parameter ky at Ordinary Temperature Among Various $L1_2$ Type Intermetallic Compounds
Among those for which data is available, ky is indicated as temperature dependent. Data on NiAl at ordinary temperature and 400° is added.

Compositional displacement from stoichiometric composition has a major influence on ductility and toughness. For example, wth Ni_3Al and Ni_3Ga, the improvement of ductility by adding B is effective on the Ni-excess side, but no effect can be observed on the Al-excess side. Also, with NiAl, such an effect of B has not been observed. Of compounds with the same $L1_2$ structure as Ni_3Al, those with ductility are Co_3Ti, Cu_3Au, Cu_3Pt, Ni_3Fe, and Ni_3Mn; of compounds with the same B2 structure as NiAl, those with ductility are NiTi, FeCo-V, and CuZn. On the other hand, many brittle compounds contain B subgroup elements. From these facts, it seems that excellent ductility can be found in compounds with strong metallic bond factors, i.e., compounds of transition metals, compounds with regular-irregular deformation points and compounds without cavity type structural defects. This seems to be related to the fact that ductility of Ni_3Al and Ni_3Ga can be improved by adding B on the Ni-excess side. This will be a suggestion for improving the ductility of NiAl. For example, it is believed that adding a transition metal element as a substitute for Al will be effective.

What kind of a structural defect appears by compositional displacement depends on the types of crystal structure and kinds of composition elements to be combined. Studies by the authors based on cavity formation energy and interatom bond energy are currently under way. As a result, it has been found that cavity type structural defects do not appear easily in compounds with closest packed structure and Kurnakov compounds with regular-irregular deformation points. Predictions with considerable accuracy are becoming possible.

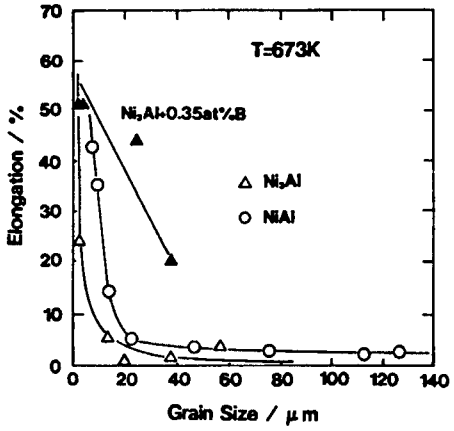

Figure 5. Crystal Grain Size Dependency of Elongation of Ni_3Al and NiAl in a Tensile Test
Effects of the improvement in ductility can be observed with Ni_3Al added with B.

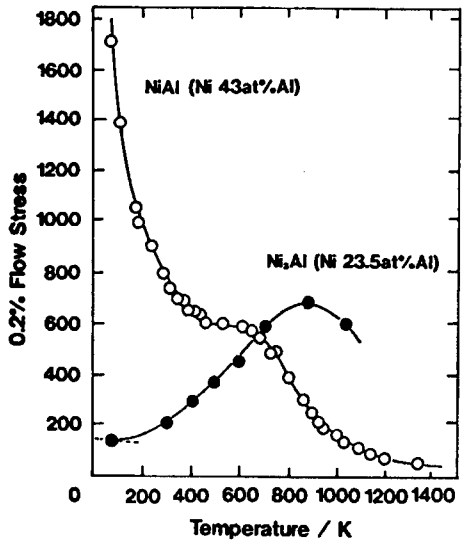

Figure 6. Temperature Dependency of Strength of Ni_3Al and NiAl
Ni_3Al has a positive temperature dependent strength and NiAl has a rapid increase in strength at low temperature.

3.2 Crystal Grain Size Dependency of Mechanical Properties

Figure 4 shows ky, Hall-Petch coefficients of various compounds. While by value of pure metals and solid solution alloys range from 0.05~0.2 MPa/m^2, those of intermetallic compounds range from 0.5~1.3 MPa/m^2, one digit greater. With intermetallic compounds, crystal grain size dependent strength is extremely great. In this drawing, both Ni_3Al and NiAl have values of almost the same level. As a general trend, temperature dependency of ky decreases as temperature increases. While there are various reasons for this, with respect to Ni_3Al, it is because of the slippage in the grain boundary.

Figure 5 shows crystal grain size dependency of the elongation in a tensile test at 673 K. With fine crystal grains, no major difference in points where the elongation rapidly increases can be observed between the two intermetallic compounds. It is found from the drawing that with Ni_3Al, toughness is remarkably improved by adding B. With intermetallic compounds, the crystal grain size to enable ultraplasticity to appear is—as is the same with ceramics—at a submicron level, one digit smaller than those of metals and alloys.

4. Grain Size Dependency of Mechanical Properties

As shown in Figure 6, while positive temperature dependent strength exists in Ni_3Al, the intensity decreases as temperature rises in NiAl, but a plateau can be observed in the middle temperature range. Also, a phenomenon unique to bcc metals, i.e., a phenomenon in which the intensity rapidly increases as

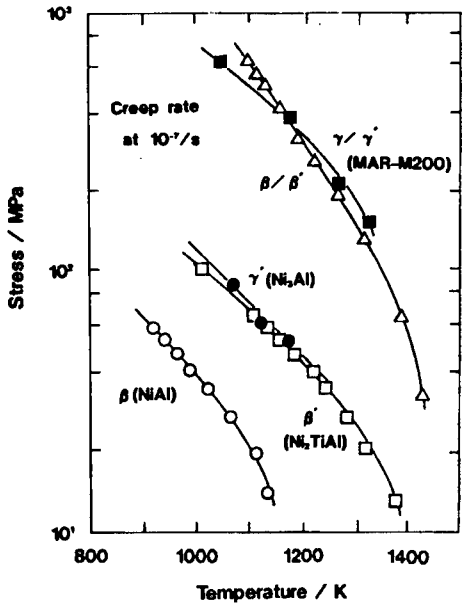

Figure 7. Relationship Between Stress and Temperature Which Shows Constant Creep Velocities of Various Single Phase Intermetallic Compounds and Their Composite Structure Alloys
Data on $\gamma'(Ni_3Al)$ is added.

temperature decreases at ordinary temperature or below, can also be observed in NiAl with regular bcc structure. No data for comparing intensity in the high temperature area is available. It is believed that NiAl with a higher melting point is superior in intensity to Ni_3Al, but Ni_3Al seems to be superior in creep resistance.

It can be observed with any compound that ductility increases as temperature rises; there is no data available for comparing the two. With Ni_3Al, <111> slippage system to a maximum strength, <001> slippage system in crystal orientation with the stress axis away from (001) at this temperature or above, and <111> slippage system in the stress axis close to (001) function. With NiAl, <001> slippage system functions in (011) orientation at every temperature and <111> slippage system in (001) orientation, causing multiple kinks.

5. Creep Resistance

Figure 7 compares creep resistance $\gamma'(Ni_3Al)$ and $\beta(NiAl)$. The drawing also shows creep resistance of $\beta'(Ni_2TiAl)$ with Heuslar type crystal structure ($L2_1$) induced from B2 structure. It is found that $\gamma'(Ni_3Al)$ is superior in creep strength to $\beta(NiAl)$. It can be said that a characteristic of $\gamma'(Ni_3Al)$ is that it enables solid solution of various elements. Solid solution of a third element causes creep strength to greatly increase. While little data is available on high temperature strength and creep resistance with respect to $\beta(NiAl)$, the addition of a third element will be an effective means of improving them. Figure 7 shows that the addition of Ti as a third element caused the crystal structure to change into Heuslar type regular configuration but that creep resistance of $\beta'(Ni_2TiAl)$ increased as much as $\gamma'(Ni_3Al)$.

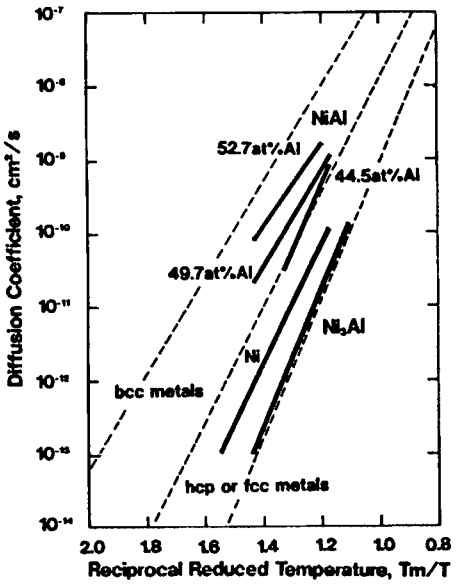

Figure 8. Temperature Dependency of NiAl's Diffusion Coefficient Is Contained in the bcc Metal Band

Data on Ni_3Al and Ni is added, which is contained in the fcc metal band.

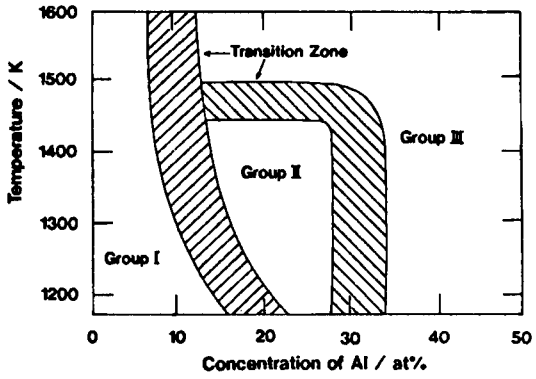

Figure 9. Division of Oxidation Behavior of Ni-Al Alloys

The greater the Al content, the better the oxidation resistance.

6. Diffusion Speed

With regular lattice alloys (Kurnakov compounds), diffusion speeds can be compared between the regular state and the irregular state with respect to the same composition. In diffusion in a regular lattice comprising several sub-lattices, only positional exchange of the closest atoms results in disturbed configuration and diffusion speed generally becomes lower than in the irregular state.

Figure 8 compares diffusion speed between Ni_3Al and NiAl. In this drawing, temperature is indicated with T_m/T normalized at their melting points. It is found that diffusion speed in fcc and hcp metals with closest packed structure is different from that in bcc metals with a coarser structure. The closer the packing, the lower the diffusion speed. Ni_3Al based on fcc, together with Ni, is in the fcc metal band. NiAl is in the bcc metal band, but diffusion speed is lower on the Ni-excess side than on the Al-excess side, which is because the existence of cavity type structural defects on the Al excess side has facilitated the diffusion. It was concluded that substitutable type structural defects exist in Ni_3Al since no such difference is observed on either side of stoichiometric composition.

In this drawing, although no comparison can be made for the same temperature, diffusion speed at 1,400 K is 4.9×10^{-11} with NiAl and 1.6×10^{-11} with Ni_3Al, and at 1,500 K, 1.3×10^{-10} with NiAl and 7.0×10^{-11} with Ni_3Al. In any event. Ni_3Al is slower in diffusion than NiAl, which corresponds to creep resistance. NiAl will be advantageous in terms of specific strength.

7. Oxidation Resistance

The greater the Al concentration, the better the oxidation resistance, because large Al concentrations facilitate the formation of continuous, close oxide covering. Figure 9 shows a binary constitutional diagram of Ni–Al with oxidation resistance divided into three areas. A comparison of two compounds, Ni_3Al and NiAl, finds that the one with higher Al content is naturally more advantageous. Few studies have been done with respect to either Ni_3Al or NiAl which examine the effect of adding a third element in terms of the improvement in oxidation resistance. Substitution of Cr and Si in these compounds seems to be effective in improving their oxidation resistance.

8. Effect of Adding a Third Element

An additional element greatly affects various characteristics of components depending upon whether a third element is substitutable for Ni site, Al site, or both sites. Substitution behavior can be predicted to some extent by simple approximation.

Figure 10 shows: the substitution site of an additional element in Ni_3Al can be divided into the upper and the lower side of the slant line; an experiment confirming that elements shown in a circle, a triangle, and a square are those of Al site substitution, both site substitution, and Ni site substitution, respectively; and the confirmation of every B subgroup element positioned in the upper part of the slant line and substitutable for Al.

Detailed substitution behavior with NiAl has not yet been examined. However, it is predicted that the position of the slant line to divide substitution sites in Figure 10 will be dislocated slightly upwards. In other words, the number of types of transition metal elements substitutable for Ni site will increase. However, the state in which B subgroup elements are substituted for Al site remains unchanged. It should be pointed out that substitution behavior is very likely to undergo changes when composition is displaced from stoichiometric composition or a fourth element is added.

It is well known that solid solution of an additional element reinforces solid solution of metals, while intermetallic compounds also increase their strength by solid solution of a third element. Figure 11 shows the reinforcement quantity of solid solution of various additional elements in Ni_3Al. The horizontal line shows the lattice constant rate of change when a solute element per unit volume is added and its reinforcement quantity is shown on the vertical line. Figure 12 shows the state of reinforced solid solution when Ni of NiAl is substituted by Fe or Co and when Fe and Co of FeAl and Fe are substituted by Co and Ni. That NiAl, FeAl, and CoAl are compounds which mutually undergo full percentage solid solution is shown later in a ternary constitutional diagram of Ni–Al–Fe. No systematic examination of substitution behavior and reinforced solid solution of NiAl has so far been done.

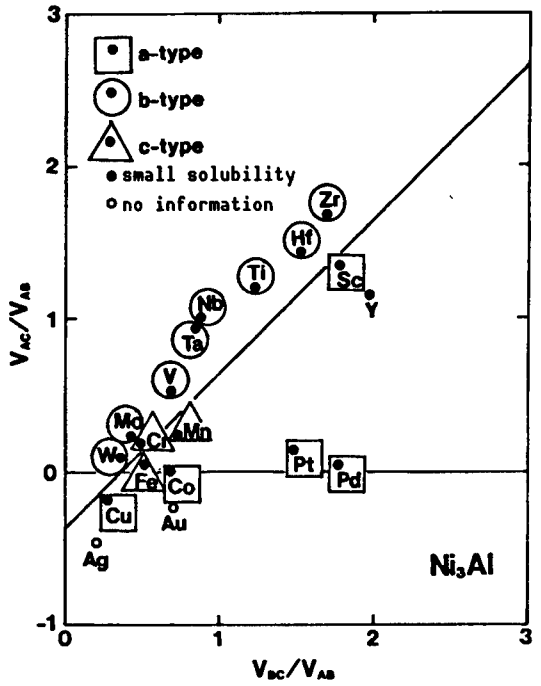

Figure 10. Substitution Behavior of Ni_3Al Third Element

An experiment has confirmed that the elements whose symbols are in circles, triangles, and squares involve Al-site, both site, and Ni-site substitution. The slant line divides substitution sites. Every B subgroup element involves Al site substitution.

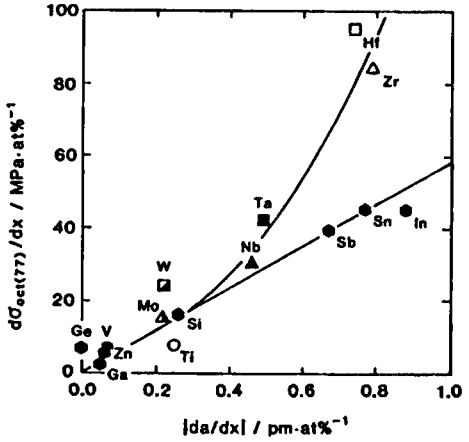

Figure 11. Reinforced Solid Solution by Substituting Third Element in Ni_3Al

The vertical line shows increments of stress at 77 K during 1 at% addition, and the horizontal line the variation of lattice constants. Every element in the drawing involves Al site substitution.

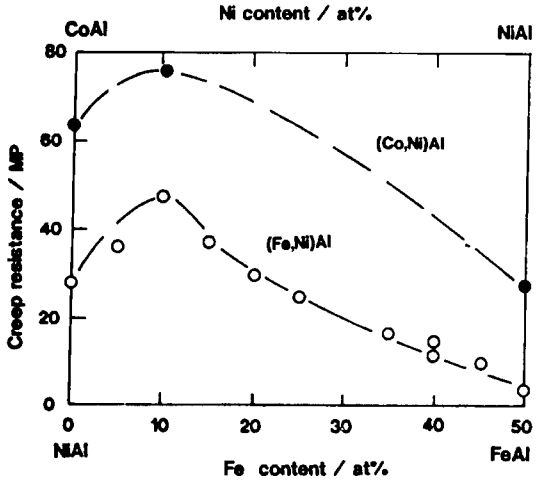

Figure 12. Compositional Dependency of Creep Resistance With β Solid Solutions of NiAl-CoAl and NiAl-FeAl

Reinforced solid solutions can be observed in intermediate composition.

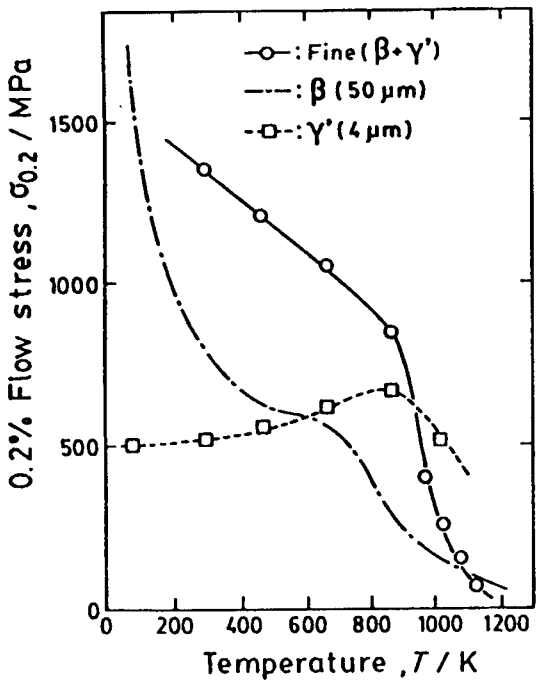

Figure 13. Temperature Dependency of Strength of Alloys With Microcomposite Structure (β(NiAl) + γ'(Ni_3Al))

Temperature dependency of strengths of the above alloys was compared with that of single phase compounds of microcrystal grains. This composite structure could be obtained by heat treatment utilizing martensite transformation.

9. Reinforcement and Improved Toughness by Composite Structure With Second Phase

There is a difference in the degree of freedom between intermetallic compounds and solid solution alloys when the state of structure coexisting with the second phase is obtained. Adjacent phases exist on either side of an intermetallic compound, so there are two choices to be made from the combination of dual phase structure. With γ'(Ni_3Al), both the state of two phases with γ(Ni) and β(NiAl) are possible.

Generally speaking, to produce a dual phase structure alloy is effective in increasing strength without losing toughness. There are also dual phase steel and dual phase stainless steel to allow two phases to share strength and toughness. In addition to the above, there is a γ'deposition reinforced type nickel heat-resistant alloy and various ultraplastic alloys with a second phase to prevent crystal grains from becoming bulky.

Composite structure should be considered a means to improve both strength and toughness for intermetallic compound. Figure 13 shows temperature dependency of strength of γ'(Ni_3Al) and that of β(NiAl) in the single phase state and alloys of these compounds in the microcomposite structure state. These

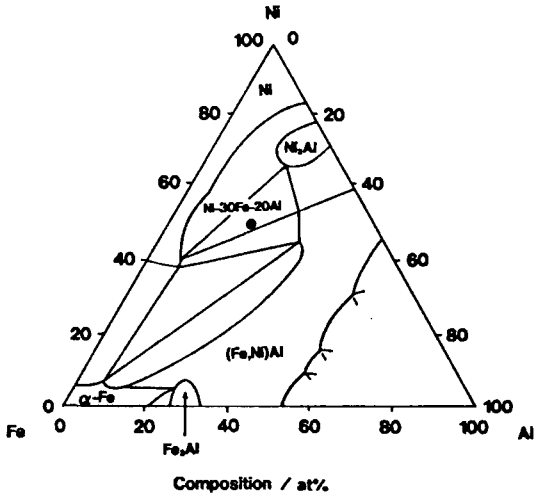

Figure 14. Ni–Al–Fe Ternary Constitutional Diagram and Composition of the Alloy Shown in Figure 15.
This alloy (Ni, 50; Al, 20; Fe, 30 at%) is in the three-phase coexisting state in equilibrium.

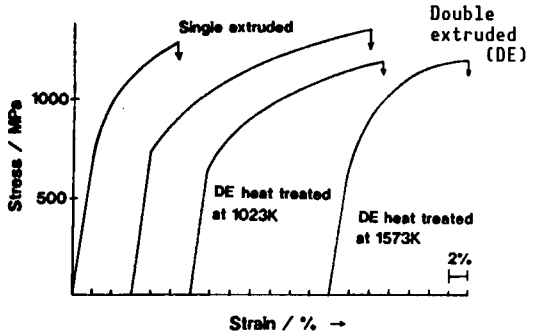

Figure 15. Stress–Strain Diagram at Ordinary Temperature of the Alloy (With the Composition Shown in Figure 14) With Microcomposite Structure ($\beta + \gamma'$)
The compositional state could be obtained by extrusion and heat treatment.

composite structure alloys have their structure refined utilizing the above martensite transformation. Figure 7 shows not only creep strength of single phase compounds as temperature functions but those of dual phase alloys. The drawing shows that the use of intermetallic compounds as composite structure is more advantageous than as a single phase in terms of heat-resistant strength. Alloys with compositional points (Ni, 50; Al, 20; Fe, 30 at%) shown in the Ni–Al–Fe ternary constitutional diagram in Figure 14 are of the three-phase coexisting state in equilibrium. The authors state that these alloys with fine crystal grains produced by extrusion are of dual phase structure of $\gamma'(Ni_3Al)$ and $\beta(NiAl)$. Figure 15 shows stress–strain curves of these alloys, showing that fine dual phase structure enables ductility to improve remarkably. It shows that dual phase structure, which is also a microstructure, is advantageous in terms of improved cold ductility.

There are various methods of obtaining the composite structure state which largely depend on alloy manufacturing processes. There are many feasible methods, such as conventional methods of dissolution, casting, plastic working, and heat treatment, powder metallurgy methods including mechanical alloying, extrusion, liquid phase sintering, and hot isostatic pressing (HIP), a method by heat flow control such as unidirectional growth and a method of achieving the formation of microstructure by liquid extra quenching.

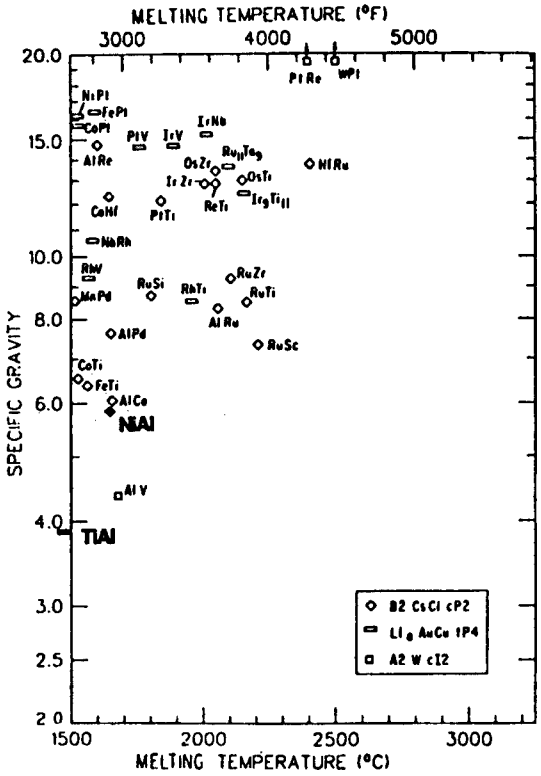

Figure 16. Fleischer's Map Showing the Relationship Between Specific Weights and Melting Points of Intermetallic Compounds With a Compositional Ratio of 1:1

Lower right is a blank area where there are no compounds, and the compounds close to the line between the blank area and the area where compounds exist are likely to be possible high-temperature materials with high specific strength. NiAl and TiAl, in particular, are indicated in bold.

10. Conclusion

A comparison from various standpoints was done between Ni_3Al—on which much data has been accumulated—and NiAl—on which more data will be collected in the future. Figure 16 shows the Fleischer relationship between specific weights and melting points of compounds. It seems that NiAl is not much inferior compared to TiAl, in attracting attention in terms of specific strength. Ni-Al intermetallic compounds feature stable processes of dissolution, etc., compared to Ti-Al intermetallic compounds; this is because of the difference between compositional elements of Ni and Ti. More active Ti will lead to various obstacles. For example, the processes of producing single crystals by the Bridgeman method and unidirectional growth involving long-time exposure to high temperature will be conducted without difficulty with respect to the Ni-Al system and contamination from crucibles during dissolution will be slight.

Every intermetallic compound mentioned in this article has both advantages and disadvantages and it is necessary to devise ways to manufacture and use them utilizing their special characteristics.

Ti-Al Intermetallic Compounds

916C1004C Tokyo KINZOKU GAKKAI SEMINA KINZOKUKAN KAGOBUTSU in Japanese
1 Jun 90 pp 21-27

[Article by Masaharu Yamaguchi, School of Engineering, Kyoto University:
"Types of Compounds and Current State of Research; TiAl; Al_3Ti"]

[Text] **1. Types of Compounds and Current State of Research**

According to the Ti-Al binary constitutional diagram in "Binary Alloy Phase Diagrams" published by ASM in 1986, five types of intermetallic compounds of Ti_3Al, TiAl, δ phase, Al_2Ti, and Al_3Ti exist in this binary system. There have been reports that compounds with Ti_2Al_5 and Ti_7Al_{11} compositions have been found in addition to the above, but compounds attracting attention as heat-resistant structural materials are Ti_3Al, TiAl, and Al_3Ti, particularly the first two with a wide compositional area. Assessing crystal structure finds that compounds with a composition close to Ti have regular structure based on hcp structure, while those with a composition of Ti/Al ratio of 1 or close to Al have regular structure based on fcc structure, whether stable or metastable. Therefore, all intermetallic compounds existing in the Ti-Al system are intermetallic superlattice compounds with regular structure based on close-packed structure, all of which are expected to show characteristics far closer to those of metals than ceramics, as far as their deformation is concerned.

Ti_3Al, TiAl, and Al_3Ti are attracting attention as stated above and a study on the practical use of Ti_3Al has already made considerable progress. Because its characteristics are similar to those of Ti alloys, it will not be likely to expect heat resistance to far exceed that of Ti alloys of this compound. Concentrated research on TiAl has been conducted in recent years with the expectation of a full-fledged lightweight heat-resistant material. However, its ductility and toughness being slightly deficient for reaching practical level is hampering its practical use, which would otherwise be possible. Compared to Ti_3Al and TiAl, Al_3Ti is far from a practical level because of its poor ductility and toughness, even compared to TiAl. Recently, it has been demonstrated that substituting Cr, Mn, V, and Ag for Al in Al_3Ti enables the crystal structure of Al_3Ti to be modified from tetragonal DO_{22} type to cubic Ll_2 type and deformability to improve substantially. Because Al_3Ti is superior in oxidation resistance compared to TiAl, much is expected from future

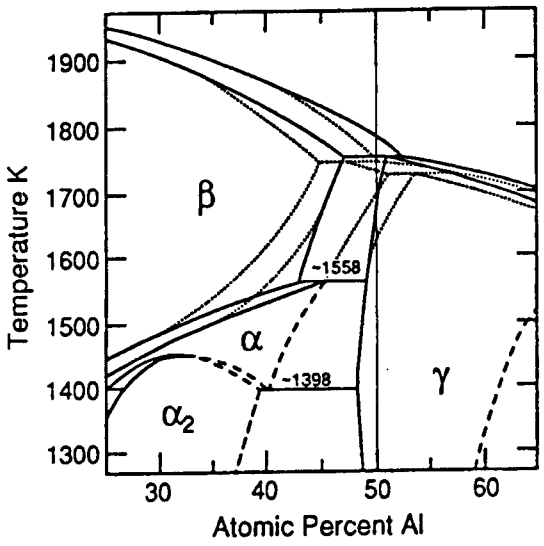

Figure 1. Part of Binary Constitutional Diagram of Ti–Al System
The solid lines and dotted lines are diverted from references (1) and (9) [not reproduced].

research in this area. In this context, this article selects TiAl and Al_3Ti, the two compounds particularly attracting attention at present, and considers basic problems involving their deformation and a method of improving their deformation, based on the latest knowledge.

2. TiAl

2.1 Solidification Process and Constitutional Diagram

Figure 1 shows part of the periphery of TiAl composition in the Ti–Al binary constitutional diagram. The solid lines are those diverted from the collection of constitutional diagrams and the dotted lines those from the constitutional diagram presented before. Recent experiments have made clear that a peritectic involving a liquid phase, β phase (bcc Ti solid solution phase), and γ phase (TiAl phase) in recent constitutional diagrams (solid lines) should be considered by dividing them into two peritectics, one involving a liquid phase, β phase, and α phase and the other involving a liquid phase, α phase, and γ phase, and the previous constitutional diagrams (dotted lines) are being reused at least in the periphery of TiAl composition. In the overall experimental results, the solidification process and solid solution deformation of the primary crystal in the composition area where β phase crystallizes can be expressed as follows: With 46–49 at%Al, they can be expressed as

$$L \rightarrow [\beta] + L \rightarrow [\beta+\alpha] + L \rightarrow [\beta+\alpha] + \gamma_s \rightarrow [\alpha] + \gamma_s \rightarrow [\alpha_2] + \gamma_s \rightarrow [\alpha_2+\gamma] + \gamma_s \quad (1)$$

and, with ≤45 at%Al close to Ti, they can be expressed as

$$L \rightarrow [\beta] + L \rightarrow [\beta+\alpha] \rightarrow [\alpha] \rightarrow [\alpha_2] \rightarrow [\alpha_2+\gamma] \quad (2)$$

With composition areas of 49~55 at%Al where α phase is crystallized as a primary crystal, on the other hand, they can be expressed as

$$L \rightarrow [\alpha] + L \rightarrow [\alpha] + \gamma_s \rightarrow [\alpha+\gamma_c] + \gamma_s \rightarrow [\alpha_2+\gamma_c] + \gamma_s \rightarrow [(\alpha_2+\gamma)+\gamma_c] + \gamma_s \quad (3)$$

where α, α_2, γ_s, and γ_c are a solid solution with composition close to that of Ti_3Al composition, a phase in which α is regularized (Ti_3Al phase), interdendritic γ-segregate and cell-shaped γ phase to appear in the boundary between primary crystal α and γ_s accompanying cooling, respectively. However, the constitutional diagram by dotted lines remains unclear, and it is conceivable that the presence of a third element or impure elements may cause the constitutional diagram to dislocate horizontally, so it should be noted that responses in the above mentioned composition areas and solidification process are not definite. It is almost certain that in the periphery of stoichiometric composition the majority of γ phases are generated by phase transformation from α_2 phase, which is extremely important in understanding typical lamellar structure (Figure 2) found in compounds with stoichiometric composition or more Ti-rich composition.

2.2 Lamellar Structure and Ordered Domain

It is known that a great number of stacking faults are involved in hcp ⇌ fcc transformation of Co to form lamellar structure. It is believed that with α_2-γ phase transformation, since α_2 and γ phases have hcp- and fcc-based constructions, respectively, γ phase is formed by laminating stacking faults in (0001) plane of α_2 phase and that transformed γ phase and α_2 phase remaining untransformed comprise lamellar structure shown in Figure 2. Therefore, between γ phase and α_2 phase in lamellar structure, the crystal orientation relationships exist, such as

$$(111)_\gamma // (0001)_{\alpha 2}$$
$$\langle 110 \rangle_\gamma // \langle 1120 \rangle_{\alpha 2}$$

predictable from the transformation mechanism as if stacking faults are stacked. Also, the fact that a great number of twins shown in Figure 3 can be observed in γ phase of lamellar structure implies that stacking faults are closely involved in $\alpha_2 \rightarrow \gamma$ transformation.

In addition, from the crystal orientation relationships between the above α_2 and γ phases, it has been shown that ordered domain is formed in γ phase comprising lamellar structure. Figure 4(a) and (b) shows atomic arrangement in (111) plane in γ phase with TiAl composition and <110> orientation (orientations of two crystals in the twin relationship are distinguished using the letters M and T since γ phase contains a large number of twins) and atomic arrangement in (0001) plane in α_2 phase with Ti_3Al composition and $\langle 11\bar{2}0 \rangle$ orientation. As is apparent from the drawing, while B and C orientations in TiAl are equivalent to each other, A orientation is not equivalent to B and C orientations. On the other hand, α, β, and γ orientations in Ti_3Al are all

Figure 2. Lamellar Structure of TiAl

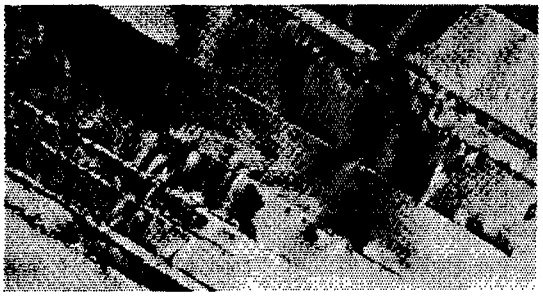

Figure 3. Lamellar Structure Observed With an Electron Microscope Band-shaped twins can be observed in TiAl phases.

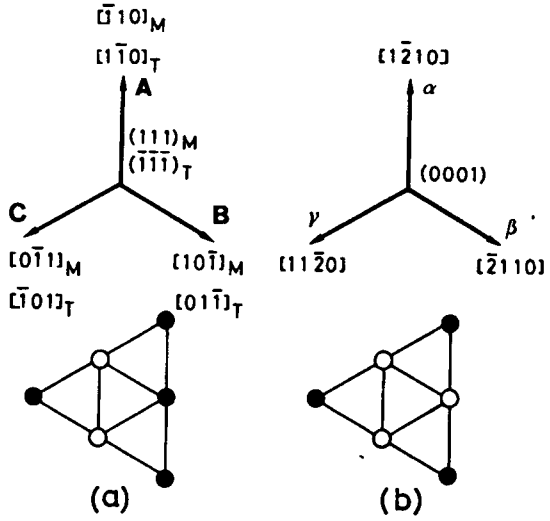

Figure 4. Atomic Arrangement and Close Packed Orientations on Close Packed Planes in TiAl(γ) Phase (a) and Ti_3Al(α_2) Phase (b) White circles represent Ti atoms and black ones Al atoms.

Figure 5. Ordered Domains in TiAl Phases Comprising Lamellar Structure

equivalent. Therefore, when (111) plane of γ phase is matched on (0001) plane of α_2 phase, three types of combinations exist

$$A//\alpha,\ A//\beta,\ A//\gamma$$

each rotating 60° around the axis vertical to the layer interface. This implies that three types of different ordered domains each rotating 60° can be formed when γ phase is formed from α_2 phase by solid solution transformation. Figure 5 shows structure (corrosion occurred after polishing) with its section vertical to the layer boundary of crystals with lamellar structure orientations aligned by unidirectional solidification, variable densities of white, black, and gray conceivable to show three types of domains. There is a relationship of [001] orientations in the three types of domains being mutually orthogonal. As is found in TiAl crystal structure shown later, the presence of domains seems to pay a role of loosening distortion resulting from the difference in lattice constant between [100] and [010] orientations and [001] orientation. In this sense, it is conceivable that the correlation is likely between the difference in lattice constant between [100] and [010] orientations and [001] orientation and domain size, with no experimental data on this point reported to date.

2.3 Lamellar Structure and Mechanical Properties

At present, as far as the TiAl system is concerned, studies aimed at practical use are concentrated on compounds with a stoichiometric composition or more Ti-rich compositions. The major reason for this is that compounds of these compositions are relatively superior in ductility. Why are the mechanical properties, especially ductility, of compounds with these compositions superior? This has not been made clear at present. However, a key to this problem lies in the lamellar structure shown in Figure 2 which is characteristic of compounds in these composition areas. Then, how is lamellar structure deformed? In order to solve this problem, the authors grew crystals with a single lamellar orientation, and attempted to clarify their deformation stress, deformability and deformation behavior.

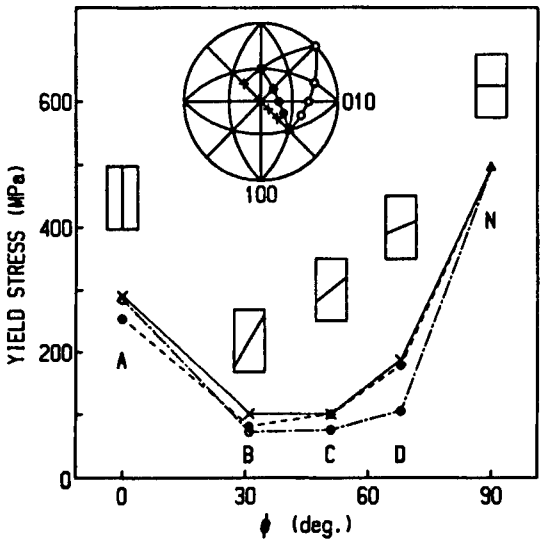

Figure 6. Relationship Between Yield Stress and Lamellar Orientation of TiAl PST Crystals
ϕ is an angle formed by the lamellar plane and the compression axis.

The crystals the authors have obtained are those with virtually a stoichiometric composition as a whole with TiAl phase still containing a large number of twins as a major phase, although they contain α_2 phase as a second phase. In relation to the term polysynthetic twinning used for minerals containing many flake twins, the authors have proposed that these crystals be called polysynthetically twinned crystals (PST crystals or peripheral twins).

Yield stress of PST crystals depends to a great extent on the relationship of relative orientation between the lamellar structure orientation and the compression axis, and, as shown in Figure 6, it becomes maximum when compression is provided vertically (N) to lamellar structure and next to maximum when provided in parallel. With intermediate orientations (B, C, and D), overwhelmingly small yield stress can be obtained, compared to the former two. Observation of the specimen surface after deformation finds that as is apparent from Figure 7, shear deformation advances over the boundary of lamellar structure when compression is provided in parallel or vertically to lamellar structure, while shear deformation advances in parallel to lamellar structure when lamellar structure is tilted against the compression axis. This difference causes lamellar orientation dependency of yield stress. This apparently implies that lamellar boundary acts as powerful resistance when shear deformation advances over lamellar boundary. Probably the resistance is provided by α_2 phase on lamellar boundary, domain boundary parallel to lamellar boundary in TiAl, and twin boundary.

Thus, it has been clarified that two modes exist in deformation of TiAl with a stoichiometric composition or a more Ti-rich composition—hard mode (shear deformation vertical to layer structure) and easy mode (shear deformation

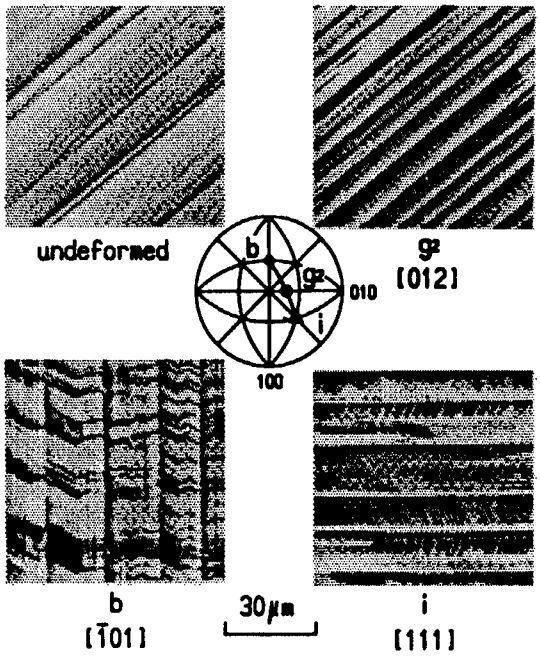

Figure 7. Relationship Between Deformation and Lamellar Orientation of TiAl PST Crystals

parallel to layer structure). Therefore, it is necessary to control the contribution by these two deformation modes to deformation in order to provide target mechanical properties to TiAl polycrystals with layer structure. It is known that Mn, V, and Cr are alloy elements effective in improving ductility of TiAl with layer structure, while it is believed that the addition of these elements causes the layer structure of TiAl to change, enabling the two deformation modes to effectively help each other, resulting in relatively great tensile ductility and strength. If Mn, V, and Cr substantially change the intrinsic dynamic characteristics of TiAl phase, effects of adding these elements should appear in Al-rich TiAl with single phase structure; there have been no such reports so far. As shown later, regarding the crystal structure of TiAl, its deformation stress can largely depend on crystal orientation. In fact, remarkable orientation dependency has been observed with deformation stress of single phase Al-rich TiAl single crystals containing no α_2 phase. In the case of PST crystals, as far as the results in Figure 6 are concerned, given that relative orientations of lamellar structure and the compression axis are the same, yield stress does not show major changes (B and C in Figure 6, for example) if crystal orientation of the compression axis changes. This implies that the presence of the three types of ordered domains enables deformation stress of both the hard mode and the easy mode to be average and isotropic.

A tensile test and a rolling experiment of TiAl PST crystals recently conducted by a group including the authors have demonstrated that active utilization of the deformation of the easy mode as shown in Figure 8 brings about rolling with a depressing ratio exceeding 50 percent at room temperature with respect to a 3 x 1.5 x 7 mm long specimen. Also, a tensile test at room temperature of PST crystals has provided ductility exceeding 6 percent, thereby proving that TiAl, at least TiAl phase comprising lamellar structure, is not intrinsically a brittle compound. Both a rolling and a tensile test

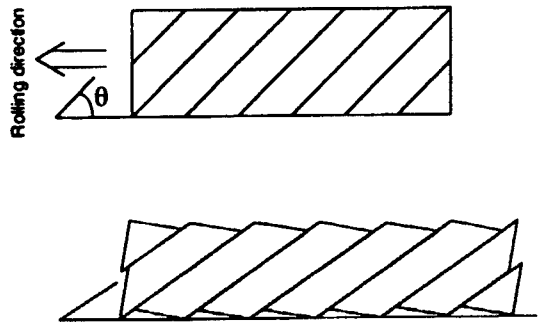

Figure 8. Rolling of TiAl PST Crystal by Easy Mode Deformation

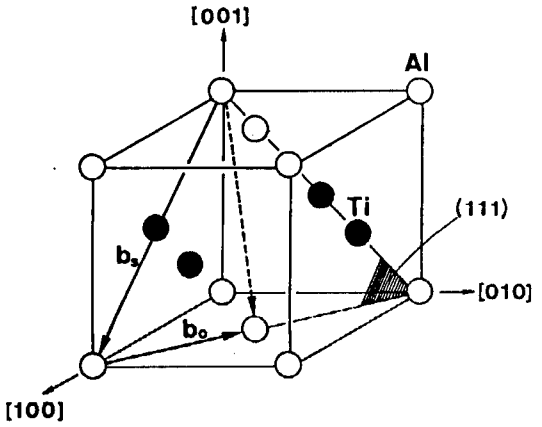

Figure 9. Crystal Structure and Burgers Vector of TiAl

have made it clear that inhomogeneity in deformation between TiAl phase and α_2 phase or crystal grains extremely different in lamellar orientation induces cracks. Therefore, structure control involving existential configuration of TiAl phase and α_2 phase, including control of lamellar structure, is indispensable for improving ductility of polycrystals.

2.4 Deformation Mechanism

Figure 9 shows the crystal structure of TiAl. It is based on fcc lattices with face centered tetragonal ($L1_0$ type) structure alternately stacking a Ti atom and an Al atom in [001] direction of three <001> directions. Without distinguishing a Ti atom from an Al atom, it results in fcc structure. Therefore, although slippage of TiAl occurs along <110> direction on {111} plane ((111) plane is shown in Figure 9), as is apparent from the atomic arrangement on the slippage plane, the magnitude of minimum translational vector is different between <110> direction vertical to c-axis [001] and <101> direction making an angle of 45° with it. Consequently, the magnitude of burgers vector of dislocation is responsible for slippage in each direction. For example, dislocation of Burgers vectors of b_s and b_o can be responsible for the slippage in [101] direction and [110] direction in Figure 9. The b_o dislocation is the same as dislocation active in fcc metals and alloys, while b_s dislocation is superlattice dislocation with Burgers vector two times as large as that. Dislocation with large Burgers vector like b_s dislocation results in large elastic energy, so it is decomposed into partial dislocation through various plane defects. Elastic energy decreases depending upon decomposition formats, but becomes inactive in many cases. However, it has been confirmed by electron microscope observation that such decomposition is likely to occur.

With TiAl, in addition to such slippage, twins which cause no disturbance to the regular arrangement of Ti and Al atoms occur. One such twin system exists in one {111}, and, with (111) plane in Figure 9. for example, the twin generated by homogeneous shear (dislocation vector of shear is 1/6 $[11\bar{2}]$) in $[11\bar{2}]$ direction along (111) plane corresponds to this. Such a twin is a deformation mechanism often found in face-centered tetragonal crystals based on fcc lattices and very important for TiAl deformation.

In fact, an observation of deformation structure of PST crystals has found that it is [110] slippage and the above type twins that are responsible for PST crystal deformation. Al-rich TiAl is inferior in ductility to Ti-rich TiAl, because with the former, <101] superlattice dislocation contributes to deformation and <110] slippage and twins should be considered in order to improve ductility of Al-rich TiAl. However, since <110] direction is converted into <101] direction when it is beyond the domain boundary, b_0 dislocation cannot be active over the domain boundary. Therefore, it is believed that ease or difficulty of the activity of b_0 dislocation sometimes determines resistance of the domain boundary, so the importance of <101] slippage cannot be denied.

As stated so far, with the Ti-Al binary system, when Ti and Al have 1:1 composition or a composition slightly close to Ti, intermetallic compound TiAl phase with α_2 phase at high temperature and γ phase at low temperature, i.e., $L1_0$ structure, is stable. In addition, since it undergoes $\alpha \rightarrow \alpha_2$ regular/irregular transformation and $\alpha_2 \rightarrow \gamma$ transformation during changing from α phase to intermetallic compound TiAl phase, and $(\alpha_2 + \gamma)/\gamma$ phase boundary is close to TiAl's stoichiometric composition, TiAl with a stoichiometric composition or a more Ti-rich composition has two-phase structure of $(\alpha_2 + \gamma)$, and the two-phase structure depends upon cooling speed and compositions. In other words, two-phase structure can be controlled by heat treatment in general, including control cooling and processing heat treatment. This is the greatest feature of TiAl with a stoichiometric composition or a Ti-rich composition, and this material should be put to practical use through the maximum utilization of this feature.

The contents of lamellar structure stated so far which is found with TiAl with a stoichiometric composition or a Ti-rich composition can be summarized as follows. Control factors of lamellar structure with respect to individual lamellar grains are:

1) thickness of layer TiAl phases comprising lamellar structure;
2) size of ordered domains in layer TiAl phases;
3) volume fraction, thickness and distribution of α_2 phases (Ti_3Al phases) comprising lamellar structure; and
4) aggregate structure.

With thin TiAl phases (fine lamellar structure), the homogeneity in deformation can increase, while with thin TiAl phases and their homogeneous distribution, hardness in the hard mode of deformation must decrease. Furthermore, with diminished domain size in TiAl phases, deformation particularly by the easy mode can be isotropic. It is believed that these effects will all lead to improved ductility of TiAl. The authors guess that the addition of Mn, V, and Cr resulted in such changes in structure. The likelihood that the relationship between structural factors and mechanical properties of lamellar structure will be explained in the future will likely lead to its more effective applications.

However, making propagation routes of cracks complicated, lamellar structure is effective in improving toughness, but not necessarily cold ductility, and some researchers have pointed out that mixed lamellar structure grains and

nonlamellar structure grains would be better. According to this, volume fraction ratio of lamellar grains to nonlamellar grains must be added to the abovementioned structural control factors of lamellar structure as a structural control factor of Ti-rich TiAl. It is believed that the dispersion of nonlamellar grains probably enables the nonhomogeneity in deformation among crystal grains very different in lamellar orientation to relax, for reasons not yet known. It has been reported that with respect to Mo-added TiAl, cold ductility exceeding 2 percent can be obtained even with two-phase structure comprising fine nonlamellar equi-axed grains and two-phase structure comprising Ti_3Al phases finely dispersing in their grain boundary. Therefore, as far as cold ductility is concerned, lamellar structure may not be essential. When considering strength, it is desirable that lamellar structure be formed in fine TiAl equi-axed grains. The nonhomogeneity in deformation among lamellar grains due to the difference in lamellar orientation can be relaxed to a coniderable extent when lamellar grains themselves become fine, so it is significant to superimpose liquid phase on fine equi-axed grain structure from the standpoint of simultaneous pursuit of Ti_3Al, ductility, and toughness. The problem is how to obtain fine lamellar grains, which may be solved by dispersing TiB_2, etc., in the future.

3. Al_3Ti

3.1 Structure and Deformation of Al_3Ti

Al_3Ti has crystal structure called DO_{22} type. This is one of a series of long-cycle structure figured out from Ll_2 type structure, a typical regular structure based on face-centered cubic lattices. Let us consider long-cycle structure obtained by introducing an antiphase boundary (APB) of displacement vector 1/2[110] on each Mth (001) plane of Ll_2 type structure in Figure 10(a). Here, DO_{22} type structure corresponds to a case where M=1, and an axial ratio (c/a) $\simeq$ about 2 (Figure 10(b)). When M=2, structure in which c/a $\simeq$ 4 called DO_{23} type shown in Figure 10(c) can be obtained. All intermetallic compound Al_3X formed among elements of VIa group, the same group as Ti, and Va group crystallize into such DO_{22} or DO_{23} type structure.

Based on face-centered cubic structure, DO_{22} structure is already a rather complicated structure, and its deformation mode which is expected to be active is actually limited. With Al_3Ti, as with TiAl, $\{111\}\langle 11\bar{2}\rangle$ system twins which do not disturb regular arrangement of Al and Ti are the main deformation mode. At high temperature, (001)<110] slippage will be active, but virtually no deformation will occur at ordinary temperature. For improved deformability of Al_3Ti, a device will be necessary to facilitate the occurrence of $\{111\}\langle 11\bar{2}]$ and (001)<110] slippage. The following are brief descriptions of an idea for the activation of $\{111\}\langle 11\bar{2}\rangle$ twins.

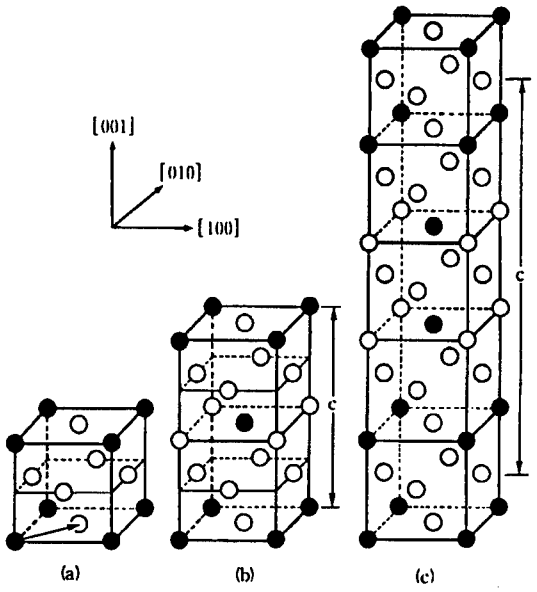

Figure 10. $L1_2$ Type (a), DO_{22} Type (b), and DO_{23} Type (c) Structure

3.2 Improvement of Deformability (Microalloying)

Figure 11(a) shows atomic arrangement on (111) atomic plane in DO_{22} type structure and the way they are stacked. With (111) atomic plane, six stacked B atoms (black circles) form, in a set, DO_{22} type structure while dislocating from 1 to 6. Here, the introduction of $(111)[11\bar{2}]$ twin (stacking fault) with minimum thickness between the third and the fourth (111) atomic plane (Figure 11(b)) will result in atomic arrangement shown in Figure 11(c) in the area of twins with minimum thickness, the same as DO_a type structure. Therefore, with element X which produces DO_a type structure compounds with Al or Ti, substituting X atoms for Ti or Al is likely to facilitate the occurrence of $(111)[11\bar{2}]$ twins in ternary compounds after substitution. This is, so to speak, a crystal chemical approach for improving the deformability, a method to expect effects of adding a trace quantity of an element while retaining DO_{22} type structure, and can be said to be an approach by microalloying. As far as the improvement of Al_3Ti's deformability is concerned, no outstanding results have been reported so far.

3.3 Improvement of Deformability (Macroalloying)

As shown in Figure 10, DO_{22} type structure and $L1_2$ type structure are extremely close to each other. While the former is tetragonal and the latter cubic, and the former is more complicated in crystal structure, the latter seems easier deformed considering the number of possible deformation modes. From such a standpoint, there is an attempt to improve the deformability of Al_3Ti by adding a third element to it and changing its crystal structure into $L1_2$ type. In this case, because of adding much of a third element, this method is sometimes called macroalloying as opposed to microalloying in section 3.2.

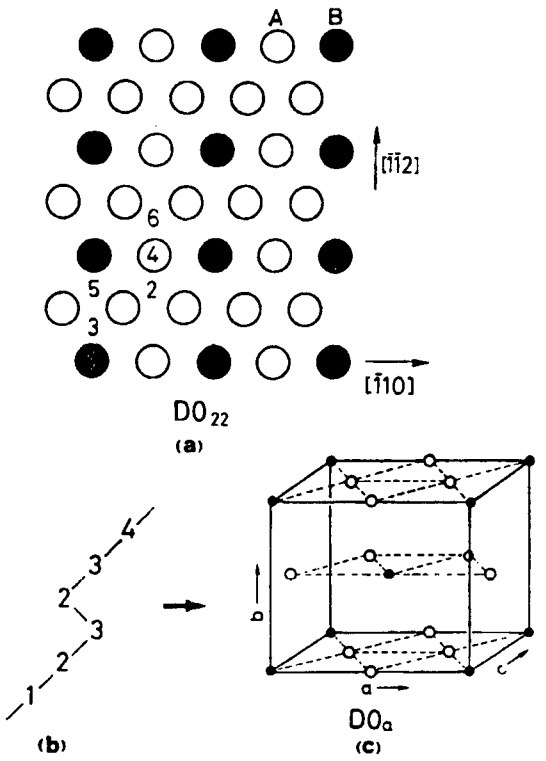

Figure 11. Atomic Arrangement on (111) Atomic Plane With DO_{22} Type Structure (Stoichiometric Composition A_3B) and the Way Atoms Stack (a), the Way (111) Atomic Planes Stack After Introducing Stacking Faults (b), and DO_a Type Structure (c)

The elements currently known as those enabling Al_3Ti's crystal structure to be converted from DO_{22} type to Ll_2 type include Cu, Ni, Fe, Zn, Cr, Mn, and Ag. The Ll_2 type ternary compounds based on Al_3Ti currently known include $Al_{67}Ni_8Ti_{25}$, Al_5CuTi_2, $Al_{66}Zn_9Ti_{25}$, $Al_{22}Fe_3Ti_8$, $Al_{67}Cr_8Ti_{25}$, $Al_{66}Cr_9Ti_{25}$, $Al_{67}Mn_8Ti_{25}$, $Al_{66}Mn_9Ti_{25}$, $Al_{66}Mn_6Ti_{23}V_5$, and $Al_{100-x-y}Ag_yTi_x$ (x=25~30, y=8~13). It is said that the deformability at room temperature of ternary alloys added with Mn, Cr, and Ag is superior. For example, Figure 12 shows stress-strain curves caused by compressing with an $Al_{67}Mn_8Ti_{25}$ as-cast material, while DO_{22} type Al_3Ti undergoes virtually no deformation at room temperature. Mn-added ternary Ll_2 type com-pound has been sufficiently deformed at room temperature although compressed. At the moment, no remarkable results have been reported on tensile ductility, but as far as oxidation resistance is concerned, it has been reported that Mn-added ternary Ll_2 type compounds are superior, similar to Al_3Ti, in spite of macroalloying, and much is expected in relevant studies in the future.

The above summarizes the current state of studies on TiAl and Al_3Ti, which reminds the authors of the explanation they wrote about a year ago that must be rewritten due to the rapid progress being made. It seems necessary to expand basic studies toward TiAl compounds with an Al-rich side and toward Ll_2 type ternary compounds with the Al_3Ti system. With research fields involving

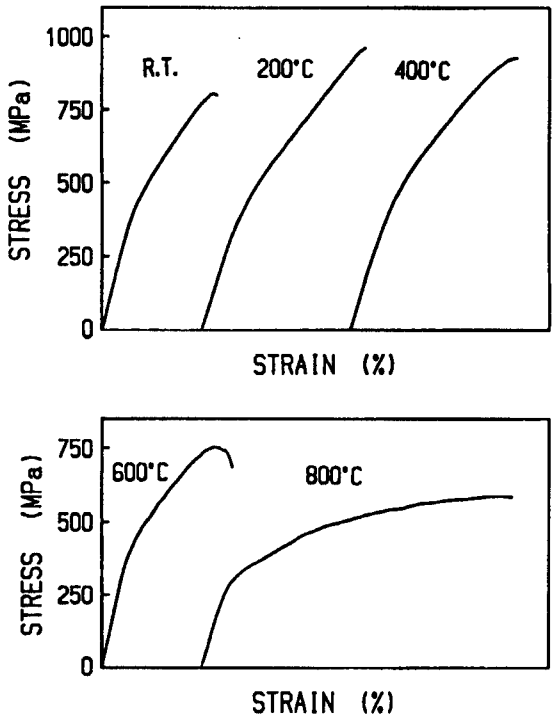

Figure 12. Stress-Strain Curves Resulting From Compression of $Al_{67}Mn_8Ti_{25}$ (as-cast)

practical applications, Ti-rich TiAl which is said to be facing immediate practical use still remains unchanged. It is hoped that Ti-rich TiAl will be put to practical use as soon as possible.

High Melting Point Intermetallic Compounds

916C1004D Tokyo KINZOKU GAKKAI SEMINA KINZOKUKAN KAGOBUTSU in Japanese
1 Jun 90 pp 29-36

[Article by Yukichi Magoshi, School of Engineering, Osaka University: "Nb_3Al-Group Aluminide; Fire-Resistant Metal Siliside; B2 and $L2_1$ Type Compounds"]

[Text] **1. Introduction**

Working critical temperature of conventional heat-resistant materials represented by Ni-group and Co-group ultraheat-resistant alloys used to be 1,000~1,200°C. However, there is demand for materials capable of withstanding use at ultrahigh temperature of around 1,500°C to be developed in recent years for high-speed aircraft and for airframes of space shuttles. High temperature strength of metallic materials, except for specific cases, begins to decrease at a temperature of $T_m/2$ or above. Therefore, with respect to materials usable at ultrahigh temperature, a melting temperature of at least around 2,000°C or above is desired. Metals, alloys, or their compounds with such high melting temperatures are limited to an extremely small number. In terms of environmental resistance under extremely harsh conditions under high temperature and atmosphere, they must contain such elements as Si, Al, Be, and Cr. From the standpoint of deformation, materials with relatively simple crystal structure with good symmetry are desirable, so those with complex crystal structure like Laves phase, for example, cannot be a candidate. In this context, this article mainly describes fire-resistant metal siliside and aluminide, with $MoSi_2$- and Nb_3Al-based compounds in particular showing promise. Also, B2- and $L2_1$-type aluminides attracting attention again due to superior oxidation resistance are mentioned although they are inferior in melting temperature at 1,600~1,700°C.

2. Nb_3Al-Group Aluminide

Nb_3Al has A15 type regular structure shown in Figure 1. Compounds with such crystal structure include Mo_3Si, W_3Si, V_3Si, Cr_3Si, V_3Sn, V_3Ge, V_3Al, Nb_3Al, and Mo_3Al. They all show high melting temperature, many of which show superconductive characteristics. It can be easily imagined from their crystal structure that slip direction of these compounds is <100>. As possible slip planes, {100} and {011} can be considered. High temperature strength has been measured with respect to V_3Si, V_3Ga, and Nb_3Sn, high strength shown at a high

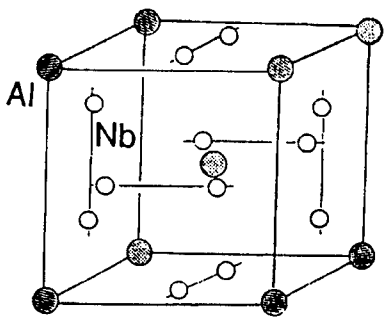

Figure 1. A15 Type Structure

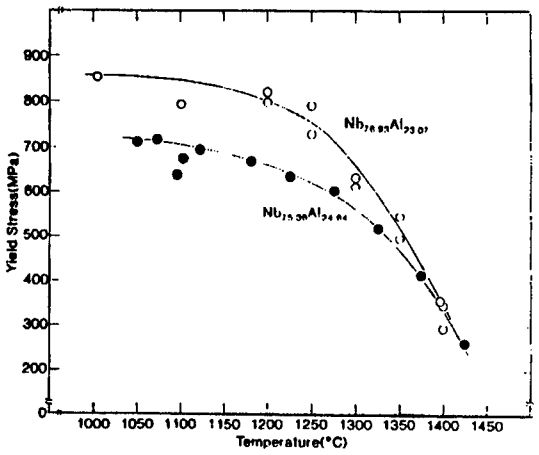

Figure 2. Temperature Dependence of Yield Stress of Nb_3Al Group Compounds

temperature of 1,200°C or above, a value of close to 350 MPa at 1,200°C reported, for example, with respect to V_3Si. With siliside, however, if <100>{011} slippage is attempted, only slip plane actually observable is {010} plane since the number of Si-Si bond couples to be cut with strong covalent bond quality is 1.4 times as many as that of <100>{010} slippage. This causes a decreased number of slip systems to be activated which partially results in the brittleness of compounds of this kind. Of such A15 type compounds, Nb_3Al which is wide and metallic in solid solution sources as far as its constitutional diagram is concerned, can be expected to have toughness, thus attracting attention as a strong candidate for ultrahigh temperature materials.

Figures 2 and 3 show temperature dependency of yield stress of Nb_3Al compounds. $Nb_{76.93}Al_{23.07}$ is actually of Nb_3Al single phase, and Nb-rich solid solution phase is crystallized with Nb side compositions from this, while Nb_2Al compound phase is crystallized with the Al side composition. Only from the standpoint of high temperature strength are the compounds of this system with Nb_3Al single phase most superior, showing a high value of about 350 MPa at a high temperature of about 1,400°C. However, the compounds rapidly become brittle at a deformation temperature of 1,000°C or below. On the other hand, whey they contain Nb-rich solid solution phases, their strength at high temperature decreases, but their brittleness-ductility transition temperature apparently decreases, proving to be effective from the standpoint of improved toughness. With an alloy containing about 20 vol% of Nb-rich solid solution phases, for example, its brittleness-ductility transition temperature decreases by about 300°C, compared to the compounds with Nb_3Al single phases. On the other hand, with Nb_3Al coexisting with Nb_2Al phases, brittleness-ductility transition temperature dislocates to the high temperature side, thus proving its ineffectiveness for improving high temperature strength.

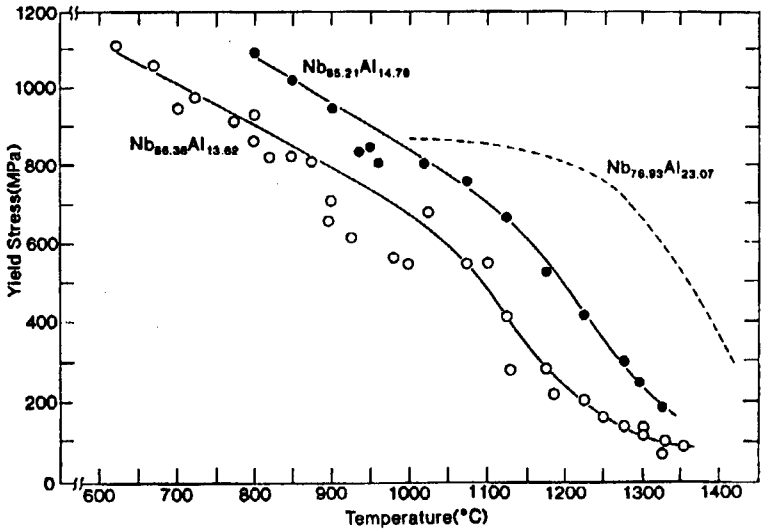

Figure 3. Temperature Dependency of Yield Stress of Nb_3Al Group Compounds

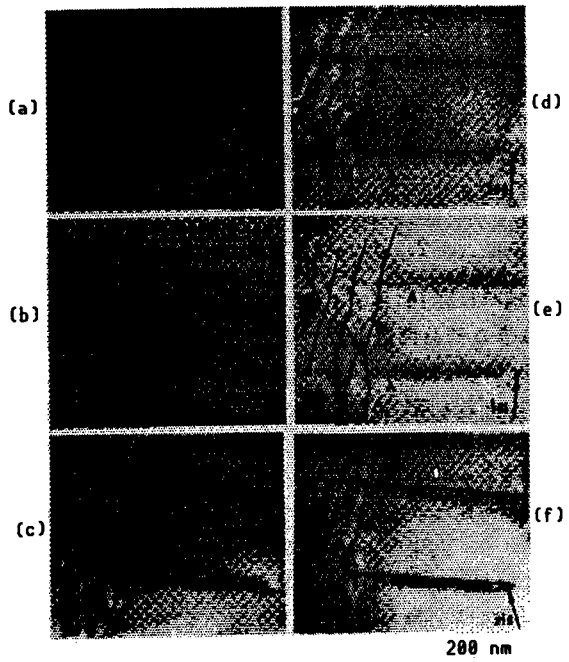

Figure 4. Dislocation Structure of $Nb_{86.38}Al_{13.62}$ Deformed at 1,300°C
A: [010]; B [001]

As shown in Figure 4, deformation of Nb_3Al is caused by <100> dislocation at any temperature with no other dislocations observable. Its slip plane is {010}, while climb motions of dislocations become active at a high temperature exceeding 1,200°C, with stress-strain curves showing a slow work hardening after showing high temperature yield. Dislocation nodes resulting from <100>

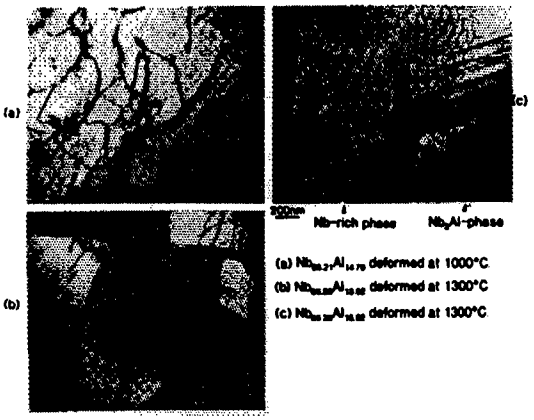

Figure 5. Dislocation Structure of Nb_3Al Group Compounds in Nb-Rich Solid Solution

interdislocation reaction can be partially observed at a high temperature of 1,300°C, while deformation remains to be rate-determined by sliding motions of dislocation, such deformation structure reflecting high strength at high temperature of the compounds.

With an Nb-rich solid solution phase, on the other hand, softening already begins at 1,000°C or below, and forms, as shown in Figure 5, dislocation nodes and networks due to remarkable climb motion of dislocation. At such high temperature, dislocation structure proving dynamic recrystallization can be observed. As stated, an Nb-rich solid solution phase does not contribute very much to reinforcement, but, as shown in Figure 5, the presence of this phase rich in processability prevents extreme accumulation of dislocations and the occurrence of cracks in Nb_3Al/Nb-rich phase interface, thus proving its effectiveness for suppressing fracture of Nb_3Al phases. Therefore, composite microdispersion alloying of Nb_3Al/Nb-rich solid solution phases will be necessary for improving mechanical quality of Nb_3Al compounds. Also, for activating {011} slippage at low temperature, substitution by more metallic elements instead of an Al-Al bond coupling should be considered.

Creep strength of its compounds is better than that of other compounds, such as $CoSi_2$(C1 type), Co_2Nb(C15 type), CoHf(B2 type), and Ti_3Sn(Do_{19} type), and higher than that of PWA1480, a practical Ni-group alloy, at a high temperature of 1,200°C or above. Steady-state activation energy of this creep shows a rather high value of 350 kJ/mol. This creep characteristic, however, is not as good as can be expected from its melting temperature, and the creep resistance should be improved by adding a third element, such as Nb_3(Al, Ta).

Nb_3Al not only has such a mechanical property problem but has a considerable problem with oxidation resistance. Figure 6 shows its oxidation resistance, which cannot be said to be superior to that of other heat-resistant materials. This is mainly because of its shortage in Al content, and, as shown in Figure 6, Al_3Nb compounds with high Al content are superior in oxidation resistance. This point will be solved before it is put to practical use by means of surface coating with Al_3Nb (DO_{22} type).

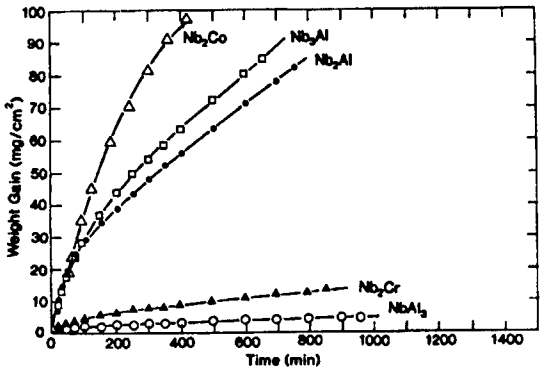

Figure 6. Oxidation Increase of Nb Components

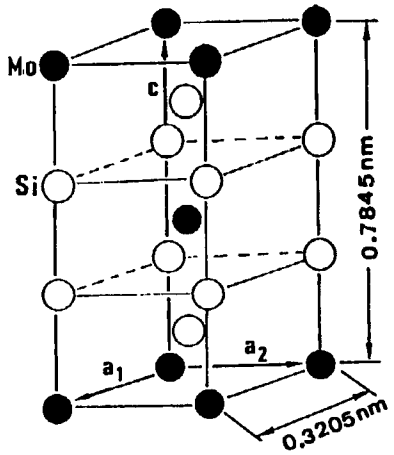

Figure 7. $C11_b$ Type Structure

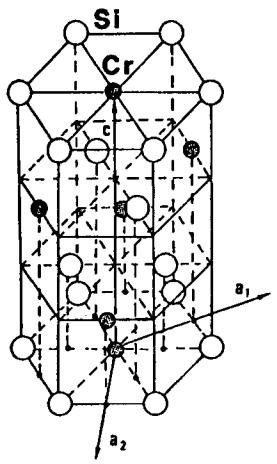

Figure 8. C40 Type Structure

3. Fire-Resistant Metal Silisides

Transition metal silisides, except for B2-, DO_3-, and $L2_1$-type structure, can be deformed structurally into a body-centered tetragonal system ($C11_b$ type) and a hexagonal system (C40 type) shown in Figures 7 and 8. This section mainly describes the deformation outcome of $MoSi_2$ ($C11_b$ type) and $CrSi_2$(C40 type). Possible slip planes of $MoSi_2$ are {110} and {013} planes and its deformation occurs in <331>, <110>, or <100> direction. Causing no disturbance to bond couples among first adjacent atoms, APB energy on {013} plane is much smaller than that on {110} plane, but its laminating period of an atomic plane is longer and more complex than that of {110}; therefore, a high deformation stress will be required for dislocation motions on this plane where it is forecast that dislocation core structure will be non-planar with low mobility.

In fact, a dislocation motion on this plane needs, as shown in Figure 9, a high deformation stress. For this reason, orientations in which {013} slippage can actually be observed are limited to those in Figure 10. The compounds, however, create no problems with respect to the number of active slip planes.

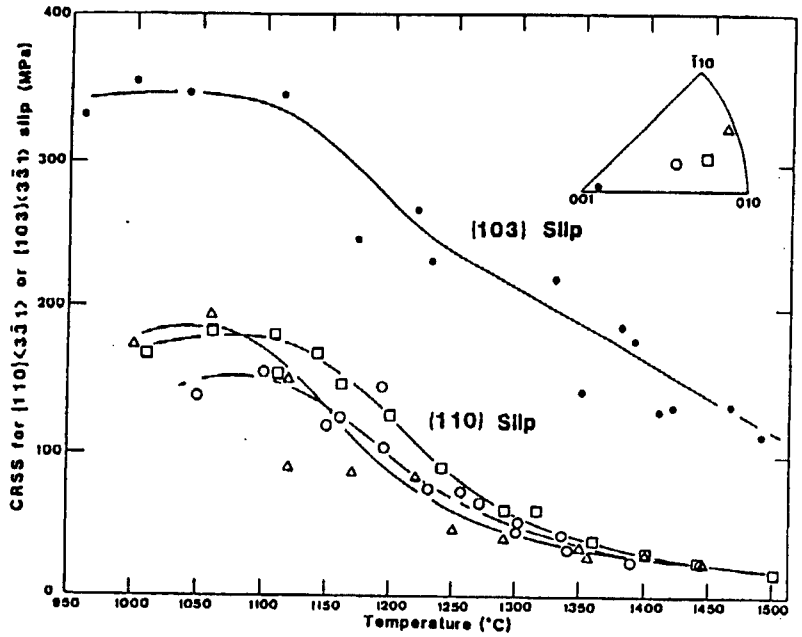

Figure 9. Temperature Dependency of CRSS of $MoSi_2$ Single Crystals

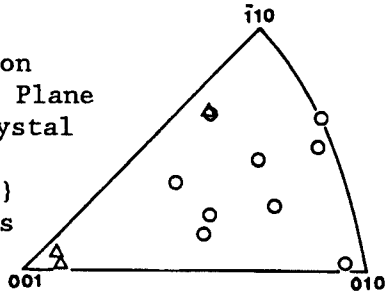

Figure 10. Crystal Orientation Dependency of Slip Plane of $MoSi_2$ Single Crystal (900°C)
Circles represent {110} slippage, and triangles {013} slippage.

The relationship of the magnitude between APB energy and critical shearing stress of {110} slippage and {013} slippage corresponds to that of {111} slippage and {100} slippage in $L1_2$ type regular alloys. In $L1_2$ type crystals, a <110> superlattice dislocation is decomposed into two partial dislocations, while in $C11_b$ type crystals, a <331> superlattice dislocation is decomposed into three partial dislocations. Despite such a difference, abnormal reinforcement at high temperature resulting from jobs in cross slip on {013} plane, as shown in Figure 11, can be expected. These two types of slippage show a remarkable difference in both temperature dependency of yield stress and the shape of stress-strain curves. With {110} slippage, softening rapidly starts around 200°C, and many <110> and <100> dislocations come to be observed among active dislocations. Parallel to dislocation activities, stress-strain curves show virtually no sign of hardening during the process after high temperature yielding, creating no problems in terms of workability. With {013} slippage, intense work hardening occurs in high temperature areas, with no work softening observed at 1,500°C, a high yield strength of about 300 MPa is shown. Activation energy of deformation obtained from strain velocity dependency and deformation temperature dependency of yield stress is as high

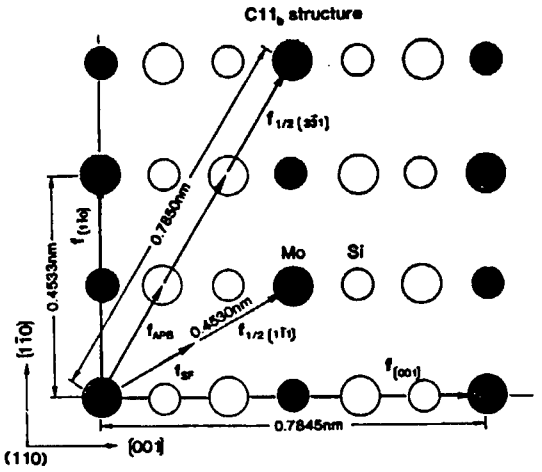

Figure 11. Atomic Arrangement of $C11_b$ Structures on (110) Plane

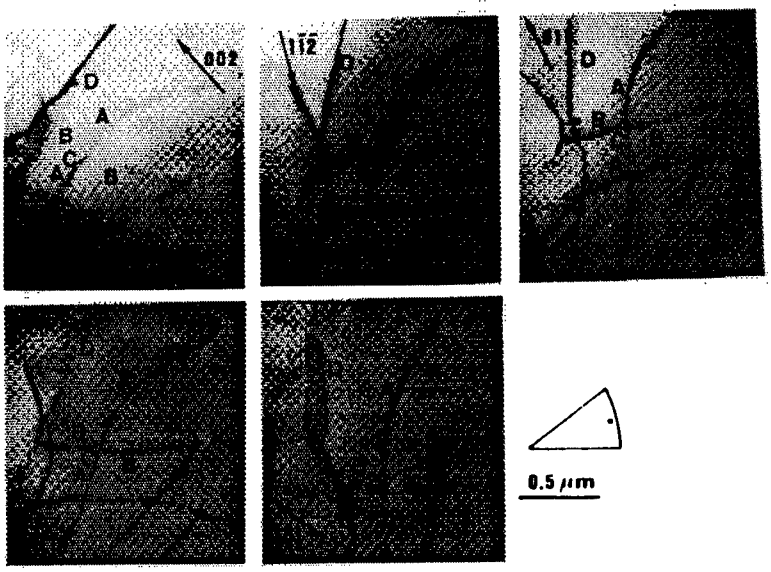

Figure 12. Dislocation Structure of $MoSi_2$ Single Crystals Deformed at 1,300°C
A: [100]; B: [010]; C: [110]; D: 1/4[111]

as about 800 kJ/mol and multiple dislocation nodes or networks can be observed as deformation structure, so creep resistance is probably superior considering diffusion rate-determination of compounds of this type. The oxidation resistance is extremely stable without damaging the specimen surface in an atmospheric test at 1,500°C. This is because Si contained in large quantity forms an SiO_2 protective coating on the specimen surface and SiO_2 works as a self-recoverable oxidation resistance protective coating with high temperature and rich viscosity.

For a more detailed study of the deformation mechanism, the atomic arrangement on {110} plane of $C11_b$ structure is shown in Figure 12. As shown in Figure 12,

Figure 13. Dislocation Structure of $(Mo_{0.97}Cr_{0.03})Si_2$ Single Crystals Deformed at 1,150°C

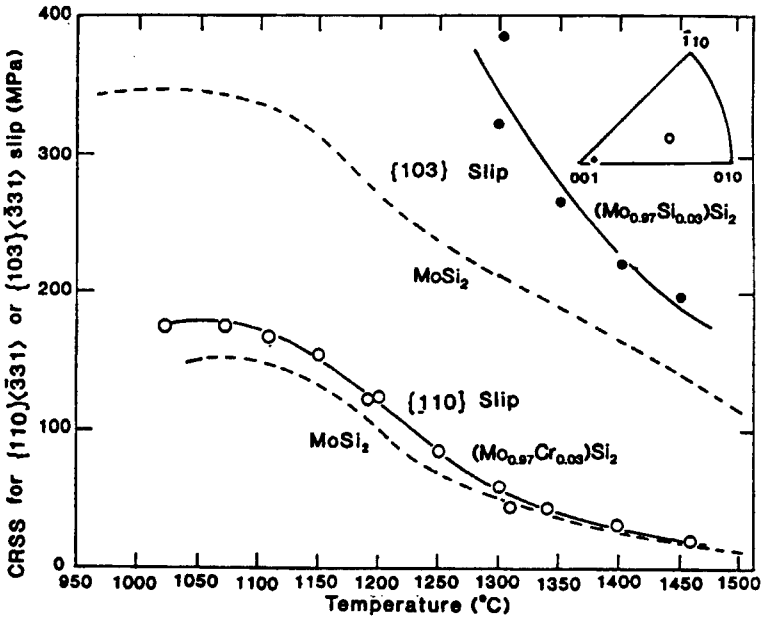

Figure 14. Cr Addition Effects of $MoSi_2$ Single Crystals' CRSS on Temperature Dependency

<110> and <100> slippage is activated at a high temperature exceeding 1,200°C, but these dislocation motions are not easy at low temperature, and to facilitate deformation at low temperature new deformation modes must be activated. In Figure 11, deformation by 1/2<111> displacement is possible, but, with low stacking fault energy in this case, decomposition into two 1/4<111> partial dislocations occurs, thereby facilitating such deformation. If such 1/4<111> displacement is provided on {110} plane of a $C11_b$ type crystal, the laminating of its atoms changes from ABAB to ABCAB, and the atomic arrangement becomes equivalent to that on (0001) plane of C40 type structure in Figure 8.

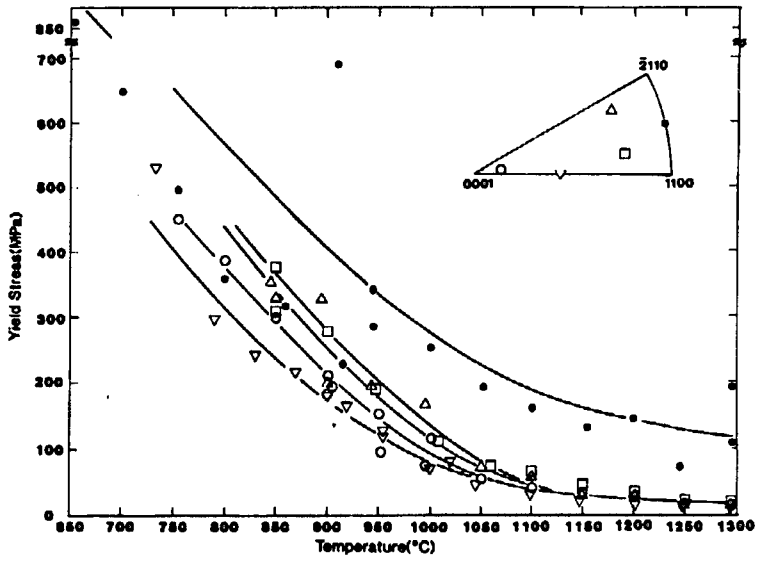

Figure 15. Temperature Dependency of Yield Stress of $CrSi_2$ Single Crystals

Therefore, the addition of an element to stabilize C40 type crystals can make the stability of $C11_b$ structure partially low and activate this slippage containing stacking faults. In fact, when part of Mo is substituted by Cr taking C40 structure as $CrSi_2$, multiple 1/4<111> couples which have been decomposed via stacking faults can be observed, as shown in Figure 13, which facilitates deformation. Figure 14 shows temperature dependency of CRSS of $(Mo_{0.97}Cr_{0.03})Si_2$ single crystals. When {013} slippage occurs, the crystals show remarkable hardening due to solid solution effects resulting from adding Cr, compared to $MoSi_2$ single crystals.

On the other hand, deformation stress required for {110} slippage undergoes no changes and is deformable up to low temperature. The difference in changes in deformation stress resulting from the difference in deformation mode is nothing but the effect of the activation of 1/2<111> dislocation via stacking faults on {119} plane. It is suggested that the brittleness is improved by alternatingly combining $MoSi_2$, WSi_2 and $ReSi_2$ which form $C11_b$ type structure and VSi_2, $CrSi_2$, $TaSi_2$, and $NbSi_2$ which form C40 type structure.

The following is a description of plastic behavior of crystals forming C40type structure using an example of $CrSi_2$. Figure 15 shows temperature dependency of yield stresses in various crystal orientation. $CrSi_2$ is deformable up to a rather low temperature compared to $MoSi_2$, but its deformation strength rapidly decreases as deformation temperature rises. Its activation energy for deformation found from strain velocity dependency and deformation temperature dependency of yield stress is 570 kJ/mol, a large value as with $MoSi_2$.

The crystal structure of $CrSi_2$ enables slip deformation of the bottom and cylindrical surfaces, but according to a result of slip line observation, slippage only occurs in the bottom surface, irrespective of crystal

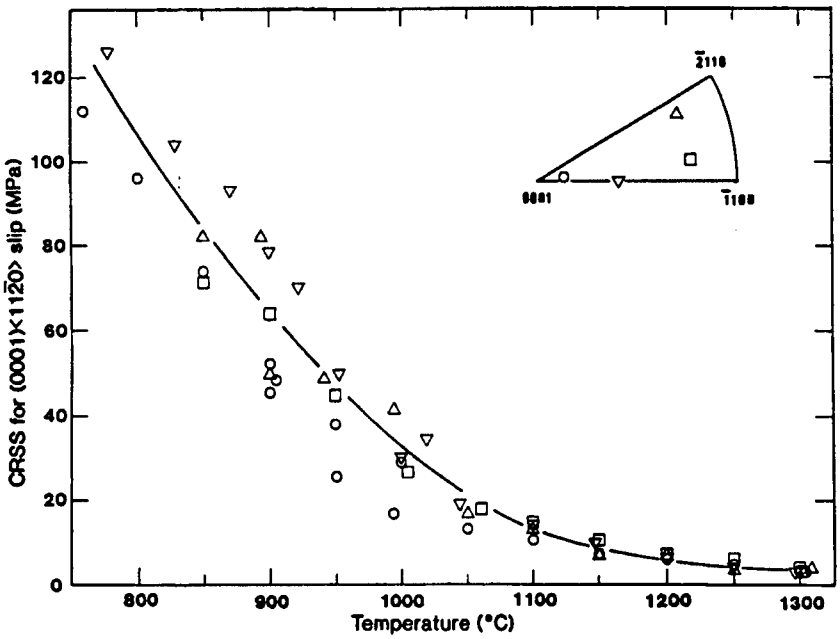

Figure 16. Temperature Dependency of CRSS of $CrSi_2$ Single Crystal

orientations. The critical shearing stress in this case shows virtually no crystal orientation dependency, as shown in Figure 16, and expected micro-cross slippage resulting from the difference in APB energy between the bottom and cylindrical surfaces.

4. B2 and $L2_1$ Type Compounds

B2 type aluminides with high melting points including NiAl, CoAl, and FeAl are expected to be used at high temperature due to their superior oxidation resistance. FeAl can be well formed at room temperature by making it fine crystal grains using Fe-side composition alloys. With NiAl, however, deformation is best facilitated in the periphery of stoichiometric composition, showing a rather different tendency from other compounds. It is difficult to deform NiAl at room temperature, compared to FeAl, which is partially because these compounds are high in regularization energy, active dislocations are consequently limited to <100> dislocations, thereby falling short of the number of slippage systems necessary for deformation of polycrystalline substances. To cope with this, adding elements for activating <111> slippage are being considered; good results have not necessarily been achieved. With many of these B2 type binary compounds, deformation by <100> dislocations become dominant at high temperature even when <111> dislocations are active, and that this slippage is prone to occur most often on {110} plane, thereby necessitating large deformation stress in {001} plane. Since these compounds are superior in high temperature strength, but inferior in creep resistance, efforts are being made to improve their creep characteristic by making dispersion less likely to occur, as for example in Figure 17, in an alloy composition, by making them pseudo-binary systems, such as FeAl-NiAl and NiAl-CoAl. With L2, type compounds, such as

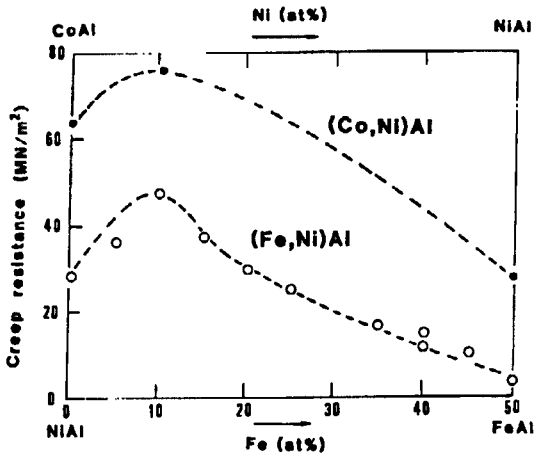

Figure 17. Creep Strength of FeAl–NiAl and NiAl–CoAl Pseudo–Binary Aluminide

Ni_2AlTi and Co_2AlTi, APB I becomes unstable and the decomposition of <111> superlattice dislocation does not occur and <100> or <110> dislocation motions sometimes rate–determine deformation. With <110> dislocations, in particular, Burgers vector is great and {001} slippage is difficult, thereby showing remarkable improvement in high temperature dependency and creep characteristic resulting from their dislocation structure. From the standpoint of practical use, microstructure of B2– and $L2_1$–type phases, NiAl–Ni_2AlTi two phases compounds, for example, are excellent.

5. Conclusion

Compounds with high melting points and high strength, i.e., stable up to high temperature, are strong in atomic bonding, and it is natural that they are under extremely harsh conditions in terms of deformation and toughness, particularly at low temperature. Of course, as can be seen in an example of (Mo, Cr)Si_2, improvement of deformability by examining in detail the deformation format and considering phase stability is one effective means. However, it is too much to expect this type of compound to have great dislocation and deformability similar to those of previous heat–resistant materials used at 1,000°C or below. It is suggested that these compounds be evaluated by their toughness and that efforts be made for alloy design to improve toughness.

With $MoSi_2$, similar to its application in fine ceramics, alloying and combination will be effective which stabilize similar crystals entailing an increase in specific volume contributing to the relaxation of concentration of stress. Also, as can be seen in an example of Nb_3Al, characteristics are likely to be improved by composite phases containing different roles including stress and toughness. Both studies to improve mechanical properties and innovations in usage are much needed since they are remarkably different in properties from their conventional counterparts.

Intermetallic Compounds as Functional Materials

916C1004E Tokyo KINZOKU GAKKAI SEMINA KINZOKUKAN KAGOBUTSU in Japanese
1 Jun 90 pp 37-44

[Article by Isao Nishida, Third Research Group, National Research Institute for Metals: "Functional Materials and Their Main Applications; Functional Sintered Bodies"]

[Text] **1. Introduction**

Materials are the base of scientific technologies of every sector and industry, and the development of new materials supports the development and progress of so-called high tech sectors, such as electronics, information, and space engineering. Along with the recent miniaturization and higher performance of industrial equipment and applied products, materials with high added values have become necessary and the development and improvement of materials with unprecedented characteristics and functions are demanded. Many types of industrial materials are used as components of such equipment, which can roughly be divided into structural and functional materials.

Functional materials have found a wide range of application in various fields, and they cannot be defined clearly by their applied fields. Copper and aluminum have a conductive function in terms of their good heat conductivity, so they are functional materials in a broad sense. However, in reality, the words functional material are used in a narrower sense, clearly meaning a material which causes a physical change. Optical and biomaterials as well as the materials used under ultrahigh temperature and pressure are also called functional materials. Except for single element semiconductors (Si, Ge) and carbon which support today's information oriented society, most functional materials are mainly alloys and compounds comprising two or more types of elements, while intermetallic compounds, even alloys, play an important role in manifestation of functionality. For example, an alnico magnet is an alloy obtained by dispersing FeCo with shape magnetic anisotropy in nonmagnetic NiAl, and a semi-rigid magnetic material obtained by changing the components and heat treatment of this alloy is used for hysteresis motors.

The types and number of functional materials used for industrial equipment and various products have increased year after year, and we are now in an age when

knowledge of various functional materials is required not only for those engaged in material development but for designers. In this context, the author asks readers to refer to a book describing the principle and its applications and manufacturing and processing technology for details of various functional materials whose characteristics undergo changes depending upon material shapes. This article describes only the classification of their functions and main applications and metals as functional materials and their compounds. Also, metallic oxides and intermetallic compounds are selected from among them, and automatic temperature control heating elements and high-performance magnets thermoelectric conversion as examples of materials in which the manifestation of functionality occurs and the performance improves because they are powder sintered bodies.

2. Functional Materials and Their Main Applications

There are a large variety of functional materials, from organic to inorganic, and, even in the case of the same substance, it shows different characteristics depending on its shape, such as gas, liquid, powder, amorphous, sintered body, polycrystal, and monocrystal. Table 1 shows functions and main applications of inorganic solid materials selected from among them. Applications with an asterisk are materials which yield functionality or improved performance when they are made sintered bodies, while those underlined are materials aimed at improved mass productivity and practicability by making themselves sintered bodies. Table 2 shows metals as functional materials and their compounds with semiconductors well known as optical and electronic materials, and oxide superconductors under material development omitted. With respect to compound semiconductors attracting attention from applied fields, such as information transmission and processing using light as a medium, microwave devices providing high-speed operation, and high-speed IC, please refer to a handbook describing their basic properties and their detailed manufacturing methods and applications.

As for characteristic applications and functional materials, the thermocouple in Table 1 is a couple of metals or alloy wires, and it is necessary for thermoelectromotive force E_0 generated at both branch ends to have linear temperature changes. This thermocouple is widely used for measuring temperature. On the other hand, the thermocouple used for the pilot light for gas appliances (preventing the flame from going out) requires large E_0 to drive an electromagnetic valve and heat and corrosion resistance. The functional characteristics have been improved by combining chromel and constantan of large E_0. The chromel of heat-resistant alloys was used as a protective cap and one end of the constantan wire was connected to the bottom of the cap. The solar cells underlined shown in two places in Table 2 are sintered bodies combining an n-type CdS and a p-type Cu_2S, featuring the applicability of the screen printing method with high mass productivity, although less efficient than amorphous and monocrystals. An (obonic) material in Table 2 is a composite material with amorphous low in thermal conductivity as a matrix with microcrystal semiconductor dispersed in it, expected to improve photoelectric and thermoelectric characteristics.

Table 1. Classification and Main Applications of Functions

Function	Property	Application
Electronic/ magnetic	Metallic quality — Conductive	Heating element, strain gauge, temperature sensor, contact/tangent point
	Metallic quality — Thermoelectric	Thermocouple, pilot flame safety device, thermocouple emitting substance
	Metallic quality — Superconductive	Josephson device, electromagnet, power storage, transmission, generator
	Semiconductivity — Conductive	Transistor, IC, FET, rectifier, magnetic field/strain gauge, switch, thermistor,* gas sensor,* pilot flame safety device*
	Semiconductivity — Photoelectric	Photoconductivity, light emitting diode, semiconductor laser, solar cell, infrared/radiation sensor, image pickup device, photosensitive plate
	Semiconductivity — Thermoelectric	Infrared (temperature) sensor,* fire alarm, thermoelectric conversion*
	Magnetism — Soft	Magnetic head, magnetic core, magnetic sensor, magnetic field, magneto-striction vibrator,
	Magnetism — Semi-rigid	Magnetic record, magnetic bubble memory, hysteresis motor
	Magnetism — Hard	Alloy magnet, ferrite magnet,* rare earth magnet
	Dielectricity — Dielectric	Large capacity condenser,* posistor,* varistor
	Dielectricity — Piezoelectric	Transmitting device,* ignition device, radio filter
	Dielectricity — Ferroelectric	Infrared sensor (ordinary temperature)* Image storage, photoelectric polarization
	Ionicity	Na·Li-S cell,* electric generation by temperature (AMTEC), oxygen gas sensor
Optical	Fluorescence	Lamp, EL, scintillator, color Braun tube
	Translucency	Transparent electrode, heat/corrosion resistant translucency
	Polarization quality	Polarization modulation, liquid crystal
	Reflection quality	Heat-resistant mirror,* single crystal laser mirror,* prevention of infrared ray reflection
	Photoconductivity	Optical fiber, (one-dimensional), wave guide line (two-dimensional)
	Absorptivity	Paint, decorative metallic sheet, radio absorption
	Radioactivity	Far infrared, infrared

[continued]

[Continuation of Table 1]

Function	Property	Application
Thermal	Cooling quality	Magnetic cooling, electronic cooling,* refrigerant
	Heat transfer quality	Insulating substrate (IC), heat pipe
	Insulating qual.	Min-K (foaming SiO_2), K_2O-TiO_2 fiber
	Expansion	Thermometer, bimetal, liquid floating temperature control
Bio-chemical	Substitute	Artificial bone,* artificial tooth,* artificial valve
	Carrier quality	Biosensor (aperture control porous substance), porous substance (catalytic carrier)*
	Catalytic substance	Porous sintered body (catalytic reaction)*
Energy related function		Solar cell, thermoelectric generation,* hydrogen storage, generating thermionic conversion,* ultrahigh temperature electrode
Mechanical function		Shape memory, heat resistant fiber, cemented carbide,* vibration prevention,* oilless bearing (ceramics, oil-bearing metal)

*: Manifestation of functionality and improved performance by sintering.
_: Improved practicability.

Table 2. Metals and Their Compounds as Functional Materials

- Magnetic material
  - Permeability
    - Power magnetic core (silicon steel, amorphous alloy, quenched high silicon steel)
    - High permeability (Sendust, ferrite, N-group alloy, B/C added quenched material)
  - Semi-rigid magnetism
    - Magnetic recording material (Cr-Co, Co-Ni, ferrite, chrome oxide)
    - Photomagnetic recording material (GdTbFe, GdFeBi, DyFe, PtMnSb, garnet)
    - Drive material (Co-Cr, Fe-Mn, Fe-Ni, Alunicl
  - Permanent magnet
    - Alloy magnet (Fe-Cr-Co, Fe-Cu-Ni, columnar crystal alnico)
    - Ferrite magnet
    - High performance magnet ($SmCo_5$, Sm_2Co_{17}, $Nd_2Fe_{14}B$ system)
  - Magnetic strain ($SmFe_2$, $TbFe_2$, $Tb_{1-x}DyFe_2$, Ni-Cu-Co ferrite, quenched material)
  - Magnetic fluid (Fe_3O_4 system, FeN_x, Fe, Co)
- Optical material
  - Reflection quality (Al, Cu, Ag, Au, TiN, W·Mo single crystal)
  - Absorptivity (coloring, coloring metal, AuN_x, WC+Co film)
  - Radioactivity (C, P, W·Mo+Pt clad, alloy heating element, SiC, Ca+ZrO_2)
- Thermal functional material
  - Temperature sensor (bimetal, thermocouple, Pt, W, Pt-Co, amorphous, magnetic substance)
  - Magnetic refrigeration (Gd, Gd-Al,Gd-Sn, $DyTi_2O_2$, $Cd(OH)_4$)
  - Thermoelectric cooling (Bi_2Te_3 system, AgTlTe-CuTlTe system, BiSb)
  - Heat pipe (Cu, Al, Ni, stainless, Inconel)
- Energy related material
  - Thermoelectric generation (Bi_2Te_3 sintered body, PbTe, Si-Ge, $FeSi_2$, amorphous, (obonic) material)
  - Thermionic conversion (W, Mo, LaB_6, HfC)
  - Temperature different cell AMTEC (As electrode Mo, W, Nb, Ti, TiN)
  - Hydrogen storage ($LaNiH_5$, $FeTiH_{\sim 1.9}$, VH_3, NbH_2, MgH_2+Ni)
  - Hydrogen generation (Ti, Pt, CdTe-(Pt·Ag), ZnTe-(Pt·Ag), GaAs, GaP)
- Mechanical material
  - Shape memory (TiNi, Ni-Al,Au-Cd, Cu-Zn, In-Tl, their alloys)
  - Bearing (Pb-Sn,Cu-Pb, Al-Sn, Cu alloys, Zn alloys)
  - Cemented carbide (WC-Co, WC-TI-Co, WC-TiC-TaC, TiN, TiB_2, Cermet)
  - Heat-resistant fiber (B coating W, C, SiC, BN)
- Acoustic material
  - Diaphragm (Be, Mg, Al, Ni, Ti, their alloys, hard high elastic coating material)
  - Vibration prevention (12Cr steel, Mn-Cu, Ni-Ti, Zn-Al, Cu-Zn-Al, Mg alloys)
  - Musical instrument (piano wire, brass, high strength cast iron)
- Biochemical material
  - Substitute (Pt, Au, Ag, Pb, Al alloys, stainless, Ni-Co, Co-Cr, NiTi

As stated so far, many functional materials effectively utilize functions resulting from combining substances of two or more types. In order to develop materials and applications, it is necessary to understand fully manifestation mechanisms, interactions among multiple substances, and combinations of optimum substances. With different crystal structures and shapes, their manufacturing processes also differ. However, given the relationship among their functions, materials and manufacturing processes, a guideline to developing new functional materials can be provided. The following are descriptions of a few functional materials utilizing properties specific to sintered bodies to help understand this relationship.

3. Functional Sintered Bodies

3.1 Automatic Temperature Control Heating Element

Semiconductor heating elements enabling specific resistance to be remarkable as temperature rises are used for recent clean hot air type heaters and hair dryers. This heating element enables temperature to be automatically controlled since it is heated when energized, and a current decreases when a certain temperature is reached, but increases again when it gets cold, thus called an automatic temperature control heating element or a heating element device. This heating element utilizes functions of sintered bodies with crystal grains and the pore ratio of semiconductive ballium titanate controlled.

It is well known that pure ballium titanate $BaTiO_3$ is a ferroelectric substance with Curie point T_c at 393 K and an insulator with specific resistance ρ at room temperature of about $10^{10}\Omega m$. The addition of Bi, Nb, etc., rare earth elements forming donor levels, to this substance yields an n type semiconductor with low resistance whose ρ at room temperature is about $0.2\Omega m$. This semiconductive $BaTiO_3$ sintered body shows, as is found with temperature changes of ρ shown in Figure 1, abnormal positive temperature coefficient (PTC), and PTS of ρ is closely related to T_c, but does not appear with monocrystals. Such a sintered body is called a PCT thermistor or a posistor corresponding to negative temperature coefficient thermistors of general semiconductors. T_c of $BaTiO_3$ becomes variable to 300~570 K by adding Sr, Zn, and Pb and start temperature of PTC characteristic can be freely controlled in this temperature range. The applications of this characteristic requires: 1) ρ_{max}/ρ_{min}, a ratio of maximum ρ to minimum ρ before and after T_c, and PCT are large; 2) pressure proof voltage in the negative temperature coefficient area is high; and 3) PTC characteristic is stable.

It has been recognized by many researchers that a manifestation mechanism of PTC is interaction between T_c and a crystal grain boundary layer, which can be basically understood with a grain boundary blocking layer model by Heywang. Figure 2 shows energy bands of this model before and after T_c in the periphery of the grain boundary. Electrons in the periphery of the grain boundary generated by ionized donor concentration N_d in the drawing are captured by surface acceptor N_s forming a deep donor level, and a depletion with an effective width of $b = N_s/N_d$ is formed. This results in ϕ, barrier's height in the grain boundary, and the following relationship of its dependency on

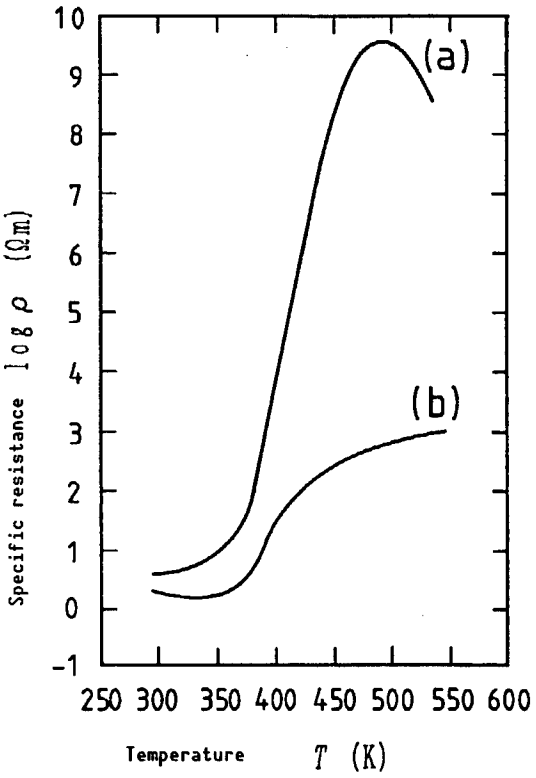

Figure 1. PTC Characteristic of Semiconductive $BaTiO_3$
(a) Fine grading structure which has become porous
(b) Grain disturbing structure which has become close

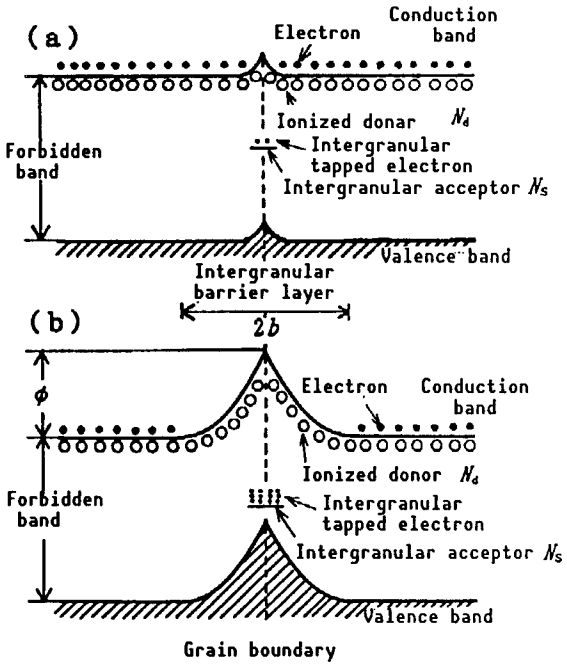

Figure 2. Heywang's Band Models Near Crystal Grain Boundary
(a) Curie point, T_c or below
(b) Curie point, T_c or above

dielectric constant ϵ can be obtained from Poisson's equation: $\phi = e_2N^2_s/(\epsilon\epsilon_0N_d)$ where e and ϵ_0 represent a raw electric charge, and a dielectric constant in vacuum, respectively. Therefore, suppose specific resistance in crystal grains were ρ_0 and Boltzmann's constant were k, the following can be obtained:

$$\rho = \rho_0 \exp\left(\frac{\phi}{kT}\right) \qquad (1)$$

A rapid increase of ρ with temperature can be explained with expression (1) since ϵ decreases according to Curie-Weiss' law of $\epsilon = C/(T-T_c)$; however, with Heywang's model, it is not clear that ρ becomes low in the area below T_c, so a manifestation mechanism of PTC has not yet been shown.

It is important in manufacturing semiconductive $BaTiO_3$ superior in PTC characteristics to consider a manufacturing process for porous sintered bodies with crystal grains whose interior has as small ρ as possible and whose surface is a high resistant layer adequately oxidized with few defects. This is also an interesting problem with respect to the clarification of a PTC manifestation mechanism.

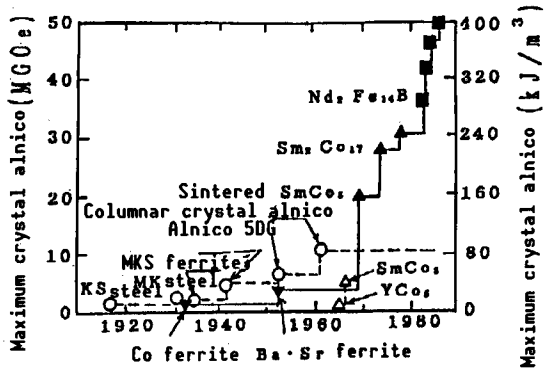

Figure 3. Changes With Year of Maximum Energy Product of High Performance Magnets

3.2 High Performance Magnets

Of all magnetic materials, a permanent magnetic material features its large coercive force H_c, and the performance of magnets is evaluated by the maximum value of the product of residual magnetic flux density B_r and H_c, i.e., the magnitude of maximum magnetic energy product $(BH)_{max}$. Thus, the conditions necessary for a high performance magnet are: 1) large saturation magnetization I_s for high B_r; 2) large uniaxial anisotropic coefficient; and 3) high Curie point temperature to prevent B_r heat deterioration. These three physical properties are specific to materials, and to find materials provided with such properties and manufacturing technology capable of enlarging H_c, an external property, while retaining these physical properties, and of coinciding magnetization direction with the ease axis are closely related to the development of high performance magnets.

Figure 3 shows changes in the maximum magnetic energy product by year used for evaluating magnet performance. Circles and white triangles represent alloy magnets, oxides, and intermetallic compound magnets, and black triangles and squares sintered magnets. Hoffer and Strnat found YCo_5 having an extremely large anisotropic coefficient, and claimed that such intermetallic compounds have high H_c. With this as a momentum, the development of rare earth magnets started, and Strnat obtained a high coercive force of 600 kA/m and $(BH)_{max}$ of 64 kJ/m^3 with $SmCo_5$, thereby demonstrating a magnet with a high coercive force.

The liquid phase sintering method, the mainstream of today's rare earth magnet manufacturing technology, was developed by Martin and Benz, which has enabled $(BH)_{max}$ to be raised higher than 160 kJ/m^3 by the in-magnetic field press/sintering method. The liquid sintering method involves the following processes: 1) an ingot material of RCo_5 with excessive rare earth metal R is made into powder; 2) the powder is allowed to undergo cold press in a magnetic field to form a compact with particles oriented in magnetization ease axis (c-axis) direction; and 3) the compact is sintered at a temperature of 1,270-1,470 K at which R excess phase with a low melting point melts. High H_c can be obtained by enabling homogenized composition and matching of crystal grain boundaries through solution processing and by reheating at lower temperature.

By this method, Charles, et al., have obtained $(BH)_{max}$ of 207 kJ/m^3 with (Sm, Pr)Co_5 with part of Sm substituted by Pr.

With I_s higher than that of $SmCo_5$ system, Sm_2Co_{17} was expected to show higher $(BH)_{max}$, but, with single phase compounds, performance exceeding that of $SmCo_5$ could not be obtained due to low H_c. However, heat treatment of an Sm_2(Co, Fe, Cu) alloy with part of Co substituted by Cu and Fe results in two-phase separated structure in which Cu excess compounds are dispersed. It is believed that the difference in magnetic wall energy between the two phases causes the magnetic wall to be pinned, thereby resulting in the birth of high H_c. This alloy is manufactured, similar to the $SmCo_5$ system, by liquid phase sintering, followed by multistage heat treatment. The addition of Zr and Ti to it results in effective two-phase separation thereby providing magnets with high performance showing $(BH)_{max}$ of 240 kJ/m^3. The literature (4) [not published] involves an explanation on the progress of $SmCo_5$ and Sm_2Co_{17} magnets, facilitating learning these magnets in general.

Tetragonal $Nd_2Fe_{14}B$, totally different in composition from the above magnets, is less expensive because it uses Nd, richer than Sm as a rare earth metal. It is manufactured, similar to $SmCo_5$ system, by liquid phase sintering, followed by heat treatment at about 870 K, with techniques specific to $Nd_2Fe_{14}B$ magnets required at every stage. Some magnets of this type have provided, although experimentally, $(BH)_{max}$ of 405 kJ/m^3, thereby attracting most attention as a high performance magnet. The magnet, however, has disadvantages of major temperature changes of B_r due to its low Curie point of 580 K and the susceptibility to oxidation because of its main component being Fe. The former can be improved by adding Co or Ga with $(BH)_{max}$ of its practical counterparts being about 290 kJ/m^3 (catalog value). The latter is improved by corrosion treatment according to service needs. Magnets by mechanical processing have currently been developed, providing $(BH)_{max}$ of about 280 kJ/m^3.

The above sintered magnets show square demagnetization curves with high H_c rather in the R excess area than in stoichiometric compositions. For example, observation with an electron microscope of an $Nd_2Fe_{14}B$ magnet finds that R-excess extremely fine layers surround crystal grains to suppress the occurrence of reverse magnetic domains, while microstructure of the crystal grain boundary is not clear before heat treatment with low H_c. Since R-excess phases, besides magnetic wall pinning, contribute to the grain boundary to improve H_c not only with an $SmCo_5$ magnet of the same reverse magnetic domain generation type but with Sm_2Co_{17} system, control of crystal grains and the grain boundary is important technology with respect to high performance magnets. Table 3 shows magnetic characteristics of main high performance magnets.

3.3 Thermoelectric Conversion

A thermocouple combining p-type and n-type semiconductors, called a thermoelectric conversion device, is one solid-state energy conversion in which carriers in semiconductors work as a Rankine cycle or a heat pump. With no mechanical factors, the energy conversion unit has no vibration or noise, thereby enabling heat↔electric energy conversion with high reliability. Its applications cover a wide range from consumer appliances to space development,

Table 3. Characteristics of Main High Performance Magnets

Composition	B_r (T)	H_c (kA/m)	$(BH)_{max}$ (kJ/m)	Manufacturing process
$SmCo_2$	1.00	790	190	Press sintering in
$(Sm_{0.42}Pr_{0.58})Co_5$	1.03	800	207	magnetic field
$Sm(Co_{0.69}Fe_{0.20}Cu_{0.10}Zn_{0.01})_{7.4}$	1.11	520	240	"
$Nd_{15}Fe_{77}B_8$	1.20	979	287	"
$Nd_{12.4}Fe_{80.7}B_{6.5}$	1.45	736	405[a]	"
$Nd_{15}(Fe_{0.8}Co_{0.2})_{77}B_6$	1.21	820	259	"
$Nd_{15}(Fe_{0.7}Ga_{0.02}B_{0.08})_{5.6}$	1.22	915	280[b]	"
$Nd_{14}Fe_{79.25}Ga_{0.75}B_6$	1.24	915	287	MQPF
$Nd_{14}Fe_{71.75}Co_{0.76}Ga_{0.75}B_6$	1.24	915	287	"

(a) Experimental scale
(b) Values at 433 K
MQPF: Upsetting of melt quenched flake powder after hot press

and thermoelements and thermoelectric cooling devices are indispensable for independent power sources for use in space and seabed and precision thermostatic control of semiconductor manufacturing processes and lasers for optical communications use, respectively.

Letting temperatures at the high temperature end and the low temperature end be T_h and T_0, respectively, the maximum generating efficiency of a material comprising a thermoelement can be expressed as

$$\eta_{max} = \frac{T_h - T_0}{T_h} \frac{M-1}{M+T_0/T_h} \tag{2}$$

$$M = \sqrt{1+Z(T_h+T_0)/2} \tag{3}$$

$$Z = \alpha^2/(\kappa\rho) \tag{4}$$

where α and κ represent thermoelectric power and thermal conductivity. Also, expression (2) can be approximated as:

$$\eta_{max} \fallingdotseq 4 \times 10^{-4} T_h^{3/2} Z^{2/3} \tag{5}$$

On the other hand, the maximum performance coefficient of thermoelectric cooling can be expressed as:

$$\phi_{max} = \frac{T_0}{T_h - T_0} \frac{M+T_h/T_0}{M-1} \tag{6}$$

When the endothermic unit is completely insulated to stop heat inflow, T_0 decreases most, and letting $\phi_{max} = 0$, the following expression is deduced:

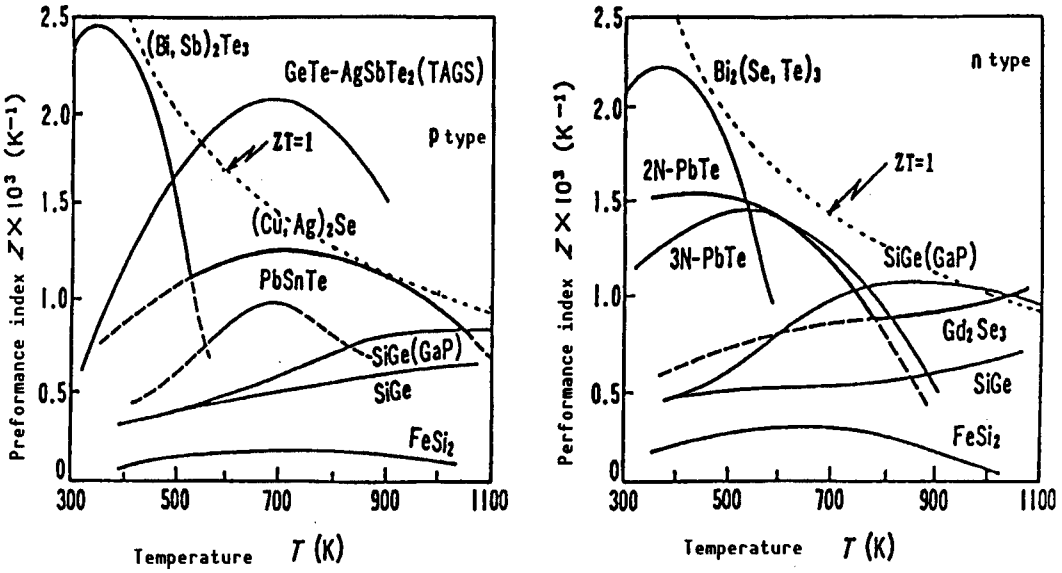

Figure 4. Relationship Between Performance Index and Temperature of Practical Thermoelectric Conversion Materials

$$(T_h - T_0)_{max} = \frac{1}{2} Z T_0^2 \tag{7}$$

In order to obtain high efficiency, as is apparent from expressions (2)~(7), a heat-resistant material with large Z enabling T_h to be high is desirable. Z in expression (4) and ZT in expression (5) are utilized for aptitude evaluation of thermoelectric conversion materials, and called performance index and dimensionless performance index, respectively. In addition, performance index of a thermoelement is expressed as $Z_{pn} = (\alpha_p - \alpha^n)^2 / (\sqrt{\kappa_p \rho_p} + \sqrt{\kappa_n \rho_n})^2$ with subscripts corresponding to p-type and n-type materials. As is found in Figure 4 showing the relationship between Z and temperature with practical thermoelectric conversion materials, the greater the Z value of a material, the greater temperature changes it undergoes to show its intrinsic value.

With a cooling device combining $(Bi,Sb)_2Te_3$ and $Bi_2(Se,Te)_3$ in Figure 4, its maximum cooling temperature is about 65 K when T_h = 300 K. $FeSi_2$, although small in Z, is useful as a consumer thermoelement utilizable in high temperature atmosphere. SiGe(GaP) is an $Si_{0.8}Ge_{0.2}$ sintered body added by 5 mass% GaP compound, a material obtained by decreasing κ and enlarging Z in expression (4). With its η_{max} reaching as high as 11.5~14.3 percent, this sintered body is currently catching attention most as a power source for space use.

The reduction of κ by sintered bodies can be obtained by effectively utilizing scattering of short wavelength phonons by crystal distortion fields obtained by solid solution of multiple elements and scattering of long wavelength phonons by the crystal grain boundary of a sintered body. The reduction effect of the latter also appears in Bi_2Te_3 compounds, a low temperature material, whose results are shown in Figure 5. The specimens in this drawing are a single crystal (broken line) and sintered bodies of the same composition with

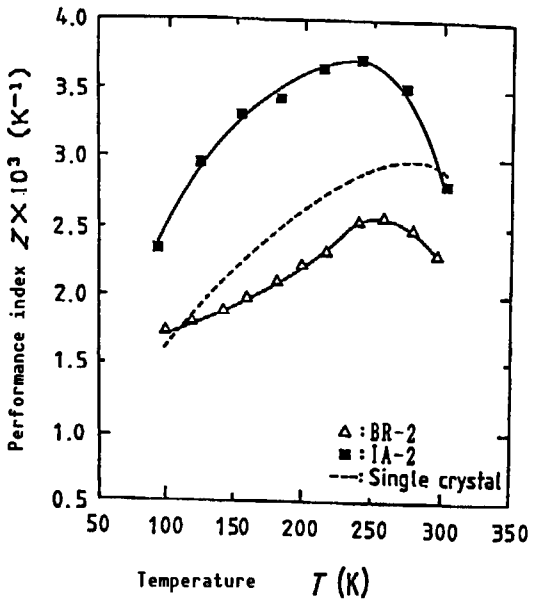

Figure 5. Relationship Between Performance Index and Temperature of n-Type $Bi_2Te_{2.85}Se_{0.18}$ Sintered Body
IA-2: Specimen obtained by heat treatment of a sintered body in hydrogen.
BR-2: Specimen obtained by hydrogen reduction of presintered powder.

carrier concentration controlled at $10^{25}m^3$. The sintered body (IA-2) heat treated in hydrogen provides mobility equivalent to that of a single crystal due to the reduction of oxygen resulting in decreased mobility, so Z becomes remarkably large in terms of a result of the effect of reducing κ by the crystal grain boundary.

4. Conclusion

Selecting a few oxides and intermetallic compounds from among various functional materials, this article has so far described only their limitations, such as functional manifestation and improved characteristics by interaction among crystal grains and grain boundaries. These functional materials seem to function themselves, but, in reality, their crystal boundaries are responsible for energy conversion. Functional devices to convert physical quantity, in particular, utilize combined effects by interaction among dissimilar materials, dissimilar characteristics and gases and liquids in the periphery of materials, multiple interesting problems remaining unsolved.

Machining of Intermetallic Compounds

916C1004F Tokyo KINZOKU GAKKAI SEMINA KINZOKUKAN KAGOBUTSU in Japanese
1 Jun 90 pp 45-51

[Article by Shuji Hanada, Metal Material Research Institute, Tohoku University]

[Text] **1. Introduction**

The intermetallic compounds NiTi, Nb_3Fe, MnAl, $Fe_3(Al, Si)$, among others, represent those which are practically available by molding and machining their ingots based on good plasticity properties. These represent the exception rather than the rule in view of all the diverse kinds and large number of intermetallic compounds. Most intermetallic compounds are characterized by their extreme hardness and brittleness and hence belong to the category of materials which are hardest to deal with by machining based on plasticity. With the progress in research on the mechanical properties of intermetallic compounds in recent years, the nature of brittleness has been clarified, mechanisms for improving ductility suggested, and research aimed at establishing new machining methods is under way. In addition to research and development for machining methods of intermetallic compounds on the basis of plasticity, it is expected that R&D on other machining processes such as powder metallurgy methods and precision casting methods will become more prevalent for brittle intermetallic compounds. Along with this trend, it is conceivable that development of the machining method based on plasticity will grow in importance with the aim of effectively utilizing the high productivity, improved quality, and high uniformity of the product that characterizes the method. This paper gives an introductory description of the recent research on the machining of intermetallic compounds and outlines the control of material-science factors important in machining intermetallic compounds.

2. Structural Type $L1_2$

The compound Ni_3Fe is among the few ordered alloys that allow various plastic machining methods such as forging and rolling even for a large ingot. The alloy is easily subjected to plastic machining, but suffers, though very infrequently, cracking during forging, and particularly those alloys which involve additional elements for improvement of magnetic properties do.

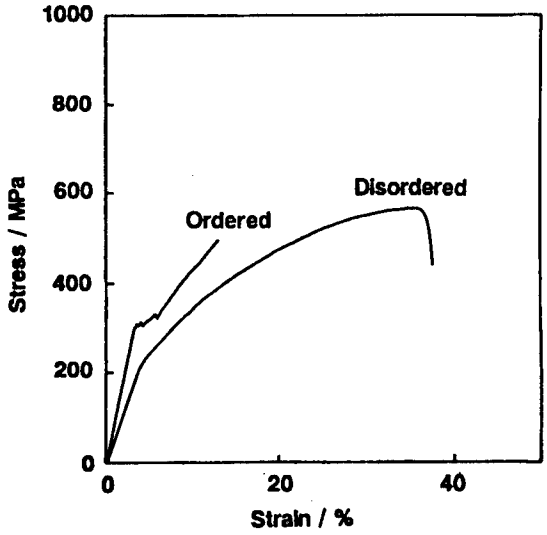

Figure 1. Strain–Stress Curve for the Randomly Oriented Polycrystal Ni_3Fe

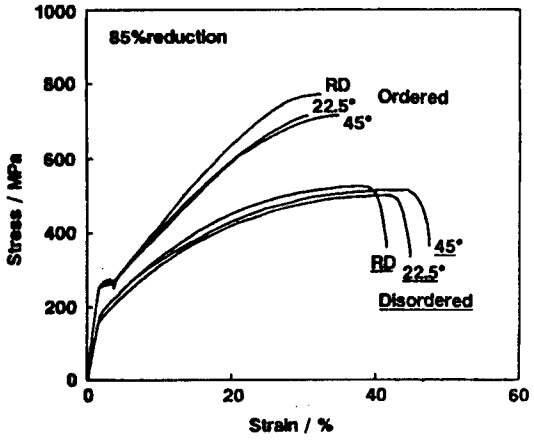

Figure 2. Strain–Stress Curve for Ni_3Fe Polycrystal (Reduction of 85 percent prior to recrystallization)

It is extremely important to clarify the mechanism of fracture—a study which will also serve to add to the understanding of the fracture mechanism of the Ll_2 type alloy in general.

With the ordered–disordered transition taking place at 516°C, the degree of the order may be changed extensively by heat treatment. The heat treatment will also contribute to a major change in the aggregation structure following recrystallization, since the treatment allows development of cubic orientation as the aggregate structure. Therefore, the heat treatment allows a systematic investigation of the effect of the degree of order and grain boundary structure on Ll_2 type alloys. Figure 1 shows a plot of the stress–strain curve for the (random) polycrystals of the alloy Ni_3Fe of grain diameter 30 μm, which completely lacks a priority orientation. The ordered specimens have a high yield strength and a limited elongation and undergo rupture without local shrinkage in contrast to the disordered specimens that have a low yield strength and a large elongation and rupture with local shrinkage. The ruptured surface of the former is covered with grain boundary rupture whereas that of the latter is with dimples located within grains.

Figure 2 shows the same curve for specimens subjected to an 85 percent reduction prior to recrystallization and in which cubic orientation is developed to some extent. The direction of the tensile strength makes an angle of 0°, 22.5°, or 45° with the direction of rolling (RD). Increase in elongation for the ordered specimen is notable as compared with Figure 1. At a reduction rate of 97 percent, a sharp cubic orientation develops as an aggregation structure following recrystallization, thereby allowing increases in elongation. The relation between the development of cubic orientation in ordered specimens and the relevant stress–strain curve is shown in Figure 3 which proves that local shrinkage emerges with increasing development of cubic orientation and hence

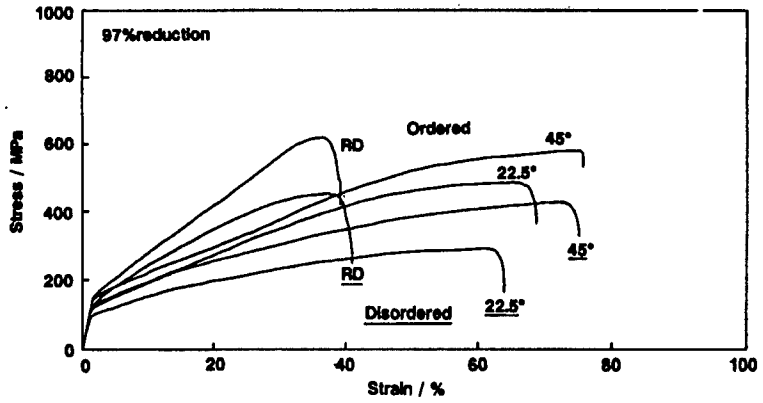

Figure 3. Strain-Stress Curve for Ni_3Fe Crystal (Reduction of 97 percent prior to recrystallization)

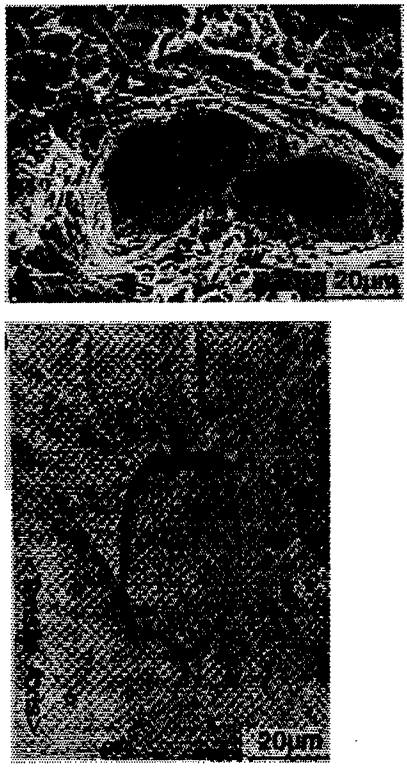

Figure 4. (a) Grain-Boundary Facet Seen Over the Fractured Surface Having Undergone Reduction (of 97 percent) (b) Grain-Boundary Crack Seen Over the Surface of the Specimen

with increasing elongation. Observation of the ruptured surface proves that the area ratio of the ruptured grain boundaries is 100 percent for the random, nonoriented specimens and falls to 85, 60, and 5 percent with reduction-rate increases to 85, 90, and 93 percent, respectively, reaching below 1 percent at 97 percent reduction. A picture of the ruptured grain boundaries for specimens with intensively developed cubic orientation at 97 percent reduction is shown in Figure 4. A grain boundary facet observed in ruptured surfaces is shown in (a) and a grain boundary crack found over the specimen surface in (b).

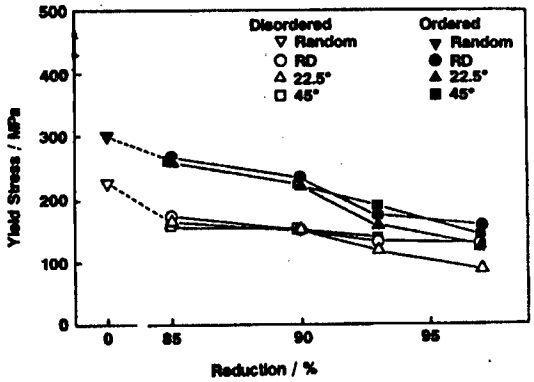

Figure 5. Effect on Yield Stress of the Rate of Reduction Prior to Recrystallization

Notable in (b) is the fact that the direction of slipbands for grains located at the center is different from those in surrounding areas. This proves that the grains at the center are shifted substantially from the cubic orientation since those in the surrounding areas are all confirmed to be in near cubic orientation on the ground of the direction of their slipband. It is concluded that the grain boundary crack develops in elevated angle grain boundaries. Figure 5 plots the relationship between yield stress and rate of reduction before recrystallization. In general, yield stress is high in ordered specimens, but falls with increasing reduction rate and hence with increasing development of cubic orientation. With the development of cubic orientation the number of low-angle grain boundaries increases, which allows the dislocation to easily penetrate the boundaries. In elevated angle grain boundaries, on the other hand, the dislocation is liable to accumulate, leading to grain boundary rupture. This tendency is increasingly clear with increasingly ordered specimens, a fact which was explained with consistency by King and Yoo through the use of a model for grain boundary rupture. According to their explanation, dislocations occurring inside the grain are absorbed by the grain boundary or penetrate the boundary by virtue of their reaction with grain boundary dislocations and, where this reaction is substantially blocked, numbers of dislocations accumulated in the vicinity of the grain boundary increases, leading to development of stress concentration and to grain boundary rupture. As seen in Table 1, numbers of possible dislocation reactions fall substantially where the specimens are ordered ones. The basic concept involved is that the introduction of dislocation at a grain boundary does not induce such a dislocation reaction as to disturb the ordered structure in the vicinity of the grain boundary. More intriguing in connection with the data in Table 1 is the fact that dislocations are more liable to occur in the corresponding grain boundary of $\Sigma = 3N$ than in the grain boundary of $\Sigma \neq 3N$.

Haneda, et al., studied grain boundary rupture behavior for Ni_3Al polycrystals in connection with the corresponding grain boundary and proved that low-angle grain boundaries and the $\Sigma 3$ corresponding grain boundaries are less subject to rupture than the others. This result is fully explained by use of the above model of King and Yoo. If the model is at all applicable to the alloy Ni_3Al, the alloy may have its ductility improved by adjusting its grain boundary to $\Sigma = 3N$--a grain boundary technology which has yet to be established.

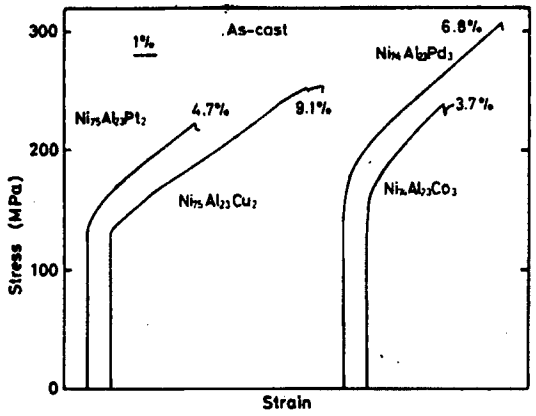

Figure 6. Strain–Stress Curve for Cast Specimen of Ni–Rich Ni_3Al Series of Alloys Involving Addition of a Third Element

Table 1. Number of Possible Grain Boundary Dislocation Reactions in $L1_2$ Alloys

	Absorption		Transmission	
	$\Sigma = 3N$	$\Sigma \neq 3N$	$\Sigma = 3N$	$\Sigma \neq 3N$
Disordered (fcc)	12	6	288	216
Ordered (pc)	3	0	72	72
	(Possible 30)		(Possible 1800)	

The ductility of Ni_3Al has been improved by the addition of B, which causes the grain boundary bonding strength to increase, but the attempt to produce a large ingot from the B-added Ni_3Al by the ordinary fusion-and-casting has encountered extreme difficulty in plastic machining, conceivably because of development of gross dendrites and resulting segregation of Al and B. Therefore, we hope to develop alloys of the Ni_3Al type which allow easy plastic machining for its large ingots and which hence are free of the segregation of their elements that causes decreased plastic machinability. The alloy is also attracting attention for its possible application in matrixes of composite materials. The question involved here is blocking interface reaction between the matrix and the reinforcement phase and hence development of methods for surface treatment for the reinforcement phase and for improvement of qualities of the matrix by adding other elements—elements which preferably increase the ductility of this alloy. From this, we have recently systematically studied the improvement of ductility of the alloy as shown in Figure 6—a stress-strain plot for as-cast specimens involving Ni-rich Ni_3Al with Pd, Pt, Co, or Cu added at 2~3 percent. The specimens, which possibly have the L2 type structure and are of single phase, exhibit 3~9 percent plastic elongation. A study on improving ductility of the alloy Ni_3Al by adding a third element has been carried out on the basis of whether the third element substitutes at the Ni or

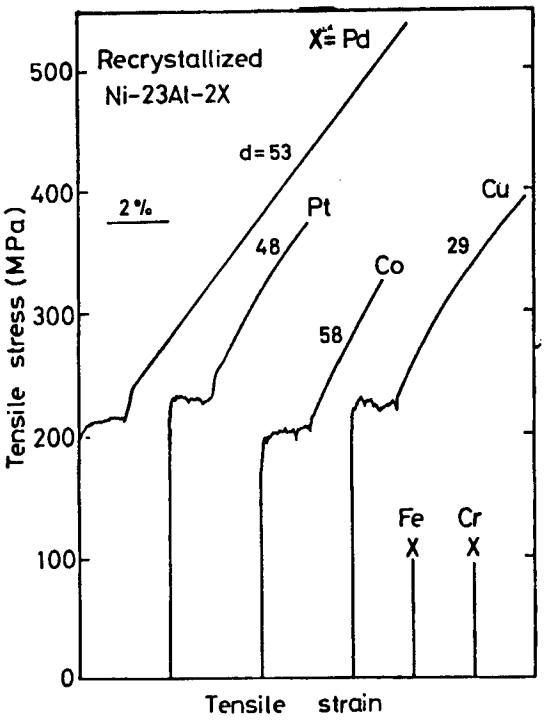

Figure 7. Strain-Stress Curve for Recrystallized Specimens of Ni-23Al-2X (X = Pd, Pt, Co, Cu, Fe, Cr)

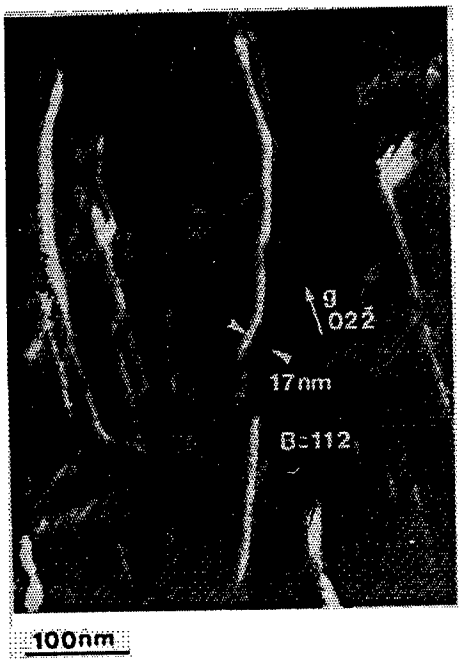

Figure 8. Ordered-Lattice Dislocation for Ni-23Al-2Pd

Al site. For example, Co and Cu have been studied in the form of $(Ni, Co)_3Al$ and $(Ni, Cu)_3Al$ because they both substitute for Ni and are classified as elements which do not contribute to improving ductility. Nevertheless, both elements provide wide ranges of solid solutions of the γ' phase when added to the alloy and hence allow evaluation of their addition effects in the form of Ni-23Al-2X. In Figure 7 is plotted stress-strain curves for the specimen of Ni-23Al-2X subjected to recrystallization following reduction (rolling). The elements Fe and Cr do not allow any plastic elongation after recrystallization, but others allow 5~10 percent elongation. Such improved ductility of the Ni-23Al-2X alloy is attributed to a breakdown of ordered lattice dislocation into partial dislocation. Figure 8 is a picture, as observed by a weak beam method, of the microstructure of the alloy Ni-23Al-2X into which dislocations have been introduced by the rolling (reduction) of the alloy. The ordered-lattice dislocations are seen to have been broken down into the ordered-lattice partial dislocations with a distance of about 18 nm, which is much larger than that of several nm for Ni-25Al reported so far. This suggests that the addition of Pd lowered the energy necessary for transition to the ordered-lattice structure. As seen in Figure 9, the temperature for ordered-to-disordered transition falls as the composition shifts from Ni-25Al to the Al-poor side.

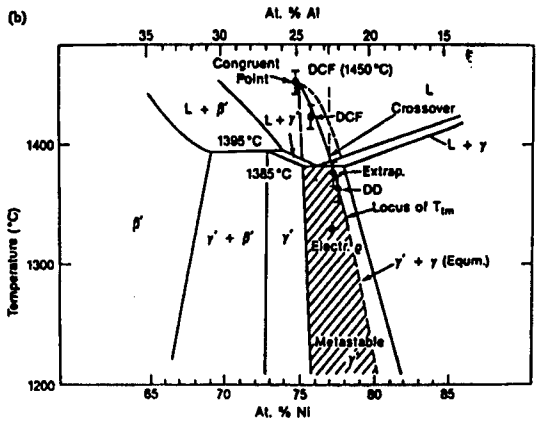

Figure 9. Effects of the Composition on the Temperature for Ordered-Disordered Transition in Ni_3Al

In response to lowering the energy required for the relevant transition, rapidly-liquid-cooled Ni-23Al allows APD (anti-phase domain) to be seen (Figure 10(a)). Addition of Pd makes this trend more distinct (Figure 10(b)).

The size of APD is as small with Cu and Co additions as it is with Pd, whereas the APD, though observable, is large in size with Fe, Mn, or Cr addition, each of which failed to improve the ductility of the alloy. In the case of X = Ti, V, or Si, the alloy Ni-23Al-2X proves to be so brittle that it does not allow reduction (rolling) treatment. The ribbons produced from this specimen do not present any observable APD. Such changes in the APD microstructure with varying alloy elements is explained by the thermodynamic stability of the γ and γ' phases of the three-element system Ni-Al-X as suggested by Jia.

Figure 11 shows the relationship between the distribution coefficient for γ/γ' phases and Ni-X, Al-X reciprocal action parameters. As can be seen, addition of γ brings about line structure and high ductility of the APD, while γ' addition produces roughness and high brittleness of the APD. It is presumed, although there is no direct evidence yet, that the improvement of ductility accompanying the fall of energy for lattice orderliness is associated with a change in the grain boundary structure and the fall of stress concentration at the boundary. Although there is no available assessment on the application of plastic machining in large ingots of the alloys of Ni_3Al series discussed above or any study on the availability of the alloy for matrixes of composite material, research on this series of alloys may conceivably be further enhanced because of the increased freedom in the designing of the alloy.

3. B2-Type Structure

The alloy NiAl, melting at 1638°C and of B2 type structure, has come to the limelight because of its possible application in single crystal alloy for high-temperature structural materials and in matrixes of composite materials, though it is highly brittle at room temperatures. The single crystal undergoes plastic deformation by compression and is more ductile in the other

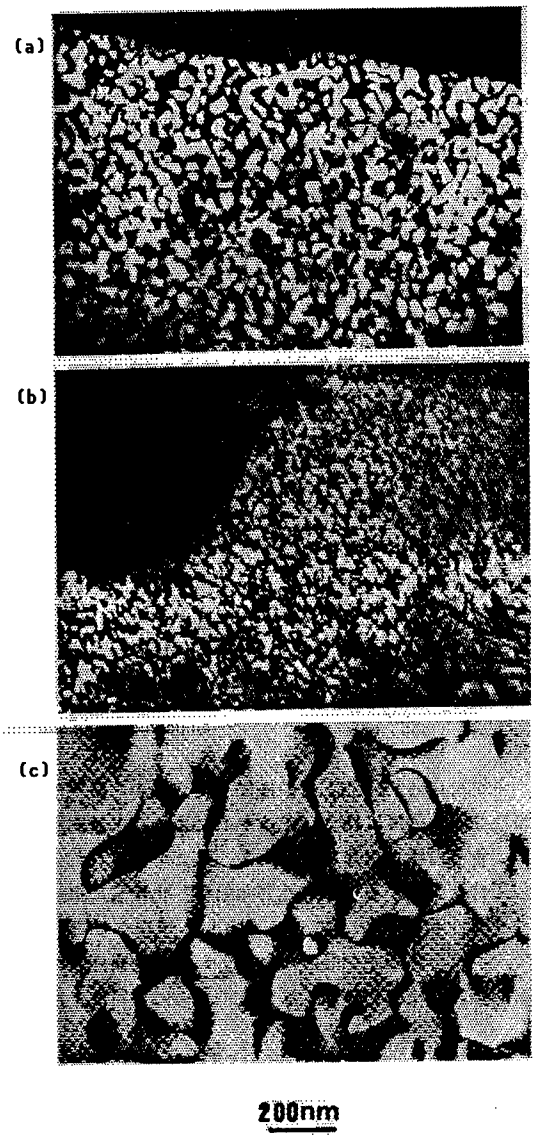

Figure 10. Anti-Phase Domain (APD) Microstructure of $L1_2$ Alloy
(a) Ni-23Al; (b) Ni-23Al-2Pd; (c) Ni-23Al-2Mn

orientations than the <100>, allowing over 50 percent plastic strain depending on directions. Yet it shows little plastic strain when subjected to deformation by extension. The active slippage system at room temperature shows 100}<001> and 110}<001>, where von Mises' conditions are not satisfied. (The <111> slippage occurs when it is compressed in the orientation <001>, where the critical breakdown shear stress is notably higher than for the other systems.) These deformation characteristics for NiAl single crystals are in striking contrast to those of Ni_3Al single crystals which affords large rupture elongation by extension and whose active slip system belongs to {111}<110>, satisfying von Mises' conditions. It hardly seems possible to improve ductility for NiAl polycrystals at room temperature. Rozner and Wasillewski, and Hahn and Vedula, reported plastic elongation of some 2 percent for the

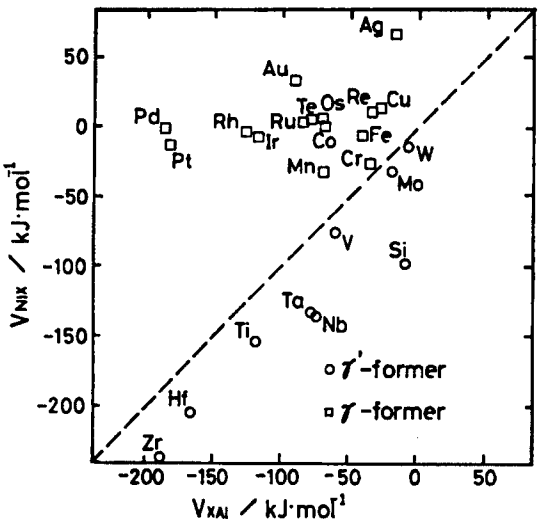

Figure 11. Relationship Between the Coefficient of Distribution for the γ and γ' Phases and Reciprocal-Reaction Parameter for Ni-X and Al-X

compound of fine particles in the stoichiometric composition with the result reconfirmed recently by George and Liu. Schulson and Barker proved that the ductility of the alloy in fine particles grows with rising temperature and exhibits an elongation of over 40 percent at 400°C for particles below 10 μm. Possible causes of increased ductility for fine particles of NiAl, though yet unconfirmed, are the formation of deformed microstructures and of preferential aggregation microstructures, active <111> slippage, and an increase in the area of grain boundaries which serve as the source of dislocation development. It has been proved recently that a coating of the surface of the alloy with oxide films lowers the deformation stress and improves the ductility. The reason is that the dislocation sources at the interface between the oxide film and the matrix allow dislocations to develop easier by virtue of relevant elastic and plastic constraints—an important finding for the understanding of the ductility of the alloy NiAl.

The addition of B to the alloy reduces its grain boundary rupture but enhances cleavage rupture inside the grain, with no ductility improvement, because of a rise in yield stress resulting from solid-solution hardening. It may also be due to the rise in yield stress, which results from introduction of structure defects by deviated compositions, that the alloy NiAl of a nonstoichiometric composition does not exhibit any plastic elongation. Among the questions involved in the development of the alloy as high-temperature structural materials is the improvement in high-temperature strength as well as that of ductility at room temperature. The fact that the alloy allows dislocation at high temperatures, such as extrusion of ingots, with comparative ease is an advantage in terms of molding process, but is not favored as a property for high-temperature structurals. One measure to counter this disadvantage is the addition to the alloy of an element that improves its high-temperature strength and that produces less solid-solution hardening and the other the use of the alloy for matrix in some composite materials.

The alloy FeAl, with a B2 type structure as the alloy Nial, is stable in the composition range of 35~50 at%Al at room temperature. The alloy is made up of cheap elements, can hold high strength up to temperatures of 500~600°C, and exhibits high resistance against oxidation. Therefore, it is subjected to research and development for intermediate- and high-temperature structurals. According to Crimp, et al., Fe-50 at%Al shows no elongation at room temperature, but Fe-40 at%Al does to 2 percent. In either alloy, grain boundary rupture dominates the picture, their active slippage system is identical to that of bcc, and the condition of von Mises is satisfied. The emergence of ductility in Fe-40 at%Al is closely related to a yield stress which is lower than Fe-50 at%Al, a high bonding strength of the grain boundary, and a low stress concentration of the grain boundary. It has been confirmed that, as in the case of Ni_3A and NiAl, the grain boundary bonding strength of FeAl is raised by the addition of B. The improved ductility by the addition of B has been observed in Fe-40 at%Al alone, and it is possible that the added B raises the grain boundary strength by segregation since the specimen shows rupture inside the grain. Leu, et al., recently showed that mechanical properties of FeAl suffer notable environmental effects. Table 2 lists various environmental effects on tensile tests. As can be seen, environmental factors have little affect on yield strength, but substantially affect elongation. Water vapor renders the alloy remarkably brittle, and high elongation in oxygen may possibly result from very low partial pressure of water vapor in oxygen as well as formation of protective oxides at the advancing front of cracks.

Table 2. Tensile Properties at Room Temperature for Fe-36.5 at%Al Tested Under Different Atmospheres

Test environment (Gas pressure)	Elongation (%)	Yield strength (MPa)	Ultimate tensile strength (MPa)
Air	2.2	360	412
Vacuum (<1 x 10^{-4}Pa)	5.4	352	501
Ar+4% H_2 (110 Pa)	6.1	378	558
Ar+4% H_2 (1670 Pa)	5.5	375	533
H_2O (67 Pa)	2.4	368	430
Oxygen (67 Pa)	11.3	373	677
Oil*	5.6	356	524

* Specimens were coated with silicone oil and tested in air.

4. DO_3 Type of Structure

The alloy Fe_3Al, of the DO_3 type of structure and with a DO_3-B2 transition temperature at about 550°C, shows high strength at high temperatures. In tensile tests, though the ruptured surface of the alloy, as a brittle one, is all covered with inside-grain cleavage ruptures, Fe-25 at%Al (grain diameter 150 μm) and Fe-31 at%Al (grain diameter 150 μm) undergo elongation of 8 and 5.6 percent, respectively, results which Mckamey, et al., claimed to have improved to an elongation of 13 percent by adding Cr^{20}, with the ruptured

surface showing inside-grain facet and inside-grain cleavage. The mechanism involved in this case has not been clarified. The regularity of DO_3 may possibly be lowered at room temperature by the addition of Cr since the addition of Cr, as is known, causes a lowered DO_3-B2 transition temperature; and improved ductility may be attributable to a decreased stress concentration at the grain boundary and a rise in cleavage strength which accompany the fall of the degree of orderliness above. The addition of Si to Fe_3Al, allows a rise in DO_3-B2 transition temperature as it does a rise in yield stress at room and high temperatures. The alloys $Fe_3(Al, Si)$, though lacking in ductility, display high resistance against oxidation and hence may have application in intermediate- and high-temperature structurals. The DO_3 type alloys with compositions around $Fe_3(Al_{0.35}Si_{0.65})$ are finding widespread application in soft magnetic materials, though they are extremely brittle at room temperature. At high temperature, however, a proper control of strain rate allows development of dynamic recrystallization grains from early-phase crystal grain boundaries and hence a fall in stress concentration at the grain boundary and thus renders the alloy highly ductile and capable of large plastic deformation and practically applicable in processing such as forging and rolling.

Intermetallic Compounds--SHS Process

916C1004G Tokyo KINZOKU GAKKAI SEMINA KINZOKUKAN KAGOBUTSU in Japanese
1 Jun 90 pp 53-59

[Article by Kinsei Miyamoto, Industrial Science laboratory, Osaka University]

[Text] **1. Introduction**

Self-propagating high-temperature synthesis, SHS for short, or combustion synthesis, is fairly well known as a method which yields instantaneous synthesis of compounds that involves high heat formation because of an exothermal chain reaction--particularly of compounds important as high-melting point materials such as carbides, borides, nitrides, and silicides, and of intermetallic compounds such as TiAl, CoAl, and TiNi. The chemical process was established by A.G. Merzhanov, et al., of the Soviet Union around 1967, but attention from the West, particularly the United States, has been drawn to it only since about 1981-1982 and from Japan since around 1984. The author, having information on the chemical process--the process translated then as an explosion method by trading companies which introduced the relevant technologies--considered it risky but intriguing. He then got the idea that the reaction may be induced under high pressure such that it would yield not only synthesis but also compaction. He immediately tested it by allowing the reaction to take place under pressure as high as 30,000 atm. by use of a superhigh-pressure press--an experiment that proved the reaction capable of simultaneous synthesis and sintering of intermetallic compounds, e.g., TiB_2, SiC, and TiC, into high density products without a promoting agent.

With the results substantially reported in newspapers and television in June 1984, research and development on this chemical process began to gradually grow in the nation. Ignition, with an arc torch of a pellet made of a mixture of powders of titanium and boron, triggers a dazzling spark which leads to instantaneous formation of the high-melting TiB_2.

Anyone observing this magical reaction, based simply on the law of nature, cannot but marvel at the wonderful scene. The scene also moved the author and his associates and pushed them to continued exploration of the chemical reaction.

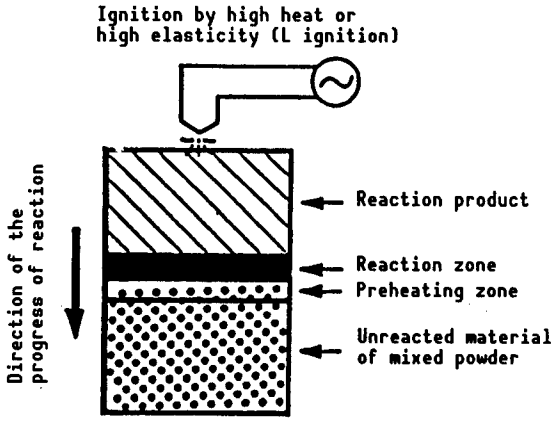

Figure 1. Propagation of Reaction in Combustion Synthesis or SHS

Since the SHS process may be available not only in the synthesis of and simultaneous synthesis and sintering of intermetallic compounds but also in coating, bonding, and other diverse applications based on different ideas, research and development of the process for application in various material processing is being carried out in the Soviet Union, the United States, Japan, etc., with practical application having partially been accomplished. In our nation, the Society for Research on SHS was organized in 1987 and with 30 corporation members and 20 individual members involved, and has been exchanging relevant information. In the United States, a similar research association was started this year. Relevant international exchanges are also going on: an international symposium for SHS was first held the year before last in San Francisco and a Japan-U.S. workshop was held in Tsukuba where Yoshiya Kaieda of the National Institute for Research of Metals served as organizer.

Triggered by research on the simultaneous synthesis and sintering, the author and his associates started R&D of synthesis of nitride composite powders and metal-nitride processing methods, both involving compression by gases coupled with SHS. This lecture deals with an introductory description of the development of the gas-pressure combustion sintering and research on the development of functionally gradient materials in which intermetallic compounds are made to involve gradient in composition by means of this new process. The functionally gradient materials represent a new composite material that has possible application in the space shuttle etc., as a super heat-resistant material capable of reducing thermal stress.

2. Simultaneous Synthesis and Sintering by SHS

Many intermetallic compounds involve heat formation as great as several ten to several hundred kJ/mol and, in the course of synthesis, give off extremely great heat, the temperature rising to 2,000~3,000 K. When a portion of the material powders mixture is ignited with explosive heat as shown in Figure 1, the relevant synthesis reaction proceeds spontaneously by the heat it produces itself, allowing synthesis of the compound in time measured in seconds without requiring heat for long hours (Table 1). The number of types of compounds thus

Table 1. Intermetallic Compounds Produced by Combustion Synthesis (SHS)

Carbide	TiC, ZrC, HiC, VC, NbC, Ta_2C, TaC, SiC, B_4C, Mo_2C
Boride	TiB_2, TiB, ZrB_2, HfB_2, HbB_2, NbB, TaB_2, TaB, MoB, MoB_2, WB
Nitride	TiN, TaN, NbN, ZrN, HfN, Si_3N_4, AlN, BN
Carbo-nitride	TiC-TiN, NbC-NbN, HfC-HfN, TaC-TaN
Silicide	$MoSi_2$, $TiSi_2$, $ZrSi_2$, $TaSi_2$, $NbSi_2$, YSi_2, $LaSi_2$
Intermetallic compound	TiNi, TiAl, NiAl,CoAl, Nb_3Al
Composite compound	$2Ti+2B+C \rightarrow TiC+TiB_2$, $3Ti+B_4C \rightarrow TiC+2TiB_2$, $Ti+Si+2C \rightarrow TiC+SiC$, $3TiO_2+4Al+3C \rightarrow 3TiC+2Al_2O_3$, $TiO_2+Zr+C \rightarrow TiC+ZrO_2$, $3SiO_2+4Al+3C \rightarrow 3SiC+2Al_2O_3$ $SiO_2+2Mg+C \rightarrow SiC+2MgO$, $2B_2O_3+4Al+C \rightarrow B_4C+2Al_2O_3$, $Wo_3+2Al+C \rightarrow WC+Al_2O_3$

produced exceeds 300. The product is in either powder form or in aggregate and pressure must be applied during reaction if the product is to be made compact. Diverse methods are presently being tested for applying pressure effectively and economically. Currently, various methods using monoaxial pressure by hot press and spring load, isotropic pressure by gas or liquid, shock consolidation, and centrifugal force are being experimented in many places. Although the authors have demonstrated the possibility of simultaneous synthesis and sintering by applying pressures as high as 30,000 atm. using a superhigh press, the method of pressure application has not proved to be practical as a means of material processing and a gas pressure method using an HIP apparatus is being developed.

3. Gas-Pressure Combustion Sintering

Combustion sintering using compression with gases similar to that by HIP is superior in pressure response and may afford near net-shape structurals. Refer to Figure 2 for a diagram of the gas pressure combustion synthesis. A green mold deaerated by applying heat is placed in a deaerated pyrex glass capsule and sealed, just as it is with the capsule method for HIP, and ignition of the mold is accomplished by the heat emitted by an ignition agent surrounding the capsule. A simple coating of BN powder was applied to the surfaces of the green mold and the capsule in order to prevent the rupture of the capsule as a result of its reaction with the green mold and the ignition agent. Any powder for SHS suffices as the ignition agent if the amount of heat liberated from it is sufficient. Thus, it can be chosen on the basis of price and on the availability of the product as a ceramic powder. The present choice is a mixture of Ti and C powders, an ignition agent which affords a temperature of 3,300 K and allows the temperature in the capsule to rise as high as 1,873 K. Argon is used for the pressurization gas, but the cheaper nitrogen gas may also be available depending on the kind of ignition agents used.

The procedure for the gas pressure combustion synthesis is as follows: The high pressure vessel is first heated to a temperature of 700°C such that the

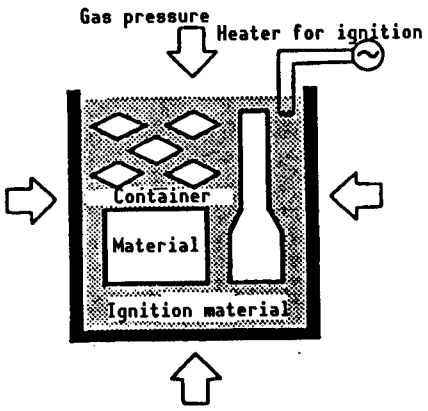

Figure 2. Diagram of the Apparatus for the Gas Pressure Combustion Sintering

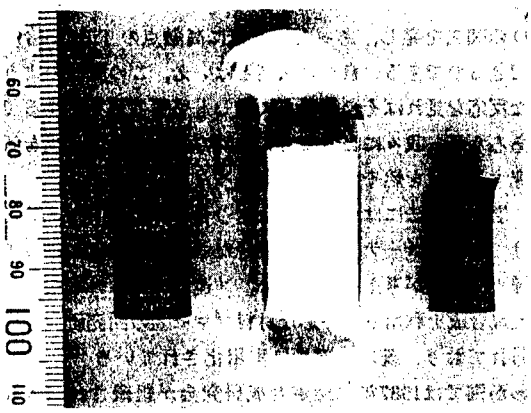

Figure 3. Specimens Produced by Gas Pressure Combustion Sintering (Left: material powders of Ti, C, Ni yet to be sintered; Middle: the material sealed into a Pyrex capsule; Right: resulting sintered TiC-Ni)

glass capsule be softened and then the argon-gas pressure is raised to a maximum of 100 MPa. Second, a current of 80 A is applied for 3 seconds to the ignition heater to start the simultaneous combustion and sintering of the material as a result of the combustion of the ignition agent. Several specimens are allowed to undergo combustion at one time by use of the ignition agent under gas pressurization. Figure 3 shows a specimen for Cermet TiC-Ni on the laboratory scale made from the powders of Ti, C, and Ni.

Combustion propagation characteristics at room temperature of an ignition agent made from Ti and C is shown in Figure 4. With increasing packing density of the agent, the cohesive force of the particles increases and the combustion is accelerated, whereas with increasing argon pressure, the combustion is decelerated. High argon pressure may possibly suppress the basic reaction process and also induce that liberation in great amounts. At an argon pressure of 100 MPa, the reaction ceases. In the preheating period at 700°C, the reaction does proceed. In the preheating period, TiC is formed in about 20 percent of the expected amount as a result of a solid-phase reaction. Heating by the ignition agent may possibly force the material in the capsule to start the reaction immediately and pushes it at a higher rate. It takes several minutes for the temperature of the ignition agent to go down to 1,000 K and the agent, during this period, gives heat to the specimens so that the reaction proceeds more completely. It is possible to sinter ceramic powders, etc., by heat supplied exclusively from the agent, although it depends on the size of the specimen.

4. Control of the Density

The synthesis of compounds by autogenous combustion is frequently accompanied by a volume reduction of 20~30 percent. Therefore, it is necessary in subjecting a material to combustion sintering for simultaneous synthesis and compaction, to use a method of applying pressure capable of countering the

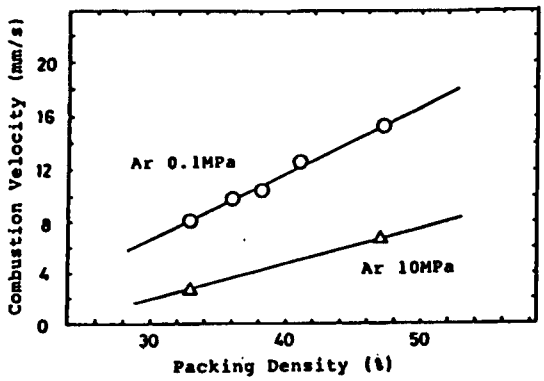

Figure 4. Velocity for Propagation of Combustion in Combustion Synthesis for Ti and C Mixture Under Argon

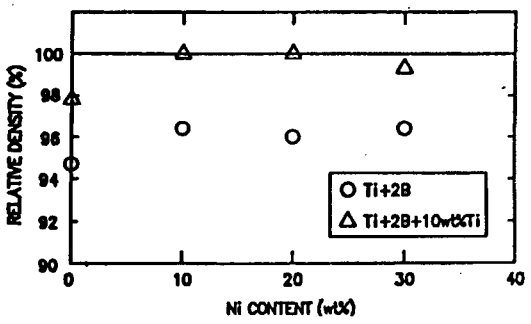

Figure 5. Density of Sintered Compacts of TiB_2–Ni Series

rapid volume reduction. Where monoaxial compression such as hot press is concerned, the friction between the die and the punch delays responses to the relevant shrinkage. The result is a lack of satisfactory density in the product, and continued heat application is often resorted to, hence, the density is raised. In the case of gas pressure combustion sintering, no question of pressure response is involved, but a vaporized compound of the material, if any is present, will prevent compaction because of the sealed system of the capsule. It is thus necessary to heat and deaerate the preconsolidated material at around 400°C as a pretreatment to remove water and other volatile matter. Figure 5 shows the density change of a sintered TiB_2–Ni made from a material mixture of Ti, B, and Ni. In cases where Ti and B are mixed stoichiometrically, the relative density remains below 96 percent, but where Ti is mixed in 10 percent excess, the density is improved and, with further addition of Ni, reaches a near complete level. Analyses of the oxygen component and observations of air pores before and after the reaction suggest that B_2O_3 contaminating the material B may be evaporated to reduce the density and that the evaporation of B_2O_3 may be blocked by the excess Ti which acts to incorporate the oxygen as a solid solution. In any of the above sintered products, TiB_2 constituted the main phase, with TiB in case of excess Ti and Ni_3Ti in case of Ni-addition being noticed in limited amounts and with no metal Ti remaining. TiB with a melting point of 2,500 K, which is lower than that for TiB_2 of 3,193 K, and liquid phase Ni may also contribute to improving density.

Figure 6 shows the density change for TiC–Ni. Where no Ni is added, the density remains below 95 percent even when pressure as high as 100 MPa is applied. The reason is not the formation of an evaporated compound but that TiC in stoichiometric composition is unstable and apt to accompany free carbon; in fact, deposition of carbon in the grain boundary is notable in relevant sintered molds. The product has near full density when the amount of C is reduced near to the formula $TiC_{0.8}$. The addition of Ni is naturally effective with a near fully-dense product produced from a mixture of the materials in the stoichiometric composition by the addition of 5 wt%Ni or by applying no more than 10 MPa of pressure if the Ni is added in larger amounts as seen in the figure.

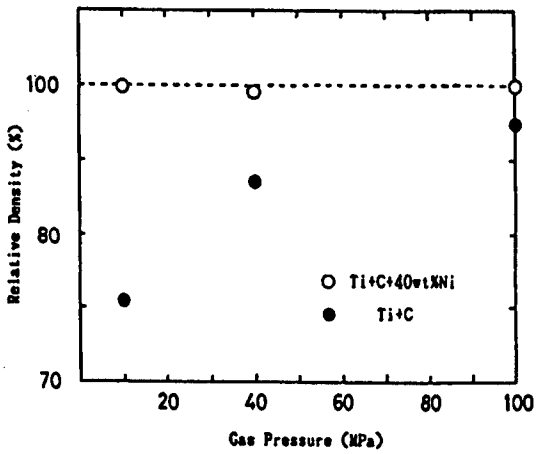

Figure 6. Plot of Relative Density Vs. Gas Pressure for TiC–Ni Series of Sintered Compacts

With causes for blocking the formation of fully dense products being different depending on different materials as described above, different measures to counter the causes are needed. Control of reaction temperature is also important since excessively high reaction temperature, for example above the boiling point of Ni of 3,003 K, may yield a large void in the specimen or cause deformation of it.

5. Control of Reaction and Microstructure

In preparing a highly functional material by means of the gas pressure combustion sintering, it is important to control the high temperature reaction produced and the microstructure of the specimen formed in short periods. The adiabatic combustion temperature for SHS in the case of TiC is computed thermodynamically on the basis of heat of formation (185 kJ/mol), specific heat, etc. The relevant temperature so computed reaches as high as 3,343 K, but is lowered by the addition of Ni.

As shown in Figure 7, the curve represents the value so estimated while values measured with a two-color radiation thermometer for the combustion temperature of the preconsolidated molds of ϕ7.7 x 10 mm and of a density around 70 percent are indicated by circles. The good agreement between the empirical and theoretical values suggests that the reaction proceeds almost adiabatically and that the added Ni scarcely participates in the reaction. The adiabatic temperatures do not directly reflect the temperature for combustion sintering because of heat supply from the ignition agent, but serve as a parameter controlling the reaction and the microstructure.

Figure 8 shows pictures of the microstructure of the sintered composite compound TiC–Ni as varying with the amount of Ni added. The grain growth of TiC is reduced with increased addition of Ni because that lowers the combustion temperature and increases the distance for transport of relevant elements. The addition of TiC also serves effectively to control the microstructure by making it finer without changing the combustion. As the amount of added Ni exceeds a level of about 50 percent, the materials are less likely to

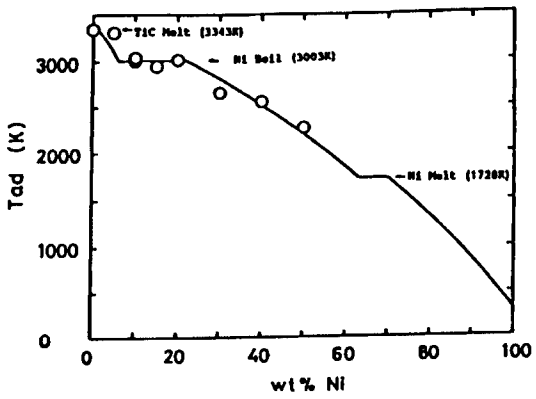

Figure 7. Combustion Temperature in the Combustion Synthesis of TiC

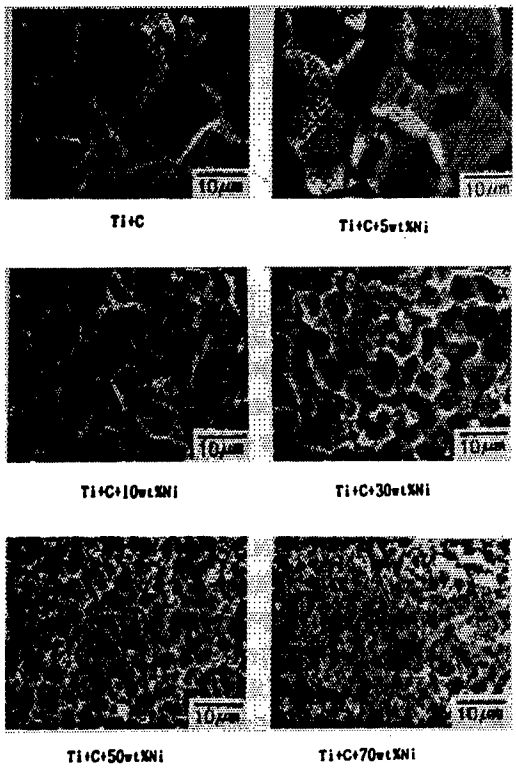

Figure 8. Changes of Microstructure for TiC–Ni Series of Sintered Compacts

a number of fine particles of TiC with developed crystal faces are seen, which may possibly have separated from the melt Ni in the cooling process.

The microstructure of sintered specimens may be controlled to some extent by adding metals or ceramics that are the same as or different from those of the product, as seen above. In particular, the addition of different kinds of ceramics may yield formation and control of unique microstructure of composite compounds.

6. Functionally Gradient Structure

Since the combustion sintering allows the process to be completed momentarily and hence prevents the constituent elements from being diffused as described above, it is favored in the preparation of functionally gradient materials whose compositions varied continuously. It is necessary to understand characteristics of each composition for gradient structures.

Vickers hardness for different functionally nongradient materials of TiC–Ni series is plotted in Figure 9. With increasing amounts of Ni added, the hardness decreases; a change in the incline of the curve is notable where Ni is added at 30~40 wt%.

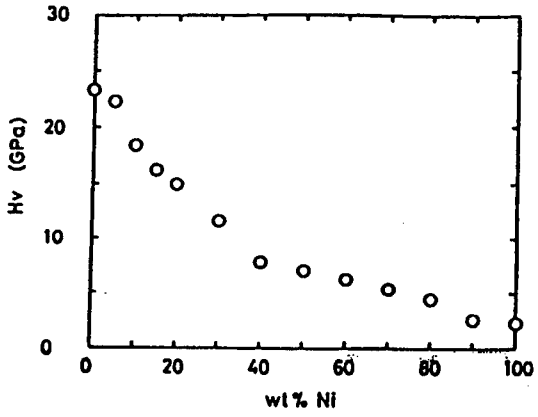

Figure 9. Changes in Vickers Hardness for TiC-Ni Series of Functionally Nongradient Material (load 9.8 N)

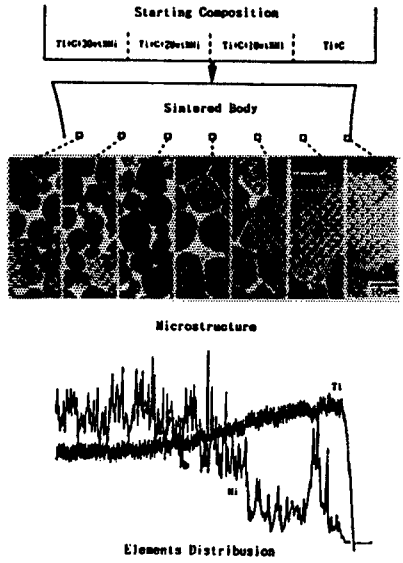

Figure 10. Microstructure of Functionally Gradient Materials of TiC-Ni Series Trial Manufactured by Gas Pressure Combustion Synthesis (Ni; 0-30 wt%)
(The right side is made up exclusively of TiC phase with Ni phase, white part, increasing in amount and TiC grains growing smaller from right to left in the pictures.)

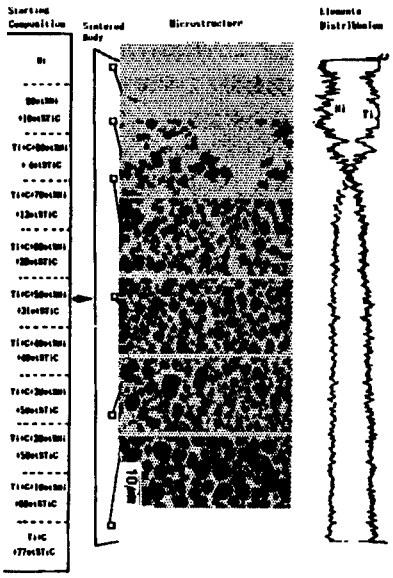

Figure 11. Microstructure of Functionally Gradient Materials of TiC-Ni Series Trial-Manufactured by the Gas Pressure Combustion Sintering (Ni; 0-100 wt%)
(TiC powder is added to each material of different composition such that the combustion temperature of every part be shifted to an identical adiabatic combustion temperature of 1,600 K. The size of the TiC particles is made approximately uniform in the entire compact.)

Together with changes in the microstructure, this may suggest a change of the matrix phase from TiC to Ni.

Fracture toughness value for simple TiC proved to be 3.6 MPa $m^{1/2}$, but rose to 17 MPa $m^{1/2}$ with the addition of Ni at 30 wt%. The three-point bending strength for TiC-10 wt%Ni was found to be 580 MPa (span 20 mm). Along with Young's modulus and other mechanical properties, thermal conductivity, thermal expansion coefficient, and other thermal properties must be considered in order to make model-computations and experiments for the composition gradient and thus to optimize the gradient value.

Refer to Figure 10 for microstructures of functionally gradient specimens of TiC-Ni series. The preconsolidated mold was a cylinder of ϕ13 x 12 mm and its Ni content varied stepwise from 0~10 to 20~30 wt%. The mold was subjected to gas pressure combustion sintering under a pressure of 100 MPa to turn out a sintered mold, the microstructure of which is shown for each portion in the figure. The sintered mold grew almost completely dense and underwent a shrinkage of some 14 percent. The right portion of the sintered body in the figure is made up of the TiC phase exclusively and the Ni phase increases gradually and continuously toward the left, initially spreading in grain boundaries and triple point and then turning to matrix. The grain also grows smaller as the Ni content increases. TiC powder may be added to the specimen such that the adiabatic combustion temperature may be uniform in every portion of the specimen and that the TiC grains thus grow in an approximately uniform size as seen in Figure 11, where the specimen has a thickness of 1 mm and the Ni content varies from 0~100 percent in 11 steps. No borders were noticed in the specimen for different compositions after sintering; Ni had diffused to the surface on the TiC side.

TiB_2-Ni may also be made functionally gradient in a like manner. Such specimens are made by simply stacking up layers of relevant material of identical thickness but of different compositions and are presently undergoing optimization of their gradient compositions by controlling the composition and arrangement of the material. One example of such cases is the functionally gradient material of $MoSi_2$-TiAl series developed jointly with Kawasaki Heavy Industries, Ltd., an outline of which will follow.

7. Manufacture of $MoSi_2$/SiC-TiAl, a Functionally Gradient Material

A functionally gradient material which seems promising as a material super-resistant against heat is one wherein the high temperature side is $MoSi_2$, a high melting material with fine antioxidation property, and the low temperature side TiAl, a heat-resistant alloy of high specific strength.

Presently, functionally gradient specimens ϕ30 x 7 mm in size are being produced by a new glass capsule method developed recently. The method involves heating of molds in vacuum in a laboratory dish with a lid upon which weight is imposed and is not only simple but also adapted to manufacture of larger specimens. The material powders Mo, Si, $MoSi_2$, SiC, TiAl, etc., are mixed and laminated on the basis of a CAD Si_2-distribution design and subjected to gas pressure combustion sintering. The arrangement of composition variation is

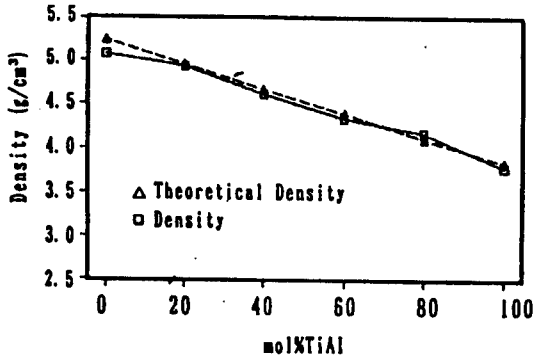

Figure 12. Density of the Functionally Nongradient Material $MoSi_2$/SiC–TiAl

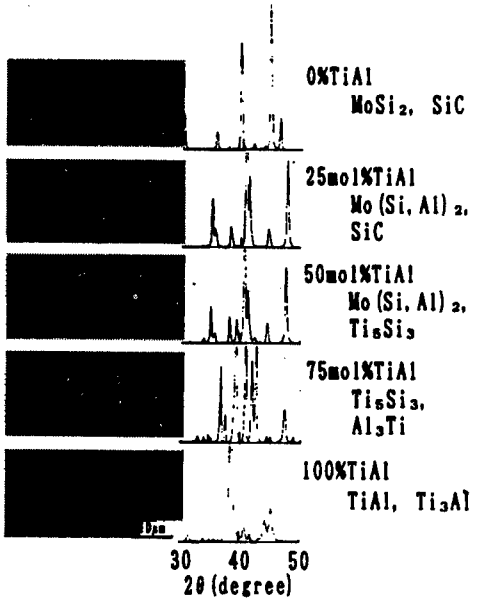

Figure 13. Microstructures and Results of Analysis of Compositions by X-Ray Diffraction for Functionally Nongradient Materials of $MoSi_2$/SiC–TiAl Series

computer-designed by the expert on the basis of the strength, the modulus of elasticity, the thermal conductivity, the thermal expansion coefficient, etc., of the relevant functionally nongradient material. SiC is added in order to improve the tensile strength of $MoSi_2$ with the amount of the addition being determined by a thermodynamic computation such that the density of the composite structure of $MoSi_2$–TiAl is made maximal.

Figure 12 shows the density of individual functionally nongradient materials and Figure 13 the result of X-ray diffraction analysis of the compositions and microstructures for the same material.

$MoSi_2$, in its composite phase with TiAl, produces reaction phases such as MO (Si, Al) and Ti_5Si_3, and thus makes it difficult to evaluate quantitatively the improvement of the density. However, study of the microstructure will show that the density improvement is fine. The microstructure of $MoSi_2$–SiC assumes a skeleton structure, yielding no reaction products between the two components. The skeleton structure turns into a diffusion structure as the amount of TiAl increases. TiAl tends to form a lamellar structure with a very small amount of Ti_3Al, a structure very important in improving the toughness of TiAl at normal temperatures according to a report.

Figure 14 shows photographs of the external appearance of the surface of the functionally gradient specimens which change as the composition-distribution parameter varies. The top picture, at n = 2, represents a composition distribution in which the amount of TiAl increases, by the parabola rule, from the surface of $MoSi_2$/SiC to that of TiAl while the bottom picture, at n = 0.5, shows a composition distribution indicated by the reciprocal function of the

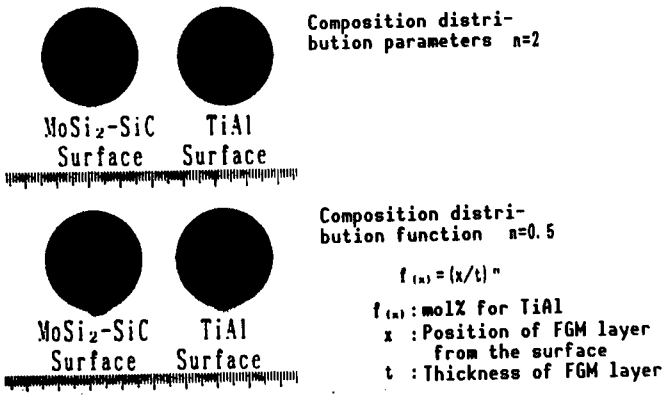

Figure 14. Effects of Composition Distribution Function on Functionally Gradient Materials of $MoSi_2$/SiC–TiAl Series

above. At n = 2, where the amount of TiAl is relatively small, cracks over the surface are notable in the $MoSi_2$/SiC side whereas not even a trace of cracking is observed at n = 0.5 where the amount of TiAl is large.

Functionally gradient materials of the thermal-stress relieving type must be capable of relieving thermal stress both at the time of its manufacture and at the time of its actual operation, the latter involving an extreme temperature gradient with a surface temperature of 2,000 K and with a temperature difference of 1,000 K. It is important that a composition distribution that keeps the residual stress below the level of rupture strength in its manufacture and an optimal composition distribution for the above temperature gradient in its operation be correlated. No materials have yet passed this severe test for temperature gradient. It seems very difficult to make a functionally gradient material from the barely moldable materials of $MoSi_2$/SiC and TiAl, except by the SHS process.

8. Conclusion

Gas pressure combustion sintering represents a process of fusing high melting intermetallic compounds, ceramics, metals, etc., by a superhigh temperature, superhigh-speed reaction at a temperature above 2,000°C produced by heat of combustion of the material itself. To overcome the brittleness and difficulty in molding intermetallic compounds—the disadvantage of the compounds—and to discover new functions from them may represent a new means of material innovation.

Near Net-Shape Synthesis of Intermetallic Compounds by Internally Heated Pseudo-HIP Method

916C1004H Tokyo KINZOKU GAKKAI SEMINA KINZOKUKAN KAGOBUTSU in Japanese
1 Jun 90 pp 61-64

[Article by Hideo Shingu, Department of Engineering, Kyoto University]

[Text] **1. Introduction**

Intermetallic compounds, compared with steel and light-metal materials, involve enormous difficulties in their casting because of reactions between the compound and the crucible, segregation of materials, and reactions with the surrounding atmosphere. The powder metallurgy method also requires complex processes such as hot isostatic pressing (HIP) and vacuum hot press. This paper deals with an introductory lecture on an internally heated pseudo-HIP method which yields simultaneous synthesis and molding of the compound in a simple but effective manner. The pseudo-HIP method is one that yields solidification and molding by means of pseudo-hydrostatic pressure produced with solid particles or sand in contrast to the HIP and cold isostatic pressing (CIP) methods known to date and the CERACON method, ROC method, and STAMP method, which all subject a preheated specimen to ordinary pressing in a preheated pressurization medium and thus achieve compression and molding under a pseudo-hydrostatic pressure at high temperatures and which are known as alternatives to the HIP since they are simpler and safer.

In the internally heated pseudo-HIP, a heat generating device is set up in sand such that a pseudo-hydrostatic pressure is produced and that heating is accomplished by the device. The major advantages of this type of pseudo-HIP are: 1) It is safe because sand is used for pressurization; 2) the internal heating type can heat the surroundings of the specimen only but not the pressurization vessel; 3) though sand particles exert pseudo-hydrostatic pressure on the specimen, the atmosphere in the space among the sand particles is under free control, that is, heating and pressurization is possible in vacuum or under any gas; 4) the internal heating type allows the specimen, a preconsolidated powder mold, to undergo reaction, synthesis, and sintering under pressure at a single site; 5) the specimen may be placed in the sand and subjected to heating and pressurization after undergoing fabrication so that the product is near net-shape.

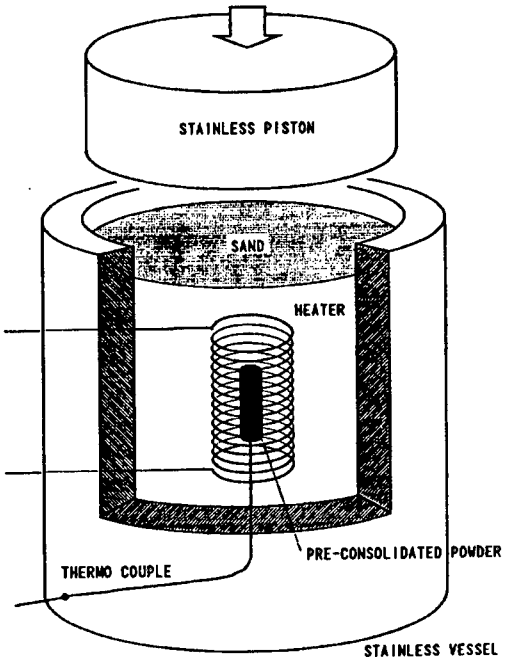

Figure 1. Diagram for a Pressure Vessel for Manufacture by Means of the Internally Heated Pseudo-HIP
(Using sand as the pressure medium, pressure is applied in vacuum or under a gas atmosphere along with application of heat so that relevant reaction and sintering is induced and that products in near net-shape are turned out.)

The disadvantages of this method, compared with the ordinary HIP, is that it is not capable of producing full hydrostatic conditions because of the sand used as the pressurization medium and that the sand causes even surfaces of the specimen by colliding with it. These disadvantages may be counteracted by such means as designing an appropriate shape for the pressurization vessel, adding lubricants to the sand, or coating the surface of the specimen with a surface sand.

2. Method and Apparatus of Experiments for the Internally Heated Pseudo-HIP

Figure 1 shows a diagram of the pressurization vessel used. Commercially available sand for casting is poured into a stainless steel vessel with an internal diameter of 110 mm and a depth of 140 mm and then a Kanthar heater of 0.5 mm ϕ and the specimen are set up in the sand. The pressure application, using a hydraulic press, is accomplished by forcing down the stainless steel piston from above the sand, as seen in the figure.

Figure 2 shows results of compression of the sand at room temperature using a pressure-sensitive paper to examine relevant pressure distribution. It shows that about half of the total pressure applied vertically is consumed in the transverse direction. The figure also shows that the pressure is high at the top of the vessel, where the piston directly presses, falling to about half that value at the bottom. In cases where the specimen undergoes the process in

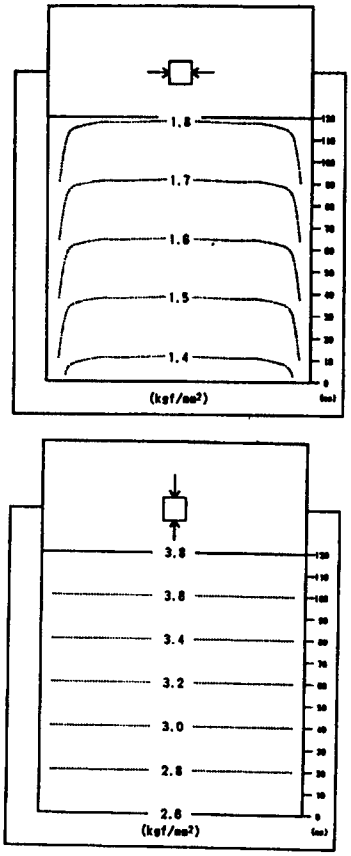

Figure 2. Pressure Distribution in the Pseudo-HIP Method
(In the above example, about half of the vertically applied pressure is exerted on the side.)

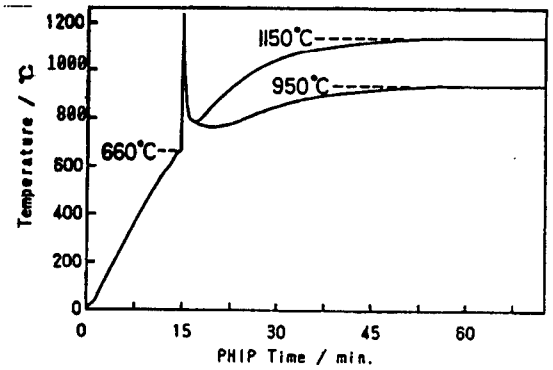

Figure 3. Plot of Temperature Vs. Time for the Reaction of Synthesis of the Compound TiAl Under the Pseudo-HIP Condition
(A steep rise in temperature is notable near the melting point of aluminum because of an autogenous exothermic reaction, SHS, taking place there.)

vacuum, the entire pressure vessel is introduced into a vacuum chamber and pressed with the piston sealed with an O-ring. The used specimen is either a rod with a diameter of about 10 mm produced by subjecting a mixture of Al and Ti particles of several ten μm in diameter to a rotary swage in a stainless steel tube or one produced by molding under pressure in a die about 20 mm in diameter. The density of the product is approximately 100 percent for the former but some 96 percent for the latter. These specimens are set at the center of the Kanthar-heater wire in coil form about 30 mm in diameter and about 50 mm in height, with its surroundings then packed with sand, and subjected next to pressuring with the hydraulic press and to heating in that order.

Figure 3 shows a plot for temperature vs. time. In this case, the rising temperature curves plateau at 950°C and 1,150°C, but a sudden rise of temperature together with rapid heat generation is noted at near 660°C, that is, at the melting point of Al in either case. The rapid rise of temperature is due to the heat of formation of an intermetallic compound (some 30 kJ/mol) by a reaction between Al and Ti and hence indicates that a self-propagating

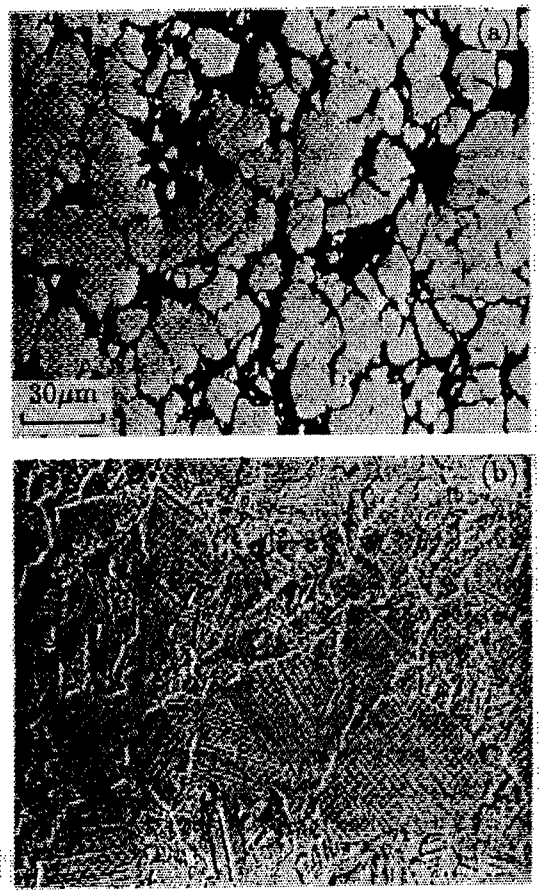

Figure 4. (a) Microstructure of the Compound Ti-50 at%Al Subjected to Rotary Swage
(b) Microstructure of the Compound Subjected to Pseudo-HIP (Particles of Ti and Al several tens of microns are mixed in (a), whereas TiAl and Ti_3Al make a lamellar structure in (b).)

high-temperature synthesis (or SHS for short) has taken place. The specimens yield compounds of a nearly true density with a specific gravity of 3.8 gr/cm^3 for the composition $Ti_{50}Al_{50}$, when subjected to this process, whereas the simple SHS process under a pressure of 1 atm forces the specimen to substantially expand. Unreacted Ti, Al, Al_3Ti compounds, etc., are notable just after the exothermal reaction in this case, but the heat treatment under raised pressures in the pseudo-HIP vessel allows the reaction to proceed further, leading to less vacant spaces initially noted by the microscope.

Figure 4 shows photographs of the microscopic picture of an alloy with the composition Ti-50 at%Al after having been subjected to a rotary swage and to a pseudo-HIP at 1,150°C for 1 hour. In (a) of the figure, the product is made of metal particles Ti and Al having been kneaded together and allows easy machining. In (b), the product has a lamellar microstructure of the two phases TiAl and Ti_3Al.

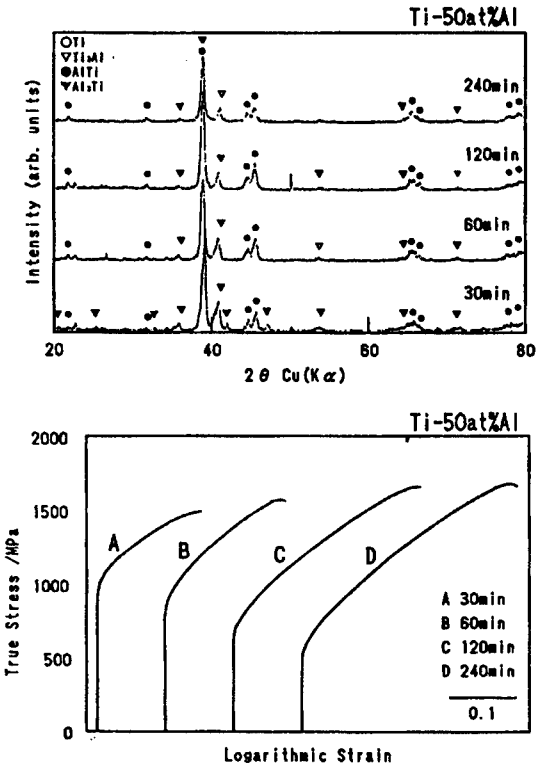

Figure 5. Phase Identification and Compression Strength After the Pseudo-HIP Treatment at 950°C for the Alloy Ti-50 at%Al

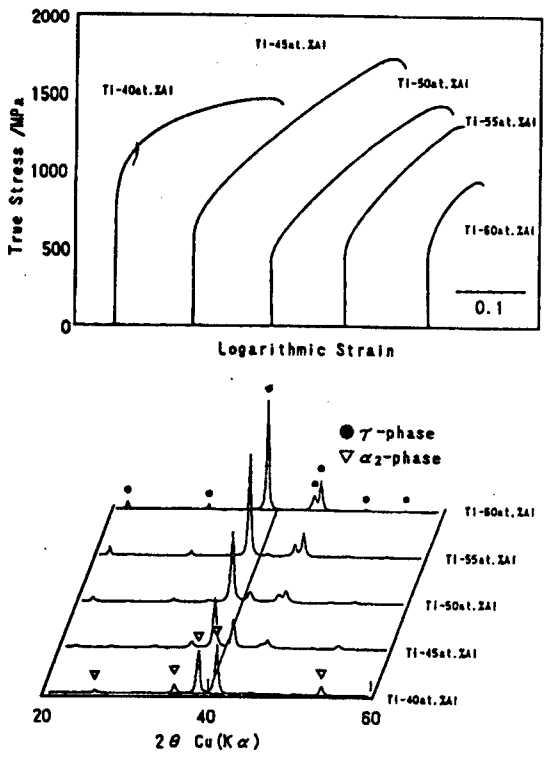

Figure 6. Compression Strength for Specimens of TiAl Subjected to Pseudo-HIP Treatment at 1,150°C in Vacuum for 2 Hours

3. Examples of Experiments for the Microstructure and Mechanical Properties of Ti-Al Alloy Series Produced by the Internally Heated Pseudo-HIP

The specimens of a mixture of Ti and Al powders having been subjected to rotary swage and then to pseudo-HIP was processed into cylindrical rods of 6 mm ϕ x 10 mm and subjected to compression strength testings. The same material was also machined into specimens of 2 x 3 x 30 mm and subjected to three-point bending testings. Figure 5 shows results of identification of alloy phases by X-ray diffraction and those of compression testings for the Ti-50 at%Al subjected to the pseudo-HIP at 950°C. Where the alloy was held at a temperature of 950°C for 30 minutes after having been subjected to the exothermal reaction of SHS, the compositions for Al comprised the three phases Ti_3Al, TiAl, and $TiAl_3$, that is, the SHS reaction between Ti and Al evidently failed to form an equilibrium phase on its own because the reaction did not involve sufficiently large enthalpy value. With the development of the lamellar structure comprised of the two phases TiAl and $TiAl_3$ as the heat treatment went on, the yield stress fell and the fracture strength grew. Figure 6 shows results of compression tests for different compositions of the specimens TiAl subjected to the pseudo-HIP for 2 hours in vacuum at 1,150°C.

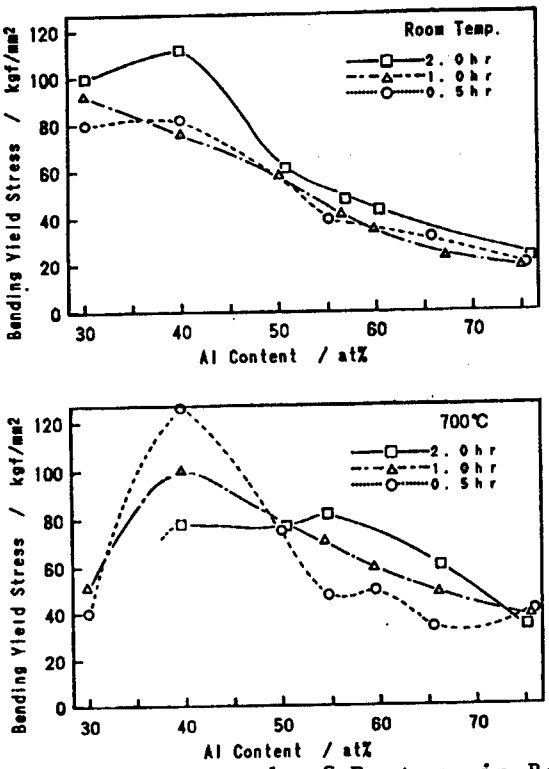

Figure 7. Strength of Rupture in Bending at 700°C and at Room Temperature for Specimen Subjected to Pseudo-HIP at 1,150°C in Air

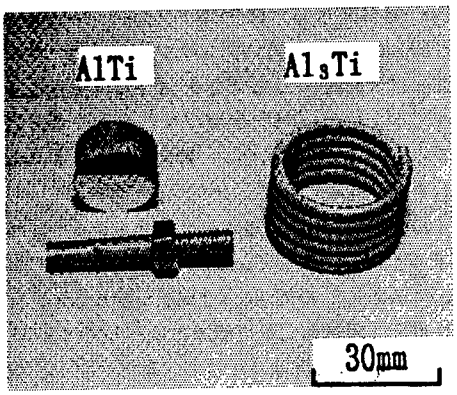

Figure 8. Products of TiAl Compound Manufactured in Near Net-Shape by the Pseudo-HIP Method

The phase of Ti_3Al singly was formed at a composition 40 at%Al whereas the phase of TiAl was at 60 at%Al, and the two phases coexisted at intermediate compositions where the plastic deformation was larger and the yield strength lower. When specimens of these compositions were subjected to a pseudo-HIP in air, the longer heat treatments led to lowering of the plastic deformation with the tendency more pronounced in specimens with lower contents of Al.

Figure 7 shows results of the bending tests for specimens subjected to pseudo-HIP in air at 1,150°C. The bending fracture strengths at 700°C are improved as compared with those at room temperature in any specimens except for those of compositions 30 at%Al and 40 at%Al subjected to heat treatment in air for two hours.

Figure 8 shows products in near net-shape turned out by compression and molding by a rotary swage or with a die, followed by machining in a metallic state and finally by pseudo-HIP treatment.

4. Conclusion

Manufacture of intermetallic compounds from material powders is accomplished satisfactorily by controlling the pressure and atmosphere involved, as reported by Tokizane, et al., for the hot press in vacuum of relevant powders mechanically alloyed. The internally heated pseudo-HIP represents a simple and

effective pseudo-HIP involving use of sand as the pressure medium and may possibly be superior in easily yielding the necessary pressure, temperature, and vacuum. The internally heated pseudo-HIP has a bright prospect for widespread application not only in the synthetic reaction of intermetallic compounds but also in the molding of composite materials, functionally gradient materials, and other metal-, compound-, and ceramic-materials.

Current Developmental Status of Intermetallic Compounds, Composite Materials

916C1004I Tokyo KINZOKU GAKKAI SEMINA KINZOKUKAN KAGOBUTSU in Japanese
1 Jun 90 pp 65-73

[Article by Shojiro Ochiai, Engineering Department, Kyoto University]

[Text] **1. Introduction**

The development of the composite material of the intermetallic compounds may largely be divided into one aimed at functionability of relevant compounds such as superconducting composite wires of Nb_3Sn and V_3Ga and one intended for utilizing high-temperature mechanical properties of the compound. This article focuses on the latter as used in high-strength structurals.

Among the first possible area of application for the composite material of intermetallic compounds in terms of its strength are space- and aircraft and jet engines. The United States started with the research and development of the composite material of intermetallic compounds for application in the space shuttle and supersonic passenger planes, with some results having been reported recently. In terms of temperature, aluminum-based composite materials are the prospective material up to 773 K, titanium alloys and the composite material of intermetallic compounds of Ti-Al series up to 1,073 K, and composite materials involving intermetallic compounds of Ni-Al series or superalloys as matrixes up to 1,373 K. Ceramic composite materials and functionally gradient materials may be available where temperature exceeds 1,373 K.

The composite material of intermetallic compounds, if prepared in an ideal manner, may possibly yield very high specific strengths and specific moduli of elasticity that can be maintained at high temperatures compared with those of simple intermetallic compounds. Figure 1 shows the dependence on temperature of theoretically predictable specific strengths of some intermetallic compounds reinforced with SiC continuous fiber, although such a high function composite material as seen in the figure has yet to be materialized. Among the methods of manufacture for the composite materials of intermetallic compounds are those involving unidirectional consolidation of alloys of eutectic composition as in the case of Ni_3Al-Ni_3Nb, those in which crystallized intermetallic compounds are subjected to plastic deformation at high temperature to turn into a fiber form, and those implanting an artificial reinforcement material

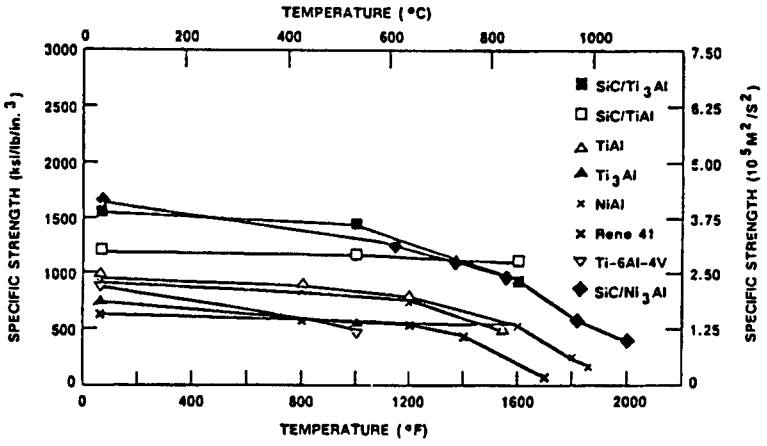

Figure 1. Dependence on Temperature of the Specific Strength—Theoretical Values—for Intermetallic Compound Matrixed Composite Materials Reinforced With Continuous SiC Fibers

in an intermetallic compound. These are all still in the research and developmental phase with many problems remaining to be resolved if they are to yield strength approaching that given in the theory and to become available practically.

This paper is an introductory review of the present state of development of intermetallic compound composite materials together with a discussion on the future trend in which research on the material is to be pushed ahead and on individual problems involved in reference to the research result for the metal-matrixed composite materials accomplished in advance of research for intermetallic compound matrix materials. In this connection, the reader is referred to References 20 and 21 for the recent progress of metal-matrixed composite materials, to References 1, 18, 22, and 23 for applications in space and aircraft engineering, and Reference 24 for automobile-related matters [references not published].

2. Examples of Research on Intermetallic Compound-Matrixed Composite Materials

2.1 Materials for Matrix and Reinforcement (Toughening)

Matrix material is largely NiAl, Ni_3Al, Ti_3Al, and TiAl. The reinforcement materials used to improve strength and creep characteristics are fibers such as those of SiC, B_4C coated B, and Al_2O_3 and the hard particles of TiB_2, TiC, Y_2O_3, etc., whereas materials used for toughening are the soft particles of Nb, Ti_6Al_4V, etc. No fibers and particles have yet been developed for exclusive use in intermetallic compound matrixed composites. Their matrixes, in contrast, have undergone diverse modifications for that purpose. In Ni_3Al, for example, B has been added for improved ductility, Cr has been added for reducing brittleness at high temperature and under oxidizing atmosphere, and Zr or Hf for improved strength at high temperature on the basis of solid solution strengthening.

Table 1. Major Methods of Manufacture and Examples of Applications for Intermetallic Compound-Matrixed Composite Materials

Method of manufacture	Application	Reference
Hot press method	Al_2O_3-short fiber/Ni_3Al SiC-continuous fiber/ TiAl(Ti_3Al) Nb-particle/TiAl	No bonding or reactions at 1,500~ 1,600 K, 20 MPa, and in 3.6 ks No bonding at low temperature; reaction yet strong at high temperature Reaction to some extent; ductility of the particles preserved
Casting under pressure	Al_2O_3-short fiber/Ni_3Al	Manufacture being possible at 1,673~1,973 K
HIP method	Al_2O_3-short fiber/Ni_3Al	At 1,373 K, 172 MPa, in 3.6 ks
RHIP method*	Al_2O_3-short fiber/Ni_3Al	At 1,073 K, 104 MPa, in 1.8 ks
High temperature extrusion	TiC-particle/Ni_3Al Al_2O_3-particle/Ni_3Al	Extrusion at 1,423 K following HIP
Mechanical alloying [MA]	Y_2O_3, Al_2O_3, ThO_2-particles/Ni_3Al	Solidification by HIP or hot press following MA
RSPD**	SiC-continuous fiber/ TiAl(Ti_3Al) TiB_2-, TiC-particle/ TiAl(Ti_3Al)	Solidification by HIP or hot press following RSPD
XD process	TiB_2-particle/TiAl (Ti_3Al) TiB_2-particle/NiAl	Particle being formed, grown in-situ; interface clean, of fine bonding; subjected to compaction by hot press or high-temperature extrusion following casting
Arc fusion in vacuum	Nb_5Si_3/Nb	In-situ mixed composite material constituted by ductile Nb and high strength Nb_5Si_3

* RHIP: Reactive hot isostatic pressing
** RSPD: Rapid-solidification plasma deposition

2.2 Method of Manufacture

Methods of manufacturing intermetallic compound-matrixed composite materials are listed in Table 1. The feature of each method may be summarized as follows.

(1) Hot Press

A preconsolidated powder is subjected to monoaxial pressure application in vacuum or under an inert atmosphere to give a composite material. This method allows control to some extent of reactions occurring at the interface between the matrix and the reinforcement material. It also has the advantage that the manufacture of articles having complicated shapes is made possible by designing a proper method of lamination and a proper mold for the green moldings.

(2) Casting Under Pressure

A fused matrix material is allowed to penetrate into vacant spaces among reinforcement fibers by application of pressure, a method which has so far been often applied in the manufacture of metal-matrixed composites and favored industrially for high quantity production. It is important in this method that the matrix and the reinforcement material wet well with each other, otherwise no composites of superior quality result. Raising relevant temperature and prolonging relevant time are available as methods for improving wetting. However, this often leads to an interface reaction that blocks development of high-quality products. It is, therefore, necessary to make the improvement of wetting and the control of interface reactions compatible and, if thermodynamics does not allow them to be compatible, a coating of the reinforcement fiber may be resorted to.

(3) HIP

A preconsolidated material is sealed in an evacuated capsule and subjected to hydrostatic pressure under a gas at high temperature and pressure such that the matrix and the reinforcement material are turned into a composite material. This method which is often used in producing metal-matrixed composites characteristically allows the density of the product to rise and, because of the application of pressure hydrostatically, it is available for near net-shape molding of components in complicated shape, for reinforcement of components, and for welding a composite with metals, if proper tooling is designed.

(4) RHIP (Reactive HIP)

RHIP involves manufacture of a composite material by means of HIP, with relevant exothermal-reaction heat being used. Ni and Al, for example, are mixed stoichiometrically and then subjected to cold isostatic pressing (CIP). After the intermediate product has been sealed into an evacuated stainless-steel capsule, it is subjected to HIP, where with the start of the reaction at a proper temperature, the low-melting constituents are turned liquid by the heat generated by the relevant reaction and immediately grow dense.

This method has the feature of allowing the intermetallic compound to form in the process of HIP at temperatures far below the melting point of the compound. Since the compatibility at the interface depends on the temperature of the reaction front and the period in which the temperature is maintained, the temperature for sintering, the speed of heat application, particle size, composite material size, reaction environment, etc., make up the keys to the good quality of the composite material yielded.

(5) High-Temperature Extrusion

This method is an effective means for the manufacture of composite materials of the particle type and the short fiber (whisker) type. The procedure is first to prepare a composite material by means of HIP, etc., followed by this method in most cases. Experiments for the manufacture of the composite material of intermetallic compounds directly from loose powder mixtures by this high-temperature extrusion are also being conducted.

(6) Mechanical Alloying

The mechanical alloying [MA] method, using high-energy ball mills, allows one powder in a mixture of powders to disperse into or to react with the others so that a dispersion reinforced type of composite material is turned out. The preconsolidated mold produced by the method is usually subjected to compaction by HIP or hot press.

(7) RSPD (Rapid Solidification Plasma Deposition)

In RSPD the matrix powder is fused by means of plasma arc and then allowed, in vacuum, to deposit on the fiber wrapping up a drum so that it is cooled and solidified immediately. Mono-tapes so produced are combined to give a composite material by means of hot press.

(8) XD-Process

Examination of relevant references by the author could not reveal the details of the XD-process. According to references 1, 12, and 15, the method, developed by the Martin Marietta Laboratories, allows the reinforcement of dispersed particles to form and grow in-situ, and does not involve a mechanical mixing of particles. The process basically involves a casting, with subsequent hot press, high-temperature extrusion, etc., being added for compaction. This method may possibly be favored because it provides interfaces that are clean and of strong bonding and thus can prevent interface reactions, a major difficulty in artificial composite materials.

(9) Vacuum Arc Fusion

Vacuum arc fusion, an effective means for fusing high-melting metals, is available for manufacturing the metal intermetallic compound type of composite materials wherein the constituent metals are not mutually fusible, for example, for Nb-Nb_5Si_3.

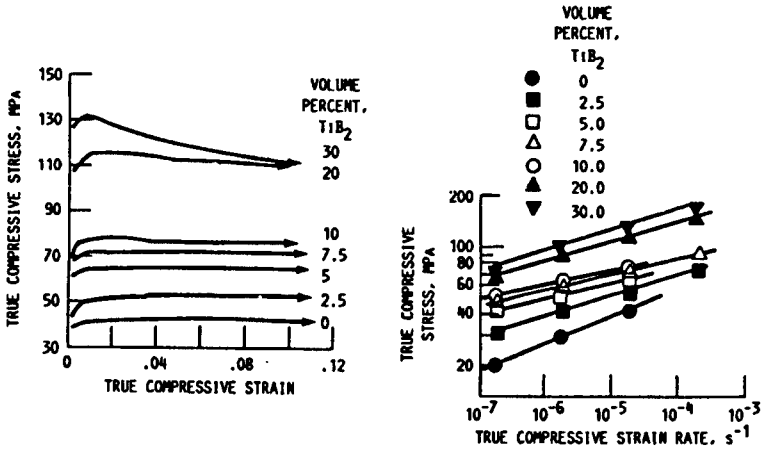

Figure 2. High-Temperature Characteristics at 1,300 K of the Composite TiB_2-Particle/NiAl

2.3 Mechanical Properties of the Composite Material

2.3.1 Ni_3Al and NiAl Composite Materials

In the case of Ni_3Al composite materials, those in which Al_2O_3 short fibers and Y_2O_3 particles are dispersed for reinforcement have been reported for yield stress, tensile strength, and elongation, but the effects in the composites are not very notable at present. The yield stress proved to be equivalent to or below that of the matrix and the tensile strength and elongation below those of the matrix, which may be attributed to poor orientation of the fiber, lack of uniformity in fiber distribution, interfaces of poor bonding, etc. According to recent report, it allowed an elongation of 10 percent in a material reinforced with 20 percent aluminum short fibers and may meet the researcher's hope in the future. It has also been demonstrated that the matrix of this composite material is capable of blocking the propagation of cracks arising from the rupture of the fiber. Selection of an appropriate material and application of an appropriate process may yield high strength and elongation and, with progress in full-scale research, still higher relevant values.

The high-temperature characteristics (at 1,300 K and in air) of a composite material, which is reinforced with TiB_2 1 μm in size on average by means of the XD-process are shown in Figure 2. The relevant value improves with increasing volume percent and, at 10 percent TiB_2, is about twice as high as that of the matrix. Steady stresses work on the specimen below the volume percent for TiB_2 of 10 percent, but above this level the specimens turn softer as they are worked on. An analysis of the dependence of fluid stress on the strain rate using the formula $\epsilon = A\sigma^R \exp(-Q/RT)$ proved that $n = 6$ and $Q = 350$ kJ/mol for the matrix and that $8 < n < 12$, and $Q = 400$ kJ/mol for the composite material. It has been demonstrated by transmission electron microscope (TEM) observation that the density for dislocation is higher for the composite material than for the matrix.

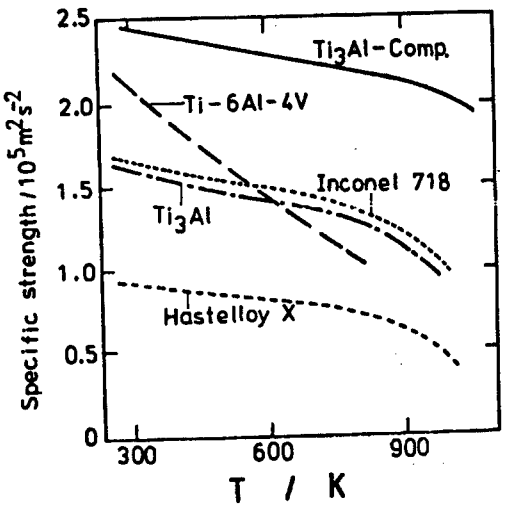

Figure 3. High-Temperature Characteristics of Composite SiC Continuous Fiber/Ti_3Al

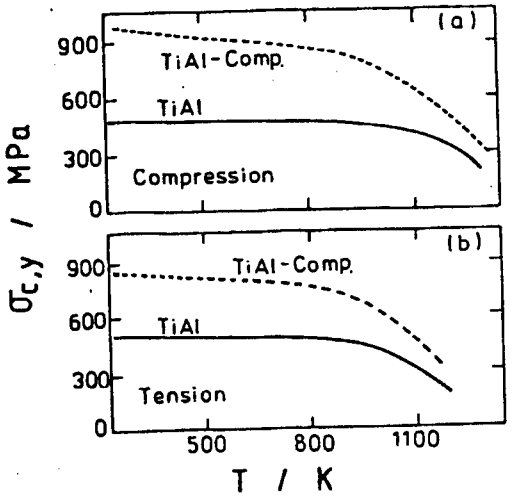

Figure 4. Dependence on Temperature of Tensile and Compression Yield Stresses of Composite TiB_2-Particle/TiAl

2.3.2 TiAl and Ti_3Al Composite Materials

Figure 3 shows the high-temperature characteristics of the Ti_3Al composite material involving reinforcement with an SiC continuous fiber SCS-6, a fiber produced by a CVD method developed for application in metal-Ti composite materials. The composite material, as developed by the RSPD above, has a volume percent for the fiber of 33 percent. As can be seen, the material maintains an extremely high specific strength up to very high temperatures compared with the existing heat-resistant alloys Inconel, Hasteloy, Ti-6Al-4V, etc., and the matrix of this material Ti_3Al. Figure 4 shows a plot of temperature vs. compression- and tensile-yield stress for the TiAl-composite materials produced by the XD-process. The composite as compared with its matrix exhibits high yield stresses in the entire temperature range.

Ductile particles, when mixed with intermetallic compounds, allow the toughness of the compound to improve largely because of a bridging effect produced by the particles. Whereas the fracture toughness at 873 K of TiAl is below 12 MPa $(m)^{1/2}$, that of the material with Nb particles implanted in some 10 percent to form a composite has a higher value of 16 MPa $(m)^{1/2}$.

3. Future Problems for the Composite Material of Intermetallic Compounds

3.1 Improvement in Manufacturing Process and Raw Material

The ideas developed in the process of development of metal-matrixed composite materials may be applied in principle to the manufacture of intermetallic compound-matrixed composite materials. One aim of the RSPD method is to block interface reactions by minimizing contact at high temperature between the reinforcement material and the matrix, just as in the case of the plasma

display method by which the mono-tape of B/Al-composite material is prepared. The wisdom of accomplishing the manufacture of composite materials by first producing mono-tapes of the material and then combining them is also based on the idea developed in the course of research for conventional composite materials. The optimization of the process, now under research, may possibly be accomplished by first analyzing the result of past research on existing composite materials and then by making modifications according to chemical properties of different materials. Systematic research is necessary for such parameters as temperature, time, pressure, and environment because of a lack of data. Development of intermetallic compounds for matrix materials that meet different objectives is also necessary: matrixes meant for strength and those for toughness may require different properties. Where B/Al composite materials are concerned, matrixes with high yield stress will raise the strength of the composite, but fail to maintain toughness. Where toughness is important, even intermetallic compound-matrixed composite materials may require increased toughness by using soft intermetallic compounds or by implanting ductile particles. It is hoped that different types of intermetallic compounds will be developed in order to be selected and applied as matrixes for different purposes. It is further hoped that reinforcement materials that are chemically and mechanically compatible with intermetallic compounds will be developed since most of the existing reinforcement materials (fibers and particles) were developed for application in metals and alloys and are not necessarily adapted to intermetallic compounds. In connection with the practical application of the material, the question of high cost which is a major snag in the development of the material never fails to emerge and must be grappled with in earnest.

3.2 Optimization of the Interface

Interface conditions make one critical element for the so-called artificial type of composite materials wherein an artificial reinforcement material is coupled with an intermetallic compound matrix, whereas the in-situ type of composite materials involves strong interface bonding and thus produce no interface reactions. In the former case the reinforcement material and the matrix are bonded in a thermodynamically nonequilibrium state which leads to changes in interface conditions as the temperature is raised. A discussion on this subject is given for the case of the fiber-reinforced type, though it is likewise available basically for the case of the particle-dispersion type. It is also necessary in discussing the optimization of the interface for the artificial type of composite materials to allow for the two factors, the interface bonding strength and the interface reaction.

3.2.1 Optimization of Bonding Strength at the Interface

In the case of fiber-reinforced materials, an ideal interface may be represented with both (a) a high capacity for transmission of stress to the fiber and (b) a capacity for blocking the propagation of a crack produced by the rupture of a fiber. Capacity (a) may be represented as one that increases with decreasing critical length lc—the length required for the fiber to display its strength—while capacity (b) as one that increases with the decreasing stress concentration factor K at which the ruptured fiber conveys the stress

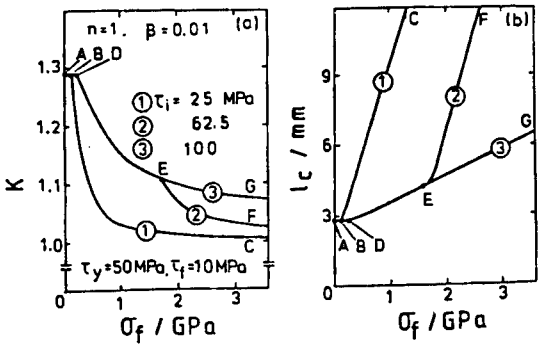

Figure 5. Plot of σ_f, the Remote Fiber Stress Vs. K, the Stress Concentration Factor, and l_c, the Critical Length, for Different τ_1's, the Interface Bonding Shear Strength, as Computed by Shear Lag Analysis Method

(In this example, the shear yield stress for the matrix τ_y is set at 50 MPa, the shear friction stress at the interface following the separation of the interface, τ_i, at 10 MPa, the fiber volume percent at 0.5, and the work hardening coefficient β, which is rated by the modulus of elasticity of the matrix, at 0.01.)

to the adjacent fiber. Such parameters as critical length and stress-concentration factor are computed by a method called shear lag analysis, as shown in Figure 5. It is evident from the figure that the stress concentration factor lowers with increasing critical length and vise versa, that is, gaining one capacity implies loss of the other; to obtain both is not possible. Where bonding strength is concerned, a rise in strength leads to shortening the critical length and thus to a rise of the strength of the composite material. The stress concentration increases with the rise of the bonding strength, resulting in lowered strength of the composite material.

The above computations indicate an essential difficulty in realizing an ideal interface for fiber-reinforced composite materials and the question of an optimization of the interface of composite materials resolves itself into how to balance the capacities (a) and (b). No improvement in properties is expected if one capacity is too high or too low. To further complicate the problem, the degree of relevant balance of capacities varies with many parameters such as physical constants including Young's modulus and the other moduli of elasticity, the volume percent of the fiber, the strength and variance of the fiber strength, the yield stress of the matrix, the rate of work hardening, and toughness. There is no useful theoretical general formula for relevant computation presently and one has to resort to a mere assumption for optimal conditions on the basis of such means as computer simulation. The author discusses below the bonding strength of the interface required for intermetallic compound matrixed fiber-reinforced composite materials in qualitative terms by Figure 6, a plot representing effects on the strength of the material of the bonding strength of the interface and of the yield stress and toughness of the matrix, as predicted by computer simulation.

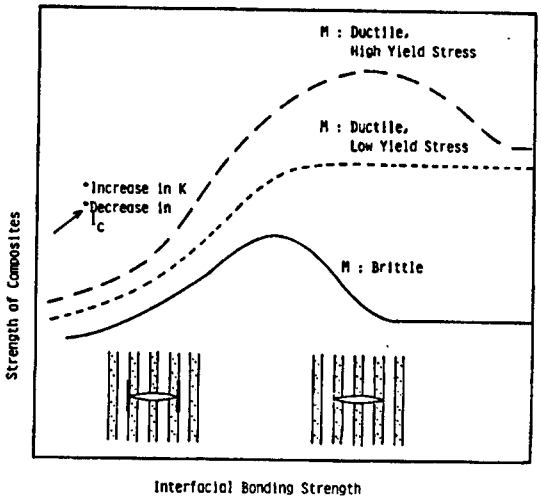

Figure 6. Effects on the Tensile Strength of Composites, of the Yield Stress of the Matrix, the Toughness of the Matrix, and the Interfacial Bonding Strength

The strength of the material varies with the bonding strength of the interface: as shown by 1) the broken line in cases where the matrix is ductile and of high yield stress; 2) the dotted line where the matrix is ductile but of low yield stress; and 3) the continuous line where the matrix lacks ductility. In the first and third cases, the maximum material strength occurs for a certain bonding strength, whereas in the second case, the material strength increases with rising bonding strength and then plateaus. From the generalization of the above result, the following may be suggested as the bonding strength of the interface appropriate for intermetallic compound-matrixed composite materials.

(a) In cases where the matrix is highly ductile and comparatively soft (or of low yield stress), the bonding strength should be as high as possible; where the matrix is highly ductile but hard, the bonding strength is somewhat low so that a separation of the interface bonding may reduce the stress concentration. It is hard to estimate quantitatively the optimal bonding strength of the interface in the latter case. However, a shear bonding strength of about equivalent to or twice that of the shear yield stress may be favored in the case where intermetallic compounds are used as the matrix of the composite. Computer experiments have demonstrated that shear bonding strength of such a value often provides high strength to hard metal matrix composite materials.

(b) Where the matrix does not have high ductility, the strength of the composite becomes maximum at the optimal bonding strength, which depends on physical constants of the constituent materials, ductility of the matrix, volume percentage of the fiber, etc. Results of computer experiments indicate that, where physical constants of the constituent materials are given, the optimal bonding strength rises with increasing ductility of the matrix and decreasing volume percent of the fiber as far as the metal-matrixed composite

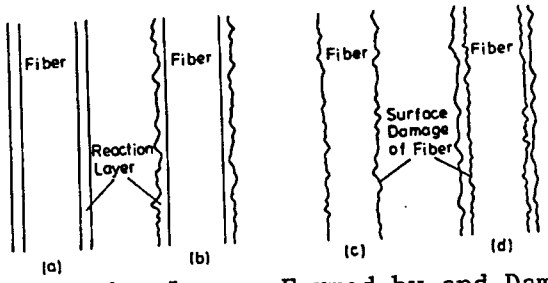

Figure 7. Reaction Layers Formed by and Damage in Fibers Resulting From Interfacial Reactions

material is concerned. As for the intermetallic compound-matrixed composite materials, prediction of the optimal bonding strength has yet to be established although it may be possible henceforth with the collection of relevant data and thus with clarification of the fracture behavior.

Where ductility of the matrix is low, the maximum strength attainable for the composite material is low even if the optimal bonding strength is provided. This is particularly true for materials with high volume percent, where relevant values predictable from the rule of compounds is far from materialization. It is imperative to develop an intermetallic compound of high ductility if a high strength for the material is to be developed.

The above discussion concerns the optimal bonding strength in connection with strength of the material and not with its ductility or creep characteristics, where the questions involved are different. Further research is needed to predict the maximum value of different properties of the composite material.

3.2.2 Interface Reaction

As seen in Figure 7, an interface reaction leads to formation of reactive layers and to damage over the surface of the fiber. Among the mechanisms leading to the deterioration of the material due to the interface reaction are formation and propagation of cracks resulting from an early fracture of the reaction layer and effect of the stress concentrated at rugged parts, pits, and other damage caused by the reaction over the surface of the fiber.

The deterioration of material due to the interface reaction for practical and near practical metal-matrixed composite materials such as carbon fiber (CF)/Al, B/Al, and B/Ti has resulted from the mechanisms mentioned above.

The deterioration of mechanical properties of the intermetallic compound-matrixed composite materials may be produced by either of the above mechanisms, although the cause has yet to be determined at this juncture. Of the intermetallic compound reactions between integrated circuits and different reinforcement materials (fibers, particles), those for the composite material Ni_3Al have been reported in comparatively greater detail. Research has proved that Ni_3Al does not react with Al_2O_3 under the thermal history required for manufacture, but violently reacts with SiC fibers, B_4C-coated B fibers, TiC particles, and TiB_2 particles.

The following three measures for preventing the deterioration of material resulting from the interface reaction which have been applied to metal-matrixed composite materials may also be available for intermetallic compound-matrixed composite materials.

(1) Manufacture and Use of a Composite Material in the Range of Temperature and Time Interval Tolerable to the Material

Since the deterioration of composite materials resulting from an interface reaction occurs when the extent of defects as introduced by the reaction and as reflected in the thickness of the reaction layers exceeds the defects inherent to the fiber itself, an actual decrease in quality may be blocked by stopping the reaction before the defects due to the interface reaction become greater than those inherent to the fiber. This implies that the temperature at which and the time interval in which the fiber makes contact with the matrix be limited to an allowable range, as in the case of B/Al composite materials used in the space shuttle. Since the interface reaction also proceeds during use of the material at high temperature, it is necessary that the temperature used be limited to a low range during the application of the material as well as during its manufacture.

(2) Coating

Coating a fiber is often resorted to in cases where the above measure fails to achieve a specific property. Selection of the coating material must be made in terms of both preventing the interface reaction and improving wetting between the fiber and the matrix. Application of TiB_2-coating for carbon fibers and B_4C- or SiC-coating for B fibers has been done successfully, leading to fine properties in case of metal-matrixed composite materials. Since the manufacture of intermetallic compound-matrixed composite materials must be carried out at higher temperatures than those for the metal-matrixed materials, it seems more difficult to both prevent the interface reaction and bond the matrix to the fiber or particle in the former materials compared to the latter, and hence the greater necessity of applying a coating to the former. Since the manufacture by means of casting has been a major theme and improvement in wetting property is a major part of developmental research regarding the latter material, it seems necessary to put particular emphasis on preventing the interface reaction in the former in view of the higher temperature involved in its manufacture and application. An element or a compound that reduces the diffusion of elements involved in the reinforcement material and the matrix may act effectively in setting up a barrier for relevant diffusion. Such carbides and oxides as HfC, Al_2O_3, and Y_2O_3 may be effective for Ni_3Al on the basis of past results for the reinforcement of Ni-matrixed superalloys with fibers. TiB_2 has been reported to be effective for TiAl and Ti_3Al due to its chemical stability.

(3) Reformation of Surface of the Fiber

Reformation of the surface of the fiber is yet another method for reducing the surface reaction. An SiC fiber, devised by AVCO Corp. and made by chemical vapor deposition (CVD), has its surface removed so that the surface layer is

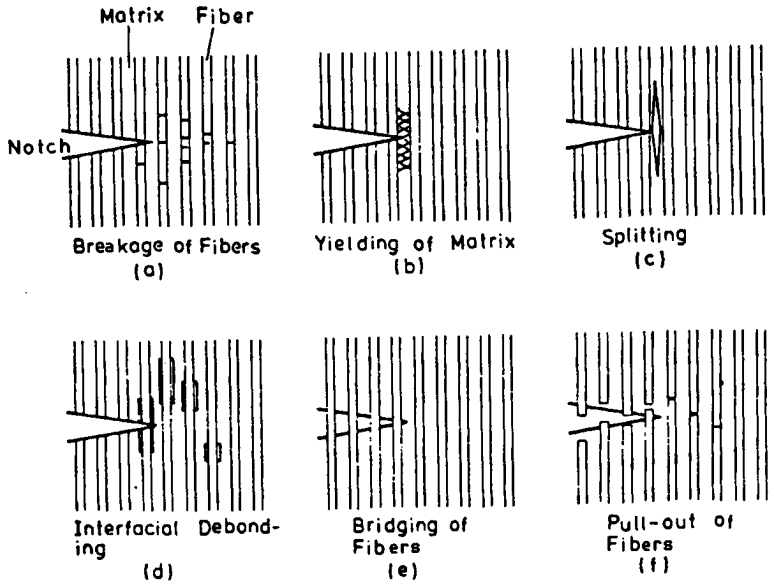

Figure 8. Phenomena Observed at Point of Notch or at Advancing Front of Cracks in Deformation of Specimen of Fiber-Reinforced Composites

rich in carbon and the deterioration due to the intermetallic compound reaction is reduced. The extent of reformation also varies to adapt the fiber to different matrix metals, i.e., SCS-6 for Ti and SCS-2 for Al, the former which can also be applied to the intermetallic compounds TiAl and Ti_3Al. The Ti_3Al-composite material, shown in Figure 3, uses this fiber and achieves a high strength, suggesting the application of surface reformation in fibers as an effective means.

3.3 Clarification and Improvement of Mechanical Properties

Strain and fracture of composite materials involves many complicated factors with many problems still remaining to be resolved. For example, phenomena notable at the advancing front of notches or cracks formed in strain include fracture of the fiber, yield of the matrix, splitting, separation of the interface, bridging of the fiber, and pull-out of the fiber, as shown in Figure 8. These, notable in combinations, are difficult to explain in quantitative terms and hence are still under research. The author describes in the following these issues and future problems for tensile strength and fracture toughness.

3.3.1 Tensile Strength and Yield Stress

The compound rule is most often used in describing the tensile strength of reinforcement fibers, but application of the rule must be done with caution because the rule does not take into account such important factors that affect the strength such as interface conditions (bonding strength, presence or absence of interface reactions, etc.), stress concentration due to fiber breakage, variance of fiber strength, internal stress, and mechanical

reciprocal reactions between the fiber and the matrix. It may be concluded from past research that a value derived from the compound rule be taken as the upper limit of relevant values and it is hoped that some new method for representing the strength that allows for the above factors be developed.

Where short-fiber reinforcement materials are concerned, Kelley's model is applied where the fiber is oriented in one direction. It should be noted here that the relevant formula does not take into account such factors as physical constants of the constituent materials, volume percent of the fiber, bonding strength of the interface, and level of the applied stress, and that the formula is properly applicable only under a limited condition in which the stress level is sufficiently high and the matrix has undergone shear yield for substantial length at the interface. It should be noted in particular that, where intermetallic compound-matrixed composite material are concerned, the yield stress of the matrix is higher than for the metal and hence the matrix may not undergo shear yield in some cases depending on the stress level. Where fiber orientation is random, no sufficient agreement between experimental and computed values has yet been achieved, though various formulas have been suggested for the transmission of stresses and for the effect of fiber stress on the direction of tensile strength, leaving the problem to be solved in the future. The effect of fiber endings also needs further study, involving the possibility of triggering serious problems where they act as sources for stress concentration, particularly in cases of intermetallic compound matrix where toughness is not satisfactory.

Where the particle type of reinforcement material is concerned, the (Orowan) mechanism may be available for the process involved as long as the particles are very fine and thus the dislocation theory is applicable. Where the particles are not very fine, no theory has yet been established, also leaving the problem to be solved in the future.

3.3.2 Fracture Toughness

The evaluation of fracture toughness of composite materials will vary depending on how to deal with the following problems: One is how to handle mathematically the damaged zone formed at the advancing front of notches as shown in Figure 8. The other is whether a composite material approximates a uniform body having physical constants which is the average of those of the constituent matrix and reinforcement material or not. If one assumes that the damaged zone behaves in the same manner that the plastic zone at the advancing front of notches in metals does and that the damaged zone as a whole approximates a uniform body, one can apply to composite materials the conventional fracture mechanics including applications of the J-integration and R-curve method. However, if one assumes that the damaged zone of composite materials behaves differently from the plastic zone of the metal and that the matrix and the fiber of composite materials must be analyzed separately, one must devise a new formula for representing the fracture toughness of composite materials. It is also possible for the sake of convenience to believe that a composite material as a whole approximates a uniform body and that in the damage zone fracture mechanics is applied separately to the matrix and the fiber. At this juncture, different formulas are being suggested for fracture toughness as

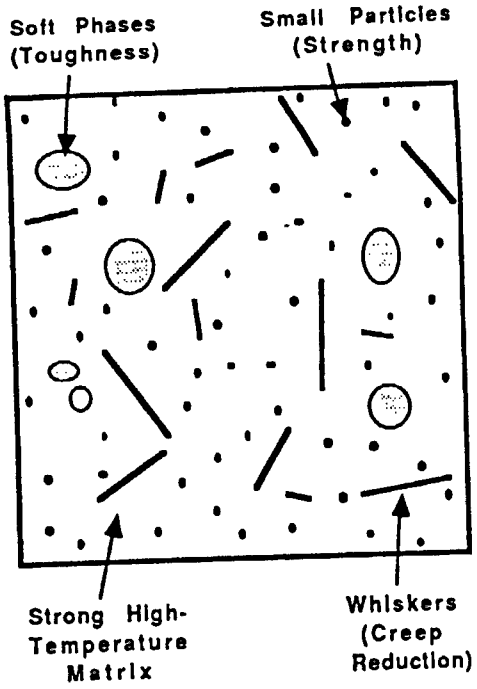

Figure 9. Diagram of the Microstructure Design

researchers take different stands, with a consensus yet to be reached. This question is not only intriguing as a theme for basic research, but is also a theme which the researcher cannot avoid tackling if practical application is to be materialized. Future development of this research theme is thus anticipated.

3.3.3 Optimal Design of the Microstructure

To turn out a design for the microstructure of composite materials that displays both strength and toughness would be ideal, and it is necessary that the mechanisms that determine the strength and toughness be explained quantitatively. At this juncture, relevant mechanism in details is yet to be known and hence the phase of microstructure design is yet to come. Nevertheless, it is known on the basis of past reports that fibers (whiskers) and particles pay the following roles in qualitative terms, depending on the consistency and size of the material: 1) fibers and whiskers bear external stresses and are effective in improving strength and creep characteristics; 2) fine particles serve to enhance strength by blocking the movement of dislocation; and 3) soft particles contribute to toughness. These factors are shown in the general diagram in Figure 9. The microstructure shown, if materialized, will provide a composite material of excellent characteristics. The question ultimately is how to design the size, the quantity, and the shape of the fiber and the whisker and how to achieve these characteristics in the composite material. Development of the microstructure control technology is anticipated along with research on the mechanism.

Other mechanical properties which must be explained are creep characteristics, dynamic properties, and thermal stress.

In addition, other questions involved include: 1) improvement of anti-oxidative, anticorrosive, and antiabrasive properties; 2) improvement of machinability and bonding characteristics; 3) establishment of testing methods; and 4) increasing reliability and establishment of relevant evaluation methods.

4. Conclusion

The research and development of intermetallic compound-matrixed composite materials have made major advances in the last several years. The emphasis of the research is still mainly on the manufacture of material of high quality rather than on the mechanical properties of the material, a research subject which remains to be resolved in the future. No doubt there are bright prospects for this type of composite material which is expected to find application first in space and aeronautical engineering in the near future. The author anticipates the role of research on this material in future material innovations.

Fracture Toughness of Intermetallic Compounds

916C1004J Tokyo KINZOKU GAKKAI SEMINA KINZOKUKAN KAGOBUTSU in Japanese
1 Jun 90 pp 75-80

[Article by Koichi Nihara, Industrial Science Laboratory, Osaka University]

[Text] **1. Introduction**

Intermetallic compounds have recently come to the limelight as new functional and structural materials that support advanced technologies. As functional materials, they have been finding wide practical application in the areas of magnetic materials, superconducting materials, semiconductors, hydrogen absorption alloys, solar-energy associated materials, and shape memory alloys. In the area of structural materials such as heat-resistant, superhard, and antiabrasive materials, their practical application at present lags behind those mentioned above because of their brittleness despite other excellent properties as structurals.

Intermetallic compounds of structurals may largely be divided into those typical metals including Ni_3Al, $Ni_3(Si \cdot Ti)$, Co_3Ti, Ni_3AlTi, NiAl, CoTi, and TiAl, and those subjected to research in the area of ceramics such as WC, TiC, TiN, Si_3N_4, BN, Fe_3N, $MoSi_2$, $Mo(Co \cdot Si)_2$, and SiC. Although the compound displays excellent properties as high-temperature structurals in both categories, it is important to overcome brittleness if the compound is to be practically available for a wide range of uses. The author gives an introductory lecture on the recent progress of those intermetallic compounds that may possibly be used as ceramics in terms of the challenge against brittleness.

2. Basic Concept for Overcoming Brittleness of Ceramics

The fracture of ceramics, the typical brittle material, arises from growth of microcracks several μm to several 10 μm in size found inside or on the surface of the material. The formula representing the fracture conditions is:

$$\sigma = (1/Y)\ (2E\gamma/c)^{1/2} = (1/Y)\ (K_{IC}/c^{1/2}) \qquad (1)$$

where Y is the shape factor of the microcrack; E, Young's modulus; γ, the fracture energy; c, the magnitude of the fracture source; and K_{IC}, the critical

stress intensity factor (fracture toughness). The K_{IC} represents a material parameter which is a measure of resistance against fracture for those materials exhibiting fracture brittleness and hence their toughness grows higher with increasing K_{IC}. The above condition for ceramic fracture is formulated on the assumption that a crack does not grow at a level below the critical stress. Cracks grow gradually at levels below critical stress in materials available, which is what is called the slow crack growth (SCG). Stress corrosion by water and slippage of and cavity formation in grain boundaries, among other things, produce SCG. Actual fracture of ceramics occurs when microcracks which have been growing in a stable state reach a magnitude that meets formula (1) above and thus starts growing in an unstable state.

If we are to overcome the brittleness of ceramics technologically, we must develop materials of limited crack growth at levels below fracture stress, or of a long lifespan, develop a manufacturing process which allows control of sources of fracture such as cracks, air-pores, coarse particles, and inclusions in size and distribution to the maximum, develop technologies for predicting the lifespan of the material by such means as nondestructive tests, fracture probability, and guarantee tests, and design machines that produce compression stress but not stress concentration. It is important in manufacturing ceramic components of high mechanical reliability by the above means that high toughness of the material be achieved, because improved toughness produces many effects such as:

(1) Materialization of high strength and easy cutting, grinding, and lapping in the material.

(2) Materialization of raising resistance against surface damage.

(3) Materialization of reduction in the number of microcracks of different characteristics or in the degree of microstructure susceptibility.

(4) Materialization of easy material- and machine-designing.

(5) Materialization of long lifespan of the material.

(6) Suppression of new fracture sources in the material during its use.

The following deals with the mechanism of toughening ceramics and the present state and future prospects of this research area.

3. Mechanism of Toughening Ceramics

Table 1 is a summary of the toughening mechanisms for ceramics. The essential mechanism that greatly contributes to the growth of fracture energy is the plastic deformation of the advancing front of cracks listed in I of the table. It is difficult for plastic deformation to occur in ceramics except at high temperature as needed in this mechanism. In general, the K_{IC} of polycrystal ceramics is substantially larger than for single crystal ceramics, which suggest that such microstructures as size, shape, air pores, grain boundaries,

Table 1. Mechanism of Toughening Ceramics

I.	Essential Improvement—Plastic Deformation
II.	Control of Microstructure Air pore, grain size, grain shape, grain boundary, microcrack, etc.
III.	Improvement of Toughness by Formation of Composite Materials
	(1) Ceramic/metal series
	(2) Ceramic/ceramic series
	(a) The reciprocal reaction between the crack front and the dispersed phase
	• Pinning of the crack front • Curving of the crack front • Deflection and twisting of the crack front
	(b) In the process zone in the vicinity of the crack front
	• Stress-induced phase transition • Formation of microcracks • Pull-out of whiskers and fibers

contaminants, microcracks, and internal stresses greatly affects the value of K_{IC} in view of differences in structure between the two types of crystals. Maximum emphasis must be placed on the control of microstructures where ceramics are concerned. Refer to Reference 1 for details on this factor.

The ceramics toughening mechanism that we must think about next is the one involving formation of composite materials, that is, involving dispersion of a second phase or an inhomogeneous material—it may be an identical material but of a crystal grain different in size and shape—thereby to improve K_{IC}. In some of the composite materials involving this mechanism, metals are used for dispersion and in other ceramics. In the former, the stress concentration at the front of a crack is absorbed in the plastic deformation of the metal. For instance, dispersion of 5~20 wt%Co in WC allows a K_{IC} of some 20 $MN/m^{1/2}$. The material is not adapted to application in severe conditions as a high-temperature structural whereas, in the latter where a ceramic is dispersed in a ceramic, the ceramic characteristics will not disappear.

The mechanism of toughening by the latter, the formation of ceramic-ceramic composite materials, is further divided into: 1) to cause "pinning of crack fronts," "curving of crack front," and "deflection of crack front," by reciprocal reactions between the crack front and the dispersed phase; and

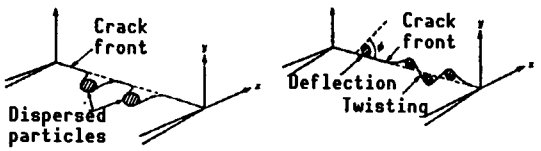

Figure 1. Reciprocal Reaction Between the Advancing Front of a Crack and the Dispersed Particles

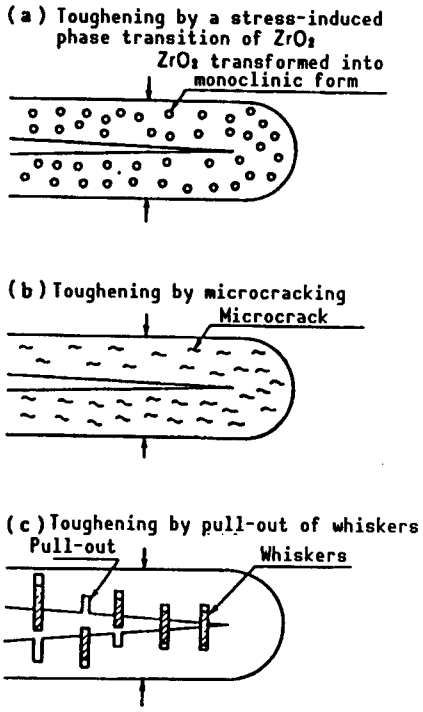

Figure 2. Toughening Mechanism by Formation of a Process Zone Which Blocks the External Stress

2) to cause "phase transformation of the dispersed phase ZrO_2 in the vicinity of a crack front," "microcracking," and "pull-out of whiskers or fibers." In the first subgroup, which of the three causes works is determined by the internal stresses around the dispersed phase arising as the material is cooled from the manufacturing temperature because of differences or anisotropy in thermal expansion coefficient and Young's modulus between the matrix and the dispersed phase. Figure 1 shows the reciprocal reaction between the matrix and the dispersion phase. The improvement in K_{IC} by the deflection of crack front, which is most effective among these toughening mechanisms, depends heavily on the shape of the dispersed phase with the deflection effect rising as the shape is changed from particle to plate and to rod.

The second subgroup that forms a process zone in the vicinity of the advancing fronts of cracks and thus blocks the advance of the external stress is shown in Figure 2. Figure (a) represents the phenomenon of 4-percent thermal expansion produced in ZrO_2 as it undergoes transition from the high-temperature cubic form to the monoclinic, b) the microcrack produced by a stress concentration at the advancing front of a crack which arises from the applied external stress and by internal stress arising around the dispersed particles, and (c) the suppression of the growth of the main crack in which the external stress is blocked by a compression stress which arises in the process zone and which results from the friction caused as the whiskers and long fibers are pulled out.

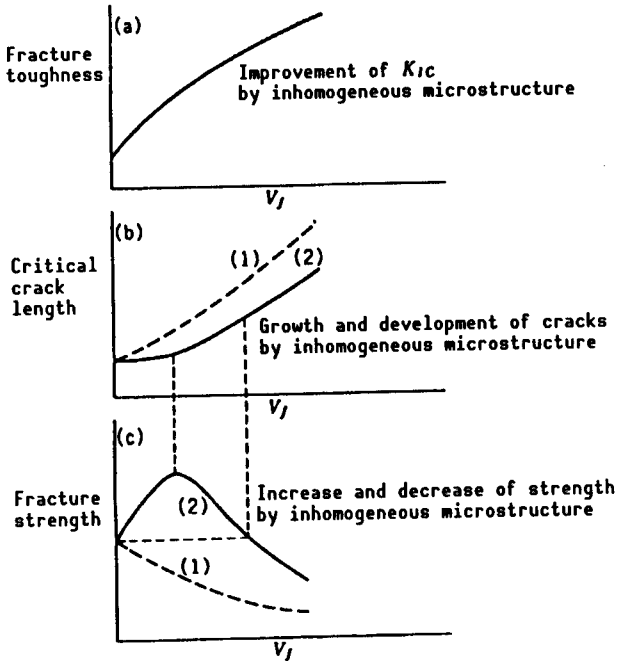

Figure 3. Dependence on Amount of Dispersed Phase of Fracture Toughness, Critical Crack Length, and Fracture Strength

An analysis of the above mechanism for toughening ceramics proves that improvement of K_{IC} is achieved in general by making the microstructure inhomogeneous, by producing modes K_{II}, K_{III}, etc., locally, and thus by making the fracture more complex (Figure 3(a)). Rendering the microstructure inhomogeneous leads to larger fracture sources as seen in the curve 1 of Figure 3(b) and the fracture strength falls as shown by the curve 1 of Figure 3(c), though toughness is enhanced. If we are to make toughness and strength of a material compatible and thus produce a material both tough and strong, we must limit the development and growth of fracture sources to a minimum and to achieve a property represented by curve 2 of Figure 3(b). In this way, a fine ceramic having both high toughness and high strength as characterized by the curve 2 of Figure 3(c) will be created. It is important in toughening a material by rendering the material inhomogeneous or by turning it into a composite that a manufacturing process be adopted or developed in which the relevant heterogenation of composite formation be limited so that increase in the fracture source be prevented and which allows control of the size of dispersed material and uniform dispersion of the material.

4. Present State of Toughening Ceramics

Many tough ceramics have recently been developed on the basis of a variety of toughening mechanisms by energetic research by ceramic researchers of the world, with most of them having been achieved by technologies for forming ceramic composites.

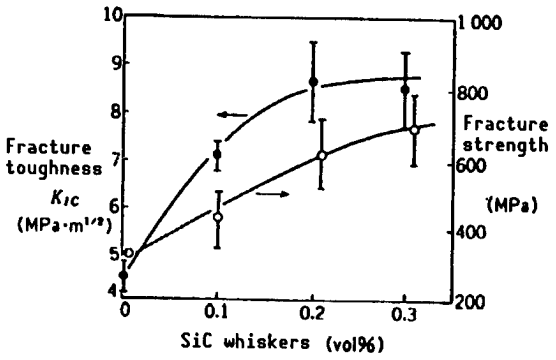

Figure 4. Toughness and Strength of Al_2O_3/SiC Whisker Composite

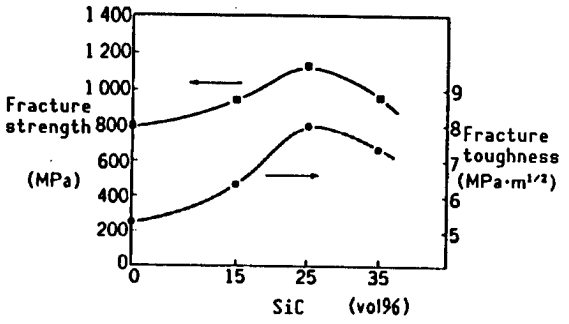

Figure 5. Dependence on Amount of SiC Whiskers of Toughness and Strength of Al_2O_3/15 vol% ZrO_2

Ceramic composite materials may be grouped largely into micro- and nano-composites depending on the size of the components of the matrix and the dispersed phase and on whether the components of the dispersed phase are located inside the grain or on the grain boundary. In microcomposites, the particles, plate-form particles, whiskers, fibers, etc., of the dispersed phase, measured in micrometers, are distributed in the grain boundary, the dispersion being aimed at toughening. In the nanocomposites, the particles and whiskers dispersed are much smaller than the matrix grain and located largely inside the grain. The crystal grain of the matrix itself, the minimum constituent unit of ceramics, is made into a composite material. It is, therefore, possible that the effect of improving toughness in this composite is not as great as for microcomposites. The nanocomposite aims at improved strength and high-temperature characteristics, as described below, rather than toughness. In the following, the author deals first with recent results in the toughening effect produced by formation of nanocomposite materials involving use of whiskers and long fibers for toughening and then with recent progress in the improvement of ceramic characteristics by formation of nanocomposite materials.

4.1 Whisker-Reinforced Composite Ceramics

Table 2 shows some of the results for toughening ceramics which have been achieved by formation of ceramic composites with use of whiskers. It is well known that toughness values above 10 MPa m$^{1/2}$ are accomplished by using stress induced phase transition of ZrO_2. tHe mechanism involved is effective only below the temperature for monoclinic/cubic transition for ZrO_2 or below 300~400°C and hence is not applicable in manufacturing high-temperature structurals. The tetragonal zirconia polycrystal (TZP)/SiC-whisker, which has been studied to overcome this disadvantage proved to have a toughness value of 11.0 MPa m$^{1/2}$, but failed to yield the necessary high-temperature strength.

Figures 4 and 5 show changes in toughness and strength for composite materials coupling Al_2O_3 with SiC whisker and Al_2O_3 with both SiC whisker and ZrO_2, respectively. In either case, not only is improved toughness and strength

Table 2. Whisker-Reinforced Ceramic Composites

Ceramic	K_{IC} ($MPa \cdot m^{1/2}$)	Mechanism for toughening
TZP/SiC whisker	6.8 → 11.0	Crack deflection, whisker pull-out
Mullite/SiC-whisker	2.4 → 4.4	" " " "
Al_2O_3/SiC-whisker	3.5 → 8.7	" " " "
Al_2O_3/ZrO_2/SiC-whisker	3.5 → 8.5	" " " "
Si_3N_4	4 → 6	Crack deflection by rod-form particles
SiC	4 → 6	" " " " "
Si_3N_4/SiC-whisker	4 → 7.5	" " " " ", Crack deflection by whiskers; whisker pull-out

achieved, but also a rise in high-temperature strength. The result seen in Figure 5 further shows the first reported case of multitoughening in which the two mechanisms of the stress-induced toughening involving ZrO_2 and the toughening by rack deflection and by whisker pull-out involving SiC whiskers worked not by addition but by multiplication and which hence may find increasing application.

In the case of Si_3N_4/SiC ceramic—noted as having the greatest prospect for application in high-temperature structurals—grains are grown in rod form which, by deflecting cracks, achieved a value of K_{IC} above 6MN $m^{1/2}$. Research on dispersion of SiC whiskers in the Si_3N_4 matrix has recently been carried out and proved to have a notable effect particularly at high temperature by the addition of the whisker as seen in Figure 6.

4.2 Long-Fiber Reinforced Ceramics

Long-fiber reinforced ceramic composites are unique in that they do not exhibit catastrophic rupture as in single-phase ceramics but the added fibers bear the external stress even if the matrix has been fractured as seen in Figure 7. Therefore, they may provide the greatest toughness at present. Table 3 shows recent results of research on these ceramic composites. As evident from the table, an SiC/carbon fiber ceramic composite and an SiC/SiC-fiber ceramic composite, which remain strong and tough up to high temperatures have been developed by a CVI method—an application of the CVD method in which the matrix component of SiC is filled effectively into the spaces among the carbon fiber or SiC fiber preform. Also developed is an Si_3N_4/carbon fiber ceramic composite which is produced from an organometallic compound precursor and

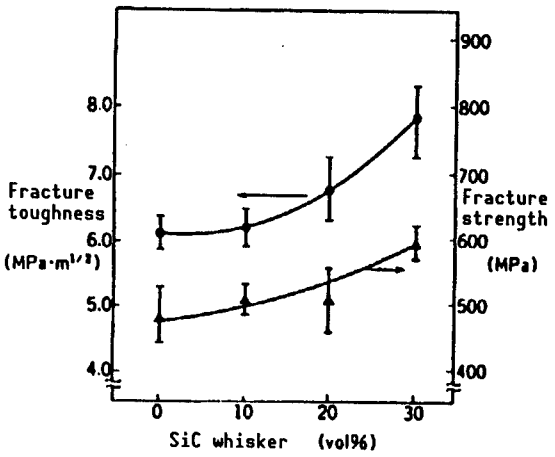

Figure 6. Toughness and Strength at 1,200°C of the Ceramic Composite Si_3N_4/SiC-Whisker

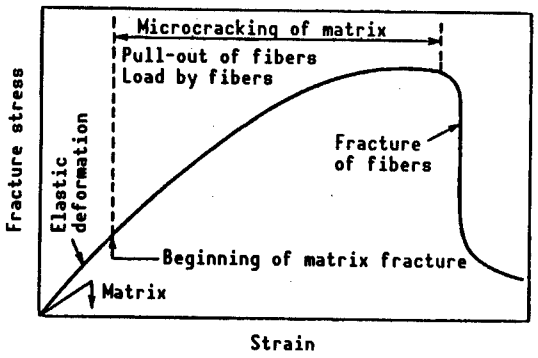

Figure 7. Stress-Strain Curve of Long-Fiber Reinforced Ceramic Composites

Table 3. Long-Fiber Reinforced Ceramic Composite

Ceramic	K_{IC} (MPa·m$^{1/2}$)	Fracture strength (MPa)		
		Room temperature	1,000°C	1,200°C
LAS/SiC fiber	1.2 → 24	850	820	
SiC/SiC fiber	3.5 → 33	300	400	280
SiC/carbon fiber	3.5 → 36	500	700	700
Si_3N_4/carbon fiber	4.6 → 29	481		443

which exhibits high strength up to 1,400°C as well as an extremely high toughness value of about 30 MPa m$^{1/2}$.

The recent progress in the research and development in this area is spectacular, with long-fiber ceramic composites about to be put to practical application. If the composite is to be developed further and to be put in wide application, many problems remain to be resolved, among which are:
1) development of long fibers of high strength and high resistance against heat; 2) development of a method that allows control of the intermetallic compound interface between the matrix and the fiber so that the pull-out mechanism works effectively for toughening the composite; 3) establishment of a simple method to assess the structure and strength of the interface;
4) establishment of a method of assessment of various properties, particularly toughness, of fiber-reinforced ceramics; and 5) development of a new cheap manufacturing process.

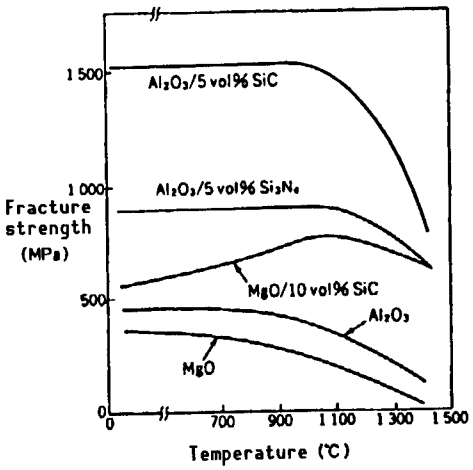

Figure 8. Strength at High Temperature of the Nanoceramic Composites Al_2O_3/SiC, Al_2O_3/Si_3N_4, and MgO/SiC

4.3 Nanoceramic Composite

In nanocomposite materials, particles or whiskers far smaller than the matrix grains are dispersed largely inside the crystal grain of the matrix and thus the crystal grain itself, the minimum constituent unit of ceramics, is turned into a composite. Nanocompounds with the above structure were initially produced by the CVD method, but an ordinary sintering method has recently been applied to prepare nanocomposites of oxide and nonoxide series as seen in Table 5. Figure 8 shows a plot of temperature vs. fracture strength for nanocompounds of oxide series produced by sintering Al_2O_3/SiC, Al_2O_3/Si_3N_4, and MgO/SiC. It is evident that their strength not only at room temperature but also at high temperatures is improved enormously compared with simple-phase ceramics Al_2O_3 and MgO. This implies that the nanocomposite technology is capable of raising the heat-resistance temperature—the temperature at which a material is available under high-stress conditions—of ceramics and, in particular, oxide ceramics. As seen in Table 4, the effect of nanocomposite formation is particularly notable in the case of MgO/SiC series where an addition of SiC particles in 10~30 Vf has allowed the heat-resistance temperature to rise by 800°C from 600°C to 1,400°C, a level equivalent to or above that of nonoxide ceramics series of SiC and Si_3N_4 which are presently in the limelight in many industrial areas as high-temperature structurals resisting severe environmental conditions. The nanocomposite technology has proved to be capable of doubling or more than doubling the value of the thermal shock resistance characteristics, a weak point of oxide ceramics.

Table 4. Improvement of Mechanical Properties by Formation of Nanocomposites

Composite system	Toughness ($MPa \cdot m^{1/2}$)	Strength (MPa)	Heat resistance (°C)
Al_2O_3/SiC particle	3.5 → 4.8	350 → 1,520	800 → 1,200
Al_2O_3/Si_3N_4 particle	3.5 → 4.7	350 → 850	800 → 1,300
MgO/SiC particle	1.2 → 4.5	340 → 700	800 → 1,400
Si_3N_4/SiC particle	4.5 → 7.5	850 → 1,550	1,200 → 1,400

Table 5. Type and Method of Manufacture for Nanocomposites of Ceramics

Composition of composite material	Manufacture method	Objective
Si_3N_4/TiN particle	CVD*	Basic research of CVD reactions
Si_3N_4/TiN whisker	CVD	Basic research of CVD reactions
SiC/lamination defect	CVD	Toughening
SiC/noncrystal or amorphite	Precursor	Machinability
Al_2O_3/SiC particle	Sintering	Strength, heat resistance improvement**
Al_2O_3/Si_3N_4 particle	Sintering	Strength, heat resistance improvement**
MgO/SiC particle	Sintering	Strength, heat resistance improvement**
Si_3N_4/SiC particle	Sintering	Strength, toughness improvement

* Chemical vapor deposition method
** Improvement in the maximum temperature for operation under high external stress.

The powders of oxide ceramics such as Al_2O_3 and MgO are manufactured more cheaply than the nonoxide ceramics Si_3N_4 and SiC and allow easy molding, sintering, and machining as well as superior cost performance. Nevertheless, they have been regarded as having slim prospects for application in high temperature structurals because of some difficulties involved in mechanical and thermal characteristics. The nanocomposite technology has now resolved the difficulties involved in oxide ceramics and is transforming them into a material comparable to nonoxide ceramics.

Among the advantages attributable to formation of nanocomposites from ceramics are: 1) making the microstructure finer, suppressing abnormal grain growth, and controlling grain shape which largely improves strength; 2) deflection of crack fronts by fine particles dispersed inside the grain and development of microcracks inside the crystal grain which raise the fracture toughness 1.5 to 4.0 times; 3) suppression of development of fracture sources by compression stress occurring inside the grain, which raises strength; 4) fracture inside the grain is induced by the tensile stress occurring around particles dispersed in the grain, serves to block delayed fracture at high temperature, and thus raises strength there; 5) pinning the movement of dislocation at high temperature by hard particles dispersed inside the grain which improves high temperature hardness, high-temperature strength, fatigue, creep resistance, and brittleness-ductility transition temperature; and 6) control of Young's modulus, thermal expansion coefficient, and thermal conductivity, which allows improvement of heat-impact resistance in connection with improved strength and toughness.

The question of which of these effects grows effective depends heavily on the type and magnitude of the stress arising from the difference between the thermal expansion coefficient, Young's modulus, and Poisson ratio of the matrix and the dispersed phase. It is necessary in the pinning effect of dislocations that the dispersed phase be capable of maintaining a high hardness at high temperature.

4.4 Super-Tough Ceramics of the Future

It has grown evident, as described in the preceding issue, that the disadvantage of ceramics being brittle or of their having low fracture toughness K_{IC} can be surmounted to a substantial extent by formation of composites with whiskers and long fibers. For example, it is no exaggeration to apply the term super tough to some of the long-fiber reinforced ceramic composites. Composites with a K_{IC} above 20 MPa $m^{1/2}$ which is comparable to those for WC/Co superhard material have been developed. Nevertheless, the strength of these composites is generally lower than those for the corresponding single-phase materials. It is imperative that the superior characteristics of single-phase ceramics of high strength and high heat resistance not become lost at the cost of improving toughness by composite formation if ceramics are to find practical application in many industrial sectors. On the contrary, ceramic composites must be designed so that the composite formation not only brings increased toughness to the resulting composite, but also strength and resistance against heat much superior to that of the original single phase.

Material designing of such a ceramic may possibly be achieved by coupling microcomposite formation—reinforcement with whiskers and long fibers—which contributes substantially to improved toughness with nanocomposite formation which induces composite formation in crystal grains themselves and which thus improves various mechanical properties; that is, a composite ceramic of superhigh toughness and superhigh strength at high temperature may be created by designing whisker- or long-fiber reinforced nanocomposites which involve a nanocomposite as the matrix and whiskers or long fibers as the reinforcement. It is also notable that nanocomposite technology proved capable of transforming oxide ceramics, which have been considered not applicable in high-temperature structurals to date into a high-temperature structural that compares with the nonoxide ceramics, SiC and Si_3N_4. Allowing for cost performance, it is possible that composite materials with oxide series of nanoceramic composite used as the matrix and whiskers or long fibers used as the reinforcement henceforth may play an important role.

5. Conclusion

The author has described whisker- and long-fiber reinforced composite materials, which have the prospect of overcoming the major disadvantage of ceramics, brittleness, and of maintaining their high strength up to high temperatures, and then nanocomposite materials, in which a technology for controlling microstructure at the level three orders of magnitude smaller than the conventional composite allows transformation of many ceramics, particularly oxide ceramics, in terms of their basic concepts, recent progress, and future development.

If these materials are to find practical application in industry, of greatest importance is to push basic research on new manufacturing methods allowing for the cost performance of the method, for example, the method of self-propagating combustion sintering, which allows molding and sintering in a very short time, and the Lanxide method in which metal melts are turned into ceramics.

- END -

NTIS
ATTN: PROCESS 103
5285 PORT ROYAL RD
SPRINGFIELD, VA

22161

Foreign Broadcast Information Service (FBIS) and Joint Publications Research Service (JPRS) publications contain political, military, economic, environmental, and sociological news, commentary, and other information, as well as scientific and technical data and reports. All information has been obtained from foreign radio and television broadcasts, news agency transmissions, newspapers, books, and periodicals. Items generally are processed from the first or best available sources. It should not be inferred that they have been disseminated only in the medium, in the language, or to the area indicated. Items from foreign language sources are translated; those from English-language sources are transcribed. Except for excluding certain diacritics, FBIS renders personal and place-names in accordance with the romanization systems approved for U.S. Government publications by the U.S. Board of Geographic Names.

Headlines, editorial reports, and material enclosed in brackets [ ] are supplied by FBIS/JPRS. Processing indicators such as [Text] or [Excerpts] in the first line of each item indicate how the information was processed from the original. Unfamiliar names rendered phonetically are enclosed in parentheses. Words or names preceded by a question mark and enclosed in parentheses were not clear from the original source but have been supplied as appropriate to the context. Other unattributed parenthetical notes within the body of an item originate with the source. Times within items are as given by the source. Passages in boldface or italics are as published.

SUBSCRIPTION/PROCUREMENT INFORMATION

The FBIS DAILY REPORT contains current news and information and is published Monday through Friday in eight volumes: China, East Europe, Soviet Union, East Asia, Near East & South Asia, Sub-Saharan Africa, Latin America, and West Europe. Supplements to the DAILY REPORTs may also be available periodically and will be distributed to regular DAILY REPORT subscribers. JPRS publications, which include approximately 50 regional, worldwide, and topical reports, generally contain less time-sensitive information and are published periodically.

Current DAILY REPORTs and JPRS publications are listed in *Government Reports Announcements* issued semimonthly by the National Technical Information Service (NTIS), 5285 Port Royal Road, Springfield, Virginia 22161 and the *Monthly Catalog of U.S. Government Publications* issued by the Superintendent of Documents, U.S. Government Printing Office, Washington, D.C. 20402.

The public may subscribe to either hardcover or microfiche versions of the DAILY REPORTs and JPRS publications through NTIS at the above address or by calling (703) 487-4630. Subscription rates will be provided by NTIS upon request. Subscriptions are available outside the United States from NTIS or appointed foreign dealers. New subscribers should expect a 30-day delay in receipt of the first issue.

U.S. Government offices may obtain subscriptions to the DAILY REPORTs or JPRS publications (hardcover or microfiche) at no charge through their sponsoring organizations. For additional information or assistance, call FBIS, (202) 338-6735,or write to P.O. Box 2604, Washington, D.C. 20013. Department of Defense consumers are required to submit requests through appropriate command validation channels to DIA, RTS-2C, Washington, D.C. 20301. (Telephone: (202) 373-3771, Autovon: 243-3771.)

Back issues or single copies of the DAILY REPORTs and JPRS publications are not available. Both the DAILY REPORTs and the JPRS publications are on file for public reference at the Library of Congress and at many Federal Depository Libraries. Reference copies may also be seen at many public and university libraries throughout the United States.